Polyoxometalates

REVIEW ARTICLE

Metal cluster confinement in MOFs and COFs: Advanced synthesis strategies and applications in photocatalysis

Irshad Ahmad,[1,2] Huan Li,[1] Ayman Al-Qattan,[3] Mohammed T. Alotaibi,[4] and Gao Li[1]

[1] *School of Chemistry and Chemical Engineering, Inner Mongolia Normal University, Hohhot 010022, China*
[2] *Department of Physics, University of Agriculture, Faisalabad 38040, Pakistan*
[3] *Energy and Building Research Center, Kuwait Institute for Scientific Research, P.O. Box: 24885, Safat 13109, Kuwait*
[4] *Department of Chemistry College of Science, King Khalid University, Abha, P.O. Box 9004, Saudi Arabia*
[§] *Irshad Ahmad Huan Li contributed equally to this work.*

Received: 3 November 2025; **Revised:** 6 February 2026; **Accepted:** 10 February 2026

Address correspondence to li_gao82@yeah.net

Cite This: ***Polyoxometalates*****, 2026, *5*, 9140122**

Read Online

ABSTRACT: Atomically precise metal nanoclusters, consisting of tens to hundreds of metal atoms, represent a unique class of catalytic materials with well-defined electronic structures and tunable surface chemistry. These features enable nanoclusters to act as versatile components in photocatalytic systems, where they regulate light absorption, charge separation, and interfacial reaction dynamics. Photocatalysis provides a sustainable pathway for converting solar energy into fuels and value-added chemicals; however, its practical application is limited by intrinsic thermodynamic and kinetic barriers, as well as catalyst stability and selectivity challenges. Recent advances have spotlighted the integration of nanoclusters with extended porous frameworks, including metal–organic frameworks (MOFs) and covalent organic frameworks (COFs), as a powerful strategy to overcome these limitations. These hybrid architectures allow precise control over active-site geometry, electronic environments, and substrate accessibility, while promoting synergistic effects such as enhanced charge transport and stabilization of reactive intermediates. This review highlights emerging synthetic methodologies, modification strategies, and recent photocatalytic applications (CO_2 reduction, H_2 evolution, H_2O_2 production, organic synthesis, pollutant removal, CH_4 conversion, *etc*) reported over the past three years. We discuss mechanistic insights, structure–function relationships, and critical challenges, including conductivity, robustness, and scalability. Finally, we propose integrated design principles for constructing hybrid nanocluster–framework photocatalysts with optimized efficiency, selectivity, and durability, offering a roadmap for the rational development of next-generation energy-conversion and chemical-synthesis platforms.

KEYWORDS: photocatalyst; nanoclusters, covalent organic frameworks (COFs), metal–organic frameworks (MOFs), modification strategies; synthesis methods

1. Introduction

Harnessing solar energy through photocatalysis has emerged as a compelling strategy for sustainable chemical transformations, offering a direct route to convert photon energy into chemical potential [1,2]. A decisive factor governing progress in this field is the ability to engineer catalytic systems with atomic-level precision, where electronic structure, spatial arrangement, and interfacial interactions can be deliberately tailored [3]. In this regard, materials that bridge molecular precision with solid-state robustness have attracted increasing attention. Among such candidates, atomically defined metal nanoclusters (NCs) exhibit distinctive advantages as light-responsive catalytic units [4,5]. Their discrete electronic states and quantized energy levels endow them with molecule-like photophysical behavior, making them highly effective in photoredox processes [6]. The precise control over atomic composition, ligand environment, and electronic configuration enables fine modulation of excited-state dynamics, charge-transfer pathways, and reaction selectivity [7]. However, despite these advantages, the practical deployment of NCs remains challenged by limited structural stability, susceptibility to aggregation, and difficulties in maintaining long-term activity under reaction conditions.

In parallel, reticular materials, including metal–organic frameworks (MOFs) and covalent organic frameworks (COFs), have emerged as highly versatile platforms for photocatalysis [8,9]. Their periodic architectures provide ordered arrays of catalytic sites embedded within porous, high-surface-area scaffolds [10]. The modular nature of these frameworks enables rational incorporation of photoactive units, catalytic centers, and conductive motifs, thereby allowing systematic control over light absorption, mass transport, and charge separation [11,12]. MOFs benefit from tunable metal nodes and coordination environments, while COFs offer extended π-conjugation and enhanced chemical robustness, making both classes attractive for photochemical applications [13,14]. Despite their complementary strengths, each

material class faces intrinsic limitations. Metal NCs suffer from instability and poor recyclability, whereas framework materials often exhibit insufficient conductivity or limited catalytic versatility [15,16]. These challenges underscore the necessity of innovative design strategies that integrate the strengths of both systems while mitigating their respective weaknesses. Notably, metal NCs and reticular frameworks share a common conceptual foundation: both enable precise manipulation of active sites and electronic structure at the atomic level [17,18]. Their atomically defined structures and tunable electronic states provide a unique platform for elucidating how charge excitation, transfer, and surface reactions evolve at the nanoscale. This conceptual convergence opens new opportunities to construct hybrid or synergistic catalytic architectures that combine molecular precision with structural order [19]. Such integration offers a powerful avenue toward unraveling structure–property relationships and advancing the rational design of next-generation photocatalysts with enhanced efficiency, selectivity, and durability [20]. In particular, metal-based NCs have attracted growing attention owing to their structural versatility, rich photophysical behavior, and capacity to mediate multielectron transformations under light irradiation.

Despite the rapid expansion of research in this area, a comprehensive and systematic overview that connects synthetic strategies, structural characteristics, modification approaches, and photocatalytic functionality of NCs remains lacking. Existing reviews have primarily focused on specific reactions or isolated material systems, leaving broader design principles and comparative mechanistic insights insufficiently addressed. Moreover, discussions on how structural modulation, such as NCs size and shape, core composition, ligand engineering, heteroatom incorporation, interfacial coupling, pore confinement, or vacancy creation, governs photocatalytic performance are often fragmented or treated superficially. Given the accelerating interest in NCs-based photocatalysts, there is a pressing need to consolidate current knowledge and establish a coherent framework that links material design with catalytic behavior. In particular, understanding how NCs interact with supporting matrices, regulate charge dynamics, and evolve under reaction conditions is essential for advancing their practical implementation. Equally important is the identification of unresolved challenges, including stability, scalability, and performance optimization across diverse photocatalytic reactions. In this review, we provide a comprehensive and critical overview of recent advances in NCs-enabled photocatalysis. Emphasis is placed on synthetic methodologies, structural regulation strategies, and mechanistic insights that govern photocatalytic activity. While particular attention is given to NCs-integrated MOF and COF systems due to their structural tunability and emerging relevance, the discussion is intentionally broadened to encompass a wide range of NCs-modified photocatalysts. By correlating material design with catalytic function, this review aims to offer a unified perspective on current progress, identify existing limitations, and highlight future directions for the rational development of high-performance photocatalytic systems.

Building on recent advances in nanocluster science, this review systematically examines the rapidly evolving field of NCs-enabled photocatalysis, with particular emphasis on metal NCs as versatile components across diverse reaction platforms. We first outline the fundamental photophysical features that endow NCs with exceptional photocatalytic potential, including discrete electronic states, tunable redox properties, and efficient interfacial charge-transfer behavior. Recent progress in synthetic methodologies is then critically assessed, highlighting emerging strategies, such as microwave-assisted, artificial intelligence–guided, co-reduction, photochemical, and sonochemical approaches that enable accelerated synthesis, improved atomic precision, and enhanced structural controllability, thereby expanding the accessible compositional and architectural space of NCs-based catalysts. Beyond synthesis, key structure–performance relationships are discussed, encompassing size and morphology regulation, core composition tuning from monometallic to alloyed systems, ligand and surface engineering, heteroatom incorporation, and interface construction with semiconducting hosts, along with advanced concepts such as spatial confinement and defect modulation to optimize charge separation and reaction selectivity. The impact of these design principles is illustrated across a broad range of photocatalytic transformations, including CO_2 reduction, H_2 evolution, H_2O_2 production, organic synthesis, environmental remediation, and CH_4 conversion. By correlating atomic-level structure with catalytic function, this review critically evaluates current challenges related to stability, mechanistic understanding, and scalability, while outlining future directions for the rational development of high-performance NCs-based photocatalytic systems.

2. Photocatalytic properties of nanoclusters

Metal nanoclusters (NCs), composed of several to a few hundred metal atoms (Fig. 1(A)), occupy a unique regime between discrete molecules and bulk solids [21]. Their well-defined atomic structures, enabled by advances in crystallography and theoretical modeling since the 1970s, make them ideal model systems for elucidating size-dependent electronic and catalytic phenomena [22]. Unlike larger nanoparticles, NCs exhibit precise compositions and atomically resolved structures, allowing direct correlation between electronic configuration and photocatalytic behavior [23]. Stabilization by organic ligands is essential to prevent aggregation and to preserve structural integrity; in particular, organosoluble ligands facilitate ordered packing and high crystallinity by avoiding protonation equilibria commonly encountered in aqueous systems [24]. Structurally, metal NCs consist of a zerovalent metal core protected by a shell of metal–ligand complexes in which surface metal atoms typically adopt a +1 oxidation state. The relative population of core and shell atoms determines the overall electronic structure and governs optical response. Owing to quantum confinement, NCs exhibit discrete electronic states rather than continuous energy bands (Fig. 1(B)), leading to molecule-like HOMO–LUMO transitions [25]. The resulting narrow energy gaps—often below 1 eV, enable efficient absorption in the visible and near-infrared regions, distinguishing NCs from conventional wide-bandgap semiconductors [26].

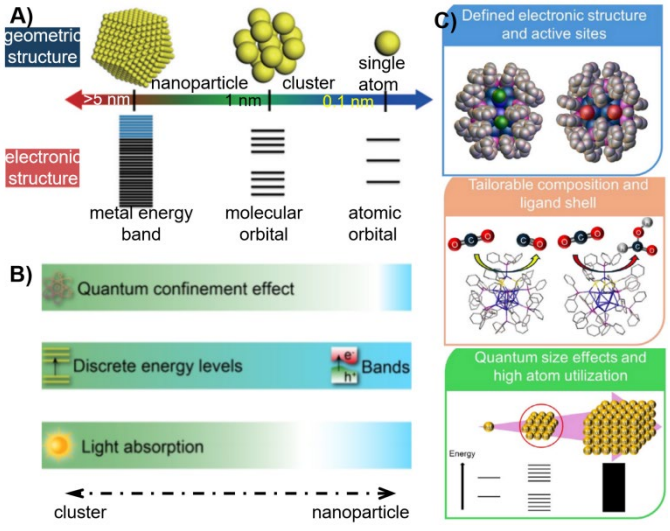

Figure 1 (A) Geometric/electronic architectures of nanoparticles, nanoclusters, and single atoms. Reproduced with permission from Ref. [21], ©America Chemical Society 2018. (B) Various physiochemical properties of metal nanoparticles and metal nanoclusters. Reproduced with permission from Ref. [25], John Wiley & Sons 2022. (C) Advantages of metal nanoclusters. Reproduced with permission from Ref. [28], John Wiley & Sons 2025.

The photocatalytic performance of metal NCs is strongly influenced by their ability to generate and separate charge carriers. In contrast to doped semiconductors, where mid-gap states often serve as recombination centers, NCs offer intrinsic tunability through size, composition, and ligand engineering [27]. Their frontier orbital energies can be precisely adjusted to match the band positions of semiconductors, enabling favorable interfacial charge transfer. When integrated into heterostructures, NCs facilitate charge separation via type-II or Z-scheme pathways, thereby suppressing recombination and enhancing photocatalytic efficiency. Surface reactivity further distinguishes NCs from larger metallic systems. The high proportion of low-coordinated atoms, coupled with quantum size effects (Fig. 1(C)) and unique surface motifs, endows NCs with exceptional catalytic activity [28]. Alloyed nanoclusters provide an additional degree of control: modulation of electronic density and upward shifts of the d-band center enhance adsorption of key reaction intermediates and improve reaction kinetics [29]. Unlike conventional noble-metal cocatalysts, which rely primarily on Schottky junctions and are limited by semiconductor type, NCs exhibit greater flexibility and stability under photocatalytic conditions [30]. Taken together, metal nanoclusters combine efficient light absorption, tunable electronic structures, and high catalytic activity within a single, atomically precise platform. Their stability against photochemical degradation and their well-defined structures make them not only highly promising photocatalysts but also ideal model systems for uncovering fundamental structure–activity relationships [31]. These attributes position metal nanoclusters as a key materials class for the rational development of next-generation photocatalytic and photoelectrochemical systems.

3. Synthesis methods

The preparation of metal NCs has traditionally relied on solution-phase chemical reduction carried out under mild conditions in the presence of stabilizing ligands. While this classical methodology is experimentally straightforward, it often suffers from prolonged reaction times, batch-to-batch variability, and limited control over cluster size and emission behavior. These shortcomings have motivated the development of alternative synthetic routes, including photochemical, sonochemical, co-reduction, and ligand-exchange strategies. More recently, data-driven and automated approaches have emerged as promising tools for accelerating NC discovery and optimization. Among these advancements, microwave-assisted synthesis has gained particular attention due to its efficiency, reproducibility, and compatibility with green chemistry principles.

3.1. Microwave-assisted synthesis

Microwave irradiation provides rapid and homogeneous volumetric heating, enabling fast reduction of metal precursors and synchronized nucleation events [32]. Compared with conventional thermal methods, microwave-assisted synthesis markedly shortens reaction times, improves product uniformity, and enhances control over nanocluster growth. Importantly, this approach often eliminates the need for harsh reducing agents and allows reactions to proceed efficiently in aqueous media, aligning well with sustainable synthesis goals [33]. The effectiveness of microwave heating has been clearly demonstrated for gold nanoclusters. Our group reported that histidine-stabilized Au NCs synthesized under microwave irradiation (850 W, 30 min) displayed markedly enhanced photoluminescence relative to materials prepared under ambient conditions [34]. The resulting clusters exhibited a single emission band centered at 471 nm with excellent photostability and temporal stability, highlighting the role of rapid and uniform heating in promoting well-defined emissive states. In a subsequent study, the same synthetic protocol was extended to solid-state histidine-protected Au NCs obtained via lyophilization [35]. These materials showed excitation-dependent dual emission at 475 and 520 nm and retained luminescence up to 150 °C, reflecting enhanced structural rigidity and strong ligand–metal interactions induced by microwave processing. Microwave irradiation has also proven highly effective for producing glutathione-protected Au NCs. Using sealed-vessel microwave heating (90 °C, 850 W, 20 min), our group obtained dual-emissive clusters with red (610 nm) and near-infrared (800–810 nm) emission bands [36]. The materials exhibited high quantum efficiency (9.9%) and unusually long excited-state lifetimes, reaching 1.8 μs in the NIR region. These optical features were attributed to rapid nucleation and efficient surface passivation enabled by microwave-driven reduction, which minimizes defect formation and enhances electronic confinement.

Beyond Au systems, microwave-assisted synthesis has been successfully applied to silver and copper nanoclusters. Shang et al. demonstrated a rapid and environmentally benign route to histidine-stabilized AgNCs by irradiating $AgNO_3$ solutions at 700 W for only 8 min [37]. The resulting clusters displayed strong blue emission at 440 nm with a quantum yield of 5.2% and nanosecond-scale lifetimes, highlighting the ability of microwave heating to control nucleation and surface coordination. Similarly, Saleh et al. reported the synthesis of pepsin-stabilized Cu NCs under microwave irradiation (850 W, 30 min), yielding uniformly sized (~2 nm) clusters with blue emission centered at 409 nm and an exceptional quantum yield of 17% [38]. The rapid heating

minimized oxidative degradation of Cu^0 species, a common limitation in copper-based nanocluster synthesis. Hence, microwave-assisted synthesis has emerged as a powerful and versatile strategy for preparing metal nanoclusters with controlled size, high stability, and tunable optical properties. Its advantages, namely short reaction times, improved reproducibility, and compatibility with green chemistry, make it particularly attractive for photocatalytic and optoelectronic applications [39-41]. Nevertheless, challenges remain, most notably the limited reproducibility across different microwave platforms. Variations in reactor geometry, irradiation power, and sample volume can significantly influence reaction outcomes. Careful standardization of experimental parameters is therefore essential for broader adoption. Despite these limitations, microwave-assisted synthesis represents one of the most efficient and scalable routes for the controlled fabrication of metal nanoclusters.

3.2. Photochemical synthesis

Photochemical synthesis has emerged as an effective and sustainable strategy for constructing metal NCs, offering a level of control that is difficult to achieve using conventional chemical reduction [42]. By harnessing light as the driving force, these methods enable temporally regulated redox processes, suppress uncontrolled nucleation, and often eliminate the need for harsh reducing agents [43]. Depending on the system, cluster formation can proceed through direct photoreduction, photoinduced electron transfer (PET), or radical-mediated pathways, allowing access to structures and oxidation states that are otherwise inaccessible [44]. A representative example was reported by Wang and co-workers, who prepared atomically precise Ag_{25} NCs using a PET-driven process under white-light irradiation [45]. The synthesis process is shown in Fig. 2(A). In this system, triethylamine served as an electron donor while molecular oxygen acted as the terminal oxidant, enabling controlled Ag^+ reduction without conventional reductants. The approach afforded structural precision comparable to $NaBH_4$-based routes but under significantly milder and greener conditions. Extending this concept, the same group later achieved the stepwise assembly of a heterometallic $Ag_{12}Cu_7$ cluster [46]. Photogenerated Ag_{19} intermediates were first formed, followed by Cu incorporation under continued irradiation, overcoming the intrinsic redox mismatch between Ag^+ and Cu^+. The resulting alloy cluster (Fig. 2(B)) displayed intense red phosphorescence (λ_{em} = 665 nm) with a lifetime of 30 μs, attributed to strong cuprophilic interactions and ligand-to-metal charge transfer. Photochemical strategies have also enabled access to group 10 metal clusters that are otherwise difficult to isolate. Fan et al. reported the first photochemically synthesized Ni and Pd nanoclusters using a light-induced redox cascade [47]. Following mild $NaBH_4$ pre-reduction, blue-light irradiation generated thiyl radicals from disulfides, which stabilized discrete metal assemblies such as $Ni_{11}(SPh)_{22}$. These clusters exhibited well-defined ring-like geometries and enhanced crystallinity compared to products obtained via thermal methods, with Ni_{11} displaying a characteristic absorption at 467 nm. From a sustainability perspective, Ferlazzo and co-workers developed an environmentally benign route to Cu nanoclusters in aqueous media using UV-activated acetone and monoethanolamine as a stabilizer [48]. The resulting ~3.5 nm clusters showed blue-green emission (λ_{em} = 489.9 nm), a quantum yield of 12%, and notable photothermal conversion efficiency (38%) under 405 nm irradiation. Importantly, the synthesis avoided toxic solvents and reducing agents, underscoring the potential of photochemistry in green nanomaterial fabrication. Collectively, these studies demonstrate that photochemical-assisted synthesis offers a versatile and environmentally responsible platform for engineering metal nanoclusters. By enabling precise control over

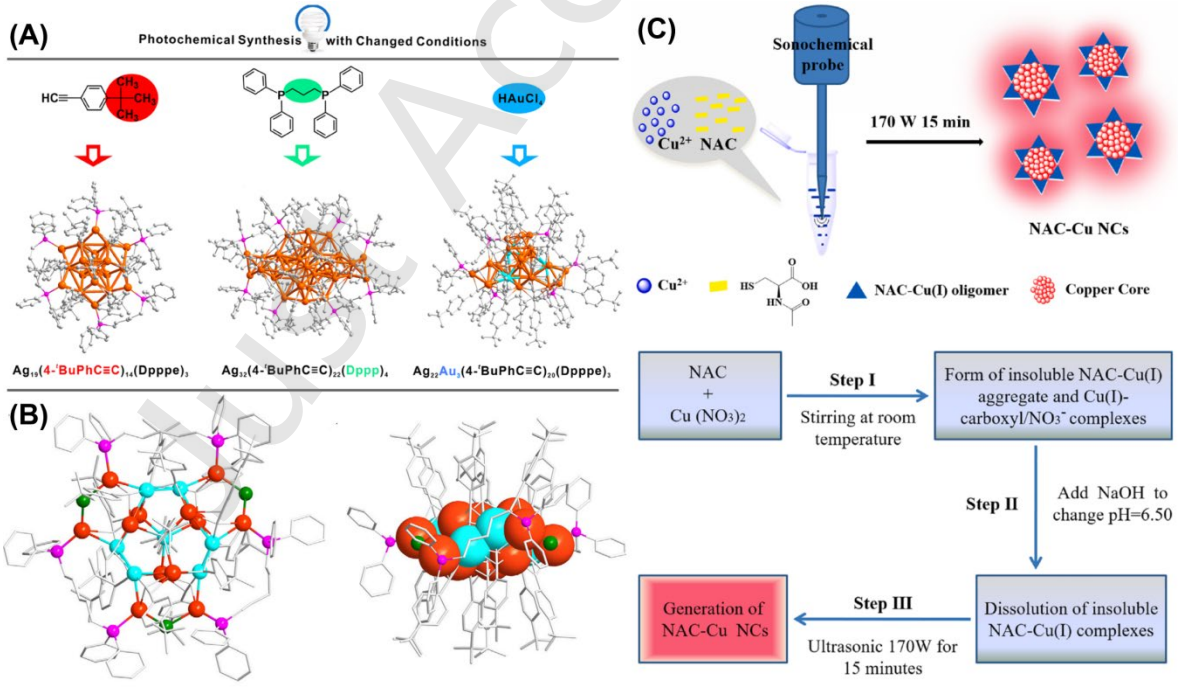

Figure 2. (A) Photochemical synthesis of Ag nanoclusters. Reproduced with permission from Ref. [45], America Chemical Society 2023. (B) Geometric structures of $Ag_{12}Cu_7$. Reproduced with permission from Ref. [46], John Wiley & Sons 2025. (C) Sonochemical synthesis of NAC-Cu nanoclusters. Reproduced with permission from Ref. [52], Elsevier B.V 2022.

nucleation, composition, and electronic structure, without reliance on aggressive reductants, this approach has become a powerful tool for accessing both noble and transition-metal clusters with tailored optical and physicochemical properties.

3.3. Sonochemical-assisted synthesis

Ultrasound-driven synthesis has emerged as a powerful alternative for fabricating metal NCs, exploiting the extreme localized conditions generated during acoustic cavitation [49]. The collapse of transient microbubbles produces short-lived hot spots with high temperature and pressure, enabling rapid redox reactions, enhanced mass transfer, and uniform nucleation [50]. Compared with conventional thermal methods, sonochemical routes often yield smaller, more uniform clusters while operating under milder and more sustainable conditions [51]. In addition, ultrasonic irradiation promotes ligand activation, improves metal–ligand coupling, and facilitates surface restructuring, making it particularly attractive for precision nanochemistry. A representative example was reported by Kang and co-workers, who developed an ultrasound-assisted route to red-emissive Cu nanoclusters stabilized by N-acetyl-L-cysteine (NAC) [52]. Remarkably, the synthesis proceeded in water within 15 minutes without any external reducing agents (Fig. 2(C)). Ultrasound promoted the stepwise reduction of Cu^{2+} to Cu^{+} and subsequently to Cu^{O}, yielding ultrasmall clusters (~1.2 nm) with strong red emission at 630 nm and an unusually large Stokes shift of 290 nm. Compared to conventional thermal treatment (12 h at 70 °C), the sonochemical route produced NCs with higher emission intensity, improved photostability, and long-term colloidal stability. The dual function of NAC as both reductant and stabilizer contributed to a prolonged luminescence lifetime (451 ns) and enhanced resistance to thermal degradation, underscoring the efficiency of ultrasound in enabling clean and rapid synthesis. Beyond copper systems, sonochemical strategies have proven effective for constructing transition-metal nanoclusters with controlled dispersion. Liu et al. employed ultrasound to fabricate Ni nanoclusters anchored on $Ti_3C_2T_x$ MXene supports [53]. In this case, acoustic irradiation simultaneously promoted MXene exfoliation and homogeneous nucleation of Ni clusters. The resulting catalysts exhibited significantly reduced particle sizes, improved electronic coupling, and a six-fold increase in turnover frequency relative to non-sonicated analogues. The enhanced catalytic activity was attributed to ultrasound-induced surface activation and the formation of electron-rich Ni sites with superior stability. Overall, sonochemical-assisted synthesis represents a rapid, scalable, and environmentally benign platform for nanocluster fabrication. By harnessing the localized energy of acoustic cavitation, this approach enables precise control over cluster size, composition, and interfacial chemistry. Its successful application across multiple metal systems highlights its growing importance in the sustainable design of high-performance nanomaterials.

3.4. Co-reduction synthesis

The co-reduction approach, often referred to as the direct reduction method, represents one of the most straightforward routes for synthesizing ligand-protected metal nanoclusters [54]. In this strategy, metal precursors and stabilizing ligands are combined in solution, followed by the introduction of a reducing agent to induce simultaneous metal reduction and cluster growth [55]. Owing to its operational simplicity, broad applicability, and compatibility with a wide range of ligands, this method has been extensively employed for the preparation of atomically precise nanoclusters [56]. To date, numerous monometallic and alloy clusters have been successfully produced using this approach [57-60]. Despite its versatility, the co-reduction route presents inherent limitations when applied to bimetallic nanoclusters (BNCs). Because cluster formation proceeds through the concurrent reduction and aggregation of multiple metal ions, mismatches in redox potentials can lead to uneven nucleation, phase separation, or preferential reduction of one component. As a result, the scope of metals that can be reliably combined through this method remains relatively narrow. In practice, successful examples are largely restricted to coinage and noble metals such as Au, Ag, Cu, Pt, Pd, and Ni, whose reduction potentials are sufficiently compatible to allow controlled co-nucleation [61]. Nevertheless, when properly optimized, co-reduction remains a powerful and accessible strategy for nanocluster synthesis, offering direct access to ligand-stabilized architectures with tunable compositions. Its continued relevance lies in its simplicity and scalability, although advanced multimetallic systems increasingly require more sophisticated, stepwise, or photochemically assisted methodologies to overcome intrinsic thermodynamic constraints.

3.5. AI-Assisted synthesis

The structural diversity and complex formation pathways of metal NCs make their rational synthesis inherently challenging. To overcome these limitations, artificial intelligence (AI), including machine learning (ML) and deep learning, has emerged as a powerful tool for predicting cluster stability, guiding synthesis, and accelerating materials discovery [62]. By leveraging data generated from high-throughput density functional theory (DFT) calculations and experimental screening, AI enables efficient navigation of the vast chemical space associated with NCs [63]. Large-scale computational databases form the foundation of AI-driven cluster design. For instance, extensive DFT datasets covering gold nanoclusters with varying sizes, ligands, and dopants have enabled the development of predictive models for structural stability and electronic properties [64]. To address the computational cost of DFT, hybrid approaches combining genetic algorithms with machine-learned moment tensor potentials have been introduced [65]. These methods significantly accelerate structural searches while maintaining near-DFT accuracy, enabling the discovery of low-energy configurations inaccessible by conventional techniques. Machine learning has also proven effective in decoding structure–property relationships. In DNA-templated silver clusters, support vector machine models were used to correlate nucleic acid motifs with optical emission behavior, enabling the targeted synthesis of near-infrared emitters and expanding functional cluster libraries [66]. Such data-driven strategies allow predictive design even in chemically complex systems with limited experimental data.

Deep learning further enables accurate evaluation of cluster thermodynamics. Graph-based neural networks, such as DeepMoleNet, have demonstrated high precision in predicting formation energies of gold clusters, guiding the successful synthesis of previously unknown structures including Au_{10} and Au_{38} species [67]. These models significantly reduce

experimental trial-and-error by preselecting thermodynamically viable targets. AI has also transformed reaction optimization. Machine learning models trained on high-throughput synthesis data can correlate reagent ratios, ligands, and reducing agents with product yield and composition. Such approaches have enabled the discovery of complex alloy clusters and improved synthetic efficiency, outperforming conventional empirical optimization strategies [68]. In catalytic applications, neural networks trained on DFT data accurately predict hydrogen adsorption energies, guiding the design of highly active alloy nanoclusters for hydrogen evolution reactions [69]. Beyond prediction, AI plays an increasing role in real-time synthesis control. Neural-network-based monitoring systems can dynamically regulate reaction parameters, enabling precise control over nucleation, growth, and dispersion. These capabilities enhance reproducibility, reduce material waste, and facilitate scalable nanocluster production. Overall, AI-driven methodologies are redefining how metal nanoclusters are designed and synthesized. By integrating computation, data science, and experiment, AI enables predictive synthesis, accelerates discovery, and opens new pathways for the rational development of cluster-based photocatalysts and functional nanomaterials.

4. Key structural features of metal nanoclusters

A fundamental understanding of the photophysical and photochemical characteristics of metal nanoclusters (NCs), together with their photocatalytic mechanisms, is essential for the rational design of nanocluster-based photocatalysts and for moving beyond empirical trial-and-error approaches. As the dimensions of metal nanomaterials approach the Fermi wavelength of electrons, electronic confinement becomes significant, leading to discretization of energy levels [70]. Consequently, ultrasmall metal NCs display molecule-like electronic structures, characterized by well-defined HOMO–LUMO gaps, step-like absorption features, and excitonic excited-state dynamics. These properties are highly sensitive to nanocluster size, geometry, composition, heteroatom doping, NCs coupling, pore confinement, vacancies and defects, and surface ligands, offering multiple levers to tune their optical and catalytic behavior for photocatalysis and related applications.

4.1. Nanocluster size and shape

Although a strict quantitative correlation between nanocluster size and the HOMO–LUMO gap (E_g) does not exist, smaller NCs generally exhibit larger E_g values [71]. A widened energy gap corresponds to higher excited-state energies, which can facilitate the activation of kinetically inert substrates. In addition, the energy gap law predicts that nonradiative decay rates increase as E_g decreases [72, 73]; thus, enlarging E_g often leads to enhanced quantum yields and prolonged excited-state lifetimes. In contrast, larger nanoparticles possess quasi-continuous electronic bands ($E_g \approx 0$) and exhibit size-dependent light absorption properties, following classical scaling laws [74]. When metal clusters reach dimensions comparable to the de Broglie wavelength of Fermi electrons (~0.5 nm), discrete electronic states emerge, giving rise to multiple excitonic transitions rather than collective plasmonic behavior [75]. Notably, the optical gaps extracted from absorption onsets of NCs deviate from classical size-scaling relationships, underscoring their nonmetallic electronic nature. A representative example is provided by Xie *et al.*, who fabricated g-C_3N_4-supported Ag NCs (0.8–2.5 nm) using formamide as both solvent and reductant, without additional reducing agents [76]. Controlled thermal treatment transformed silver nanoparticles into atomically dispersed Ag NCs on the g-C_3N_4 surface (Fig. 3(A)). Owing to the enhanced atom utilization efficiency, the resulting Ag NCs/CN photocatalyst delivered a hydrogen evolution rate of 1439.77 μmol g^{-1} h^{-1} under visible light, 2.6-fold and 19.2-fold

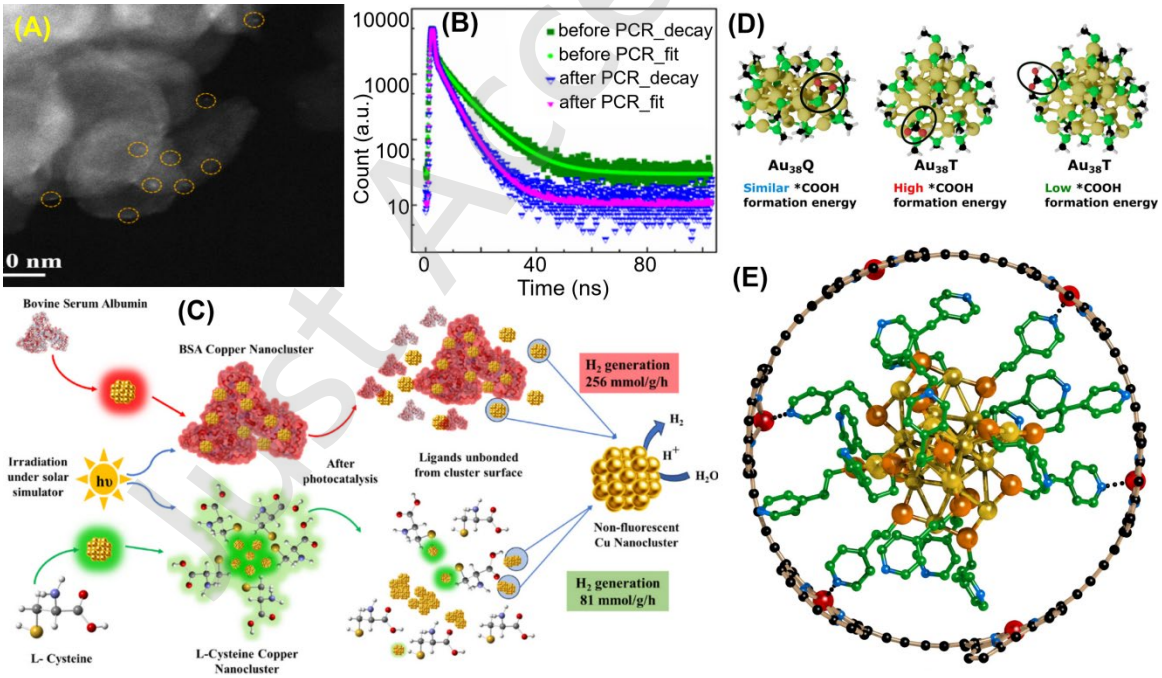

Figure 3. (A) STEM image of Ag nanoclusters/CN. (B) TRPL analysis, and (C) proposed hydrogen evolution mechanism for ligand/amino acid mediated copper nanoclusters. Reproduced with permission from Ref. [79], Elsevier B.V 2025. (D) $Au_{38}T$ shows smaller activation barrier and larger *COOH formation energy compared to $Au_{38}Q$. Reproduced with permission from Ref. [81], John Wiley & Sons 2022. (E) View of ***c***-P6*$Au_{25}PyET_{18}$-host-guest complex. Reproduced with permission from Ref. [20], John Wiley & Sons 2025.

higher than Ag NPs/CN and pristine g-C_3N_4, respectively. The superior activity was attributed to suppressed charge-carrier recombination and strong metal–support interactions, while the recyclability of formamide further reduced synthesis cost and complexity.

From a catalytic perspective, reducing cluster size increases the surface-to-volume ratio and maximizes exposure of active sites, which is beneficial for photocatalysis [77]. However, ultrasmall NCs often suffer from photoinduced instability and inefficient utilization of photogenerated charge carriers [78]. Surface ligands or surfactants play a critical role in stabilizing NCs, although their influence on photocatalytic pathways remains insufficiently understood. Busi *et al.* demonstrated that ultrasmall Cu NCs (<2 nm) exhibit strong light absorption and long carriers lifetimes (Fig. 3(B)), making them promising photocatalysts for water splitting [79]. In comparative studies, protein-stabilized BSA–Cu NCs achieved a hydrogen evolution yield of ~256 mmol g^{-1} after 12 h of solar illumination, substantially outperforming L-cysteine-stabilized Cu NCs (~86 mmol g^{-1}). The enhanced performance and higher solar-to-hydrogen efficiency (0.53% vs. 0.08%) were attributed to improved colloidal stability and prolonged excited-state lifetimes conferred by the protein ligands (Fig. 3(C)).

Beyond photocatalytic hydrogen evolution, metal NCs have emerged as structurally precise catalysts for photochemical CO_2 reduction. Compared with conventional nanoparticles, NCs possess atomically defined size, geometry, and surface chemistry, resulting in uniform active sites and highly reproducible catalytic behavior [80]. Their discrete electronic structures enable efficient charge transfer and selective stabilization of key reaction intermediates, thereby directing reaction pathways toward desired products while suppressing competing reactions. Li *et al.* showed that increasing the size of Au NCs (Au_{25} → Au_{38} → Au_{144}) enhanced the CO partial current density, whereas CO Faradaic efficiency remained largely size-independent, indicating that activity scales with surface-to-volume ratio while selectivity is governed by surface electronic structure [81]. Moreover, subtle geometric differences between Au_{38} isomers (Au_{38}Q vs. Au_{33}T) led to pronounced variations in CO_2 reduction reaction performance, with Au_{38}Q exhibiting superior CO selectivity due to more favorable *COOH formation energetics as revealed by DFT calculations (Fig. 3(D)).

An additional hallmark of metal NCs is the existence of "magic numbers," corresponding to specific atomic compositions that confer exceptional thermodynamic stability and distinct optical signatures [82]. Such clusters often display sharp absorption features and closed-shell electronic configurations, occupying deep minima on the potential energy landscape [83]. Understanding magic-number behavior not only provides insight into nonclassical nucleation and growth mechanisms but also enables atomic-level control over nanomaterial synthesis. A prototypical example is thiolate-protected $Au_{25}(SR)_{18}$, whose crystallographically resolved structure, an icosahedral Au_{13} core protected by six dimeric staple motifs, has served as a benchmark system for correlating atomic structure with optical and catalytic properties [84]. Detailed knowledge of such well-defined clusters continues to guide theoretical modeling and rational catalyst design. Collectively, these studies highlight that nanocluster size and shape profoundly influence electronic structure, excited-state dynamics, and catalytic behavior. When combined with precise control over ligands and atomic geometry, size-engineered metal NCs provide a versatile platform for advancing photocatalytic energy conversion and sustainable chemical transformations. Precise control over nanocluster size and shape thus provides a primary route to tailoring photocatalytic activity at the atomic level.

4.2. Core composition

While the size and geometric configuration of nanoclusters dictate quantum confinement and the distribution of surface active sites, the chemical identity of constituent atoms introduces an additional and equally critical degree of freedom**,** enabling modulation of electronic structure, adsorption energetics, and catalytic selectivity beyond purely morphological control [85]. Monometallic NCs already possess molecule-like electronic states with size-dependent HOMO–LUMO gaps, which favor visible-light harvesting, efficient charge separation, and multielectron transfer [86]. Noble metal NCs, especially Au NCs, are therefore widely explored as photocatalytic cocatalysts. For instance, thiolate-protected $Au_{25}(SR)_{18}$ deposited on g-C_3N_4 shows dramatically enhanced CO formation compared with Au nanoparticles, mainly due to suppressed hydrogen evolution and improved CO_2 activation [87]. The surface ligand environment plays a decisive role: hydrophobic ligands restrict water access, stabilize COOH* intermediates, and direct the reaction pathway toward CO_2 reduction. Beyond isolated clusters, hybrid systems combining Au_{25} with Ru or Ni terpyridine complexes enable efficient photoinduced charge transfer, achieving high Faradaic efficiencies and turnover frequencies in CO_2-to-CO conversion [88]. Host–guest assemblies, such as pyridinethiol-coated Au_{25} encapsulated in zinc–porphyrin nanorings (Fig. 3(E)), further amplify photogenerated reactive oxygen species and promote photocatalytic CO_2 reduction [20]. However, monometallic NCs have limited photocatalytic performance because they offer limited tunable electronic states and weaker light absorption, resulting in low performance and stability under operated conditions.

The evolution from monometallic NCs to bimetallic nanoclusters (BNCs) has opened new opportunities for tailoring structure–property relationships at the atomic scale. By integrating two different metals into a single cluster, BNCs exhibit cooperative electronic and geometric effects that are inaccessible in single-metal systems [89]. Relative to monometallic NCs, BNCs offer several advantages: (i) their electronic structures can be finely engineered by varying the type, number, or spatial position of heteroatoms [90], (ii) synergistic metal–metal interactions often lead to broadened light absorption and accelerated charge migration [91], and (iii) atomically precise structures enable direct correlation between composition, geometry, and photocatalytic behavior. These features make BNCs particularly attractive as model systems for elucidating structure–photoactivity relationships, something that is difficult to achieve with conventional nanoparticles. Introducing a second metal into Au or Ag NCs substantially enriches their structural diversity and functional performance. Among BNCs, Au–Ag systems are the most extensively studied owing to the similar atomic radii of Au and Ag (1.44 Å), which facilitates controlled substitution [92]. Ag doping subtly alters the electronic structure

of Au NCs, leading to tunable optical and catalytic properties while maintaining good stability and low toxicity [93, 94]. A prototypical example is $[Ag_{24}Au(SR)_{18}]^-$, where a single Au atom occupies the core of an Ag_{25} framework, with the precise atomic arrangement resolved by mass spectrometry and single-crystal X-ray diffraction [95]. Beyond Au–Ag clusters, Au–Cu BNCs such as Au_6Cu_6, $Au_{13}Cu_4$, and $Au_{52}Cu_{72}$ demonstrate how transition-metal incorporation reshapes both geometry and electronic structure [96]. The Au_xCu_{16-x} series highlights the sensitivity of cluster properties to single-atom substitution on the surface [97]. Even clusters with identical atomic frameworks, for example $[Au_{18}Cu_{32}(SPhCl)_{36}]^{2-}$ and $[Au_{18}Cu_{32}(SPhCl)_{36}]^{3-}$, can display markedly different physicochemical behaviors due to changes in electronic states and ligand orientations [98]. Such effects translate into improved selectivity in organic transformations and enhanced photo-to-electron conversion efficiencies, exemplified by $Au@Cu_{14}$ clusters with a quantum efficiency of 71.3% [99, 100].

Au–Pt BNCs further illustrate the power of bimetallic synergy. Pt incorporation into Au clusters (e.g., $PtAu_{24}$, Pt_2Au_{36}) significantly boosts hydrogen evolution activity by providing favorable hydrogen adsorption sites [101]. Structurally well-defined $Pt@Au_{12}$ clusters with icosahedral kernels also exhibit strong photoactivity in intramolecular [2+2] cycloaddition reactions under white light [102]. Although still less explored in photocatalysis, rational engineering of metal composition and surface ligands is expected to unlock the full potential of Au–Pt BNCs [103]. Pt-doped Ag NCs represent another important class of BNCs. Owing to the distinct electronic configuration of Pt relative to Ag, Pt incorporation allows more pronounced tuning of electronic structures compared with Au–Ag systems. A variety of Pt–Ag clusters (e.g., $PtAg_{20}$, $PtAg_{28}$, $PtAg_{42}$) stabilized by thiolates, phosphines, halides, or alkynes have been reported [104-107]. Notably, $PtAg_{24}(SR)_{18}$ can function as a near-infrared-absorbing triplet photosensitizer and cocatalyst, where Pt atoms regulate interfacial electron transfer processes [108]. Adjusting the Pt content provides a powerful handle to optimize light absorption and charge dynamics in these atomically precise photocatalysts. Monometallic NCs offer size-dependent, molecule-like electronic structures that are highly effective for light harvesting and selective photocatalysis. Bimetallic NCs go a step further by introducing synergistic metal–metal interactions, enabling finer control over geometry, electronic states, and charge transfer pathways. Overall, while monometallic NCs serve as excellent model photocatalysts, BNCs provide superior tunability and performance, making them more promising for advanced photocatalytic applications.

4.3. Surface Ligand

Beyond the intrinsic effects arising from mono- or multimetallic compositions, the interfacial chemistry defined by surface ligands plays a decisive role in governing nanocluster stability, charge accessibility, and interaction with reactants, thereby offering a powerful handle to tailor catalytic behavior without altering the metal core [109]. Surface ligands are indispensable components of metal NCs, governing not only their structural integrity but also their electronic configuration, excited-state dynamics, and catalytic behavior [110]. Beyond simple stabilization, ligands modulate metal–ligand charge transfer, redox characteristics, and photophysical processes by altering the electronic density of states at the cluster surface. Meanwhile, ligand steric bulk, rigidity, and interligand noncovalent interactions (such as π–π stacking, C–H, and H–F contacts) can suppress vibrational relaxation pathways, thereby enhancing photostability and catalytic durability. A representative example was reported by Zhu et al., who demonstrated that substituting phenylethanethiol ligands with 3,4-difluorothiophenol on Au_{25} clusters markedly improves photostability [111]. The resulting $[Au_{25}(F\text{-}Ph)_{18}]^-$ cluster benefits from a rigid ligand shell formed through cooperative interligand interactions, which stabilizes the excited triplet state. Under light irradiation, this cluster efficiently sensitizes triplet oxygen to singlet oxygen ($^1O_2$), enabling oxidative C–H functionalization of tetrahydroisoquinoline via an iminium-mediated pathway. Remarkably, the reaction proceeds under near-infrared excitation (850 nm), highlighting the advantage of NIR light penetration for scale-up. Comparative studies revealed that only $[Au_{25}(F\text{-}Ph)_{18}]^-$ preserved its structural integrity during catalysis, whereas Ag_{25} and $[Au_{25}(PET)_{18}]^-$ decomposed, underscoring the decisive role of ligand design. The same catalyst also displayed high efficiency in sulfide oxidation and β-ketoester transformations.

Peptide-based ligands provide an alternative strategy to simultaneously enhance stability and substrate recognition. Nakamura and Isozaki developed a dendritic ornithine peptide–protected cluster, $[Au_{25}(S\text{-}DOP)_{18}]^-$, which exhibits excellent photostability and efficient $^1O_2$ generation [112]. This cluster catalyzes the oxidative cyclization of tertiary amino alcohols through singlet-oxygen-mediated iminium formation followed by intramolecular nucleophilic trapping. Kinetic analyses revealed superior activity relative to $[Au_{25}(PET)_{18}]^-$, attributed to hydrogen-bonding interactions between peptide ligands and substrates, as confirmed by circular dichroism and NMR titration. Extending this concept, the same cluster was applied to photocatalytic C–H alkynylation of tertiary amines via a dual catalytic mechanism [113]. Here, the Au_{13} core acts as a photosensitizer for $^1O_2$ generation, while the $Au_2(S\text{-}DOP)_3$ staple motifs function as organometallic reaction sites. Ligand exchange with terminal alkynes generates reactive intermediates, further emphasizing the multifunctionality imparted by tailored ligand shells.

In NC–semiconductor hybrid photocatalysts, ligands play a critical role in mediating interfacial charge transfer. Because ligands form the direct electronic bridge between NCs and semiconductor surfaces, their conjugation and conductivity strongly influence carrier injection and recombination dynamics. Liu et al., systematically investigated Au_{25} clusters protected by

benzenethiol (BT), phenylethanethiol (PET), 2,4-dimethylbenzenethiol (DT), and 1-thionaphthol (TT) [114]. Despite nearly identical metal cores (Fig. 4(A)) and optical absorption profiles, TT- and DT-protected clusters exhibited enhanced electronic coupling with TiO_2 due to extended π-conjugation and hyperconjugation effects. When evaluated as photoanodes in photoelectrochemical cells, these clusters generated higher photosensitizer-normalized current densities (ja), which directly reflect intrinsic charge transfer efficiency rather than geometric electrode performance Surface ligand engineering

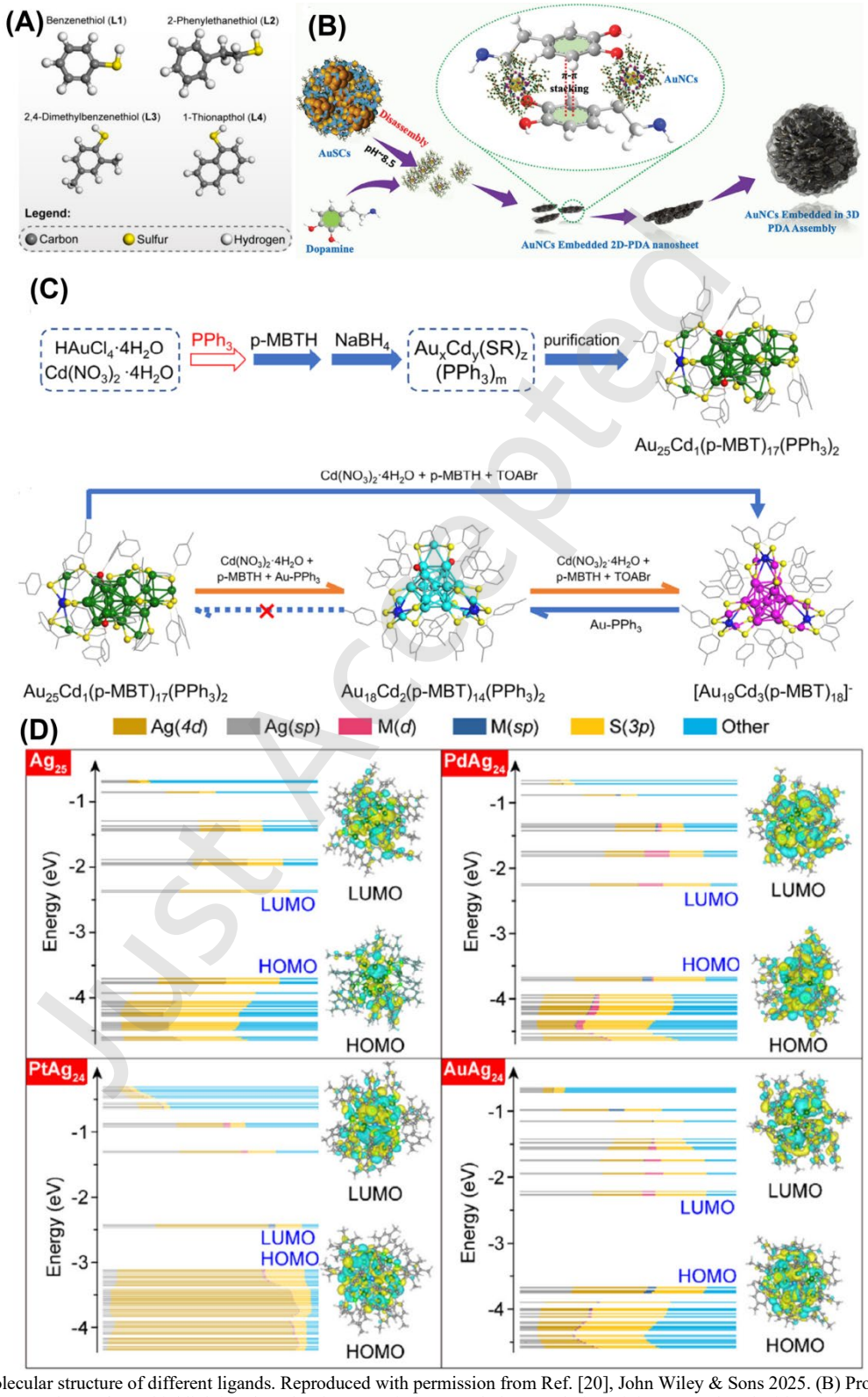

Figure 4. (A) Molecular structure of different ligands. Reproduced with permission from Ref. [20], John Wiley & Sons 2025. (B) Proposed mechanism of Au superclusters/PDA highlighting the role of Au NCs in increased photocatalytic activity. Reproduced with permission from Ref. [116], John Wiley & Sons 2025. (C) Synthesis process and conversion routes of different clusters. Reproduced with permission from Ref. [118], America Chemical Society 2024. (D) KS-orbitals and LUMO/HOMO orbitals of MAg_{24} nanoclusters. Reproduced with permission from Ref. [121], John Wiley & Sons 2023.

fundamentally dictates the stability, electronic structure, and catalytic behavior of metal nanoclusters. By controlling interfacial charge transfer, excited-state dynamics, and substrate interactions, tailored ligands unlock synergistic functions inaccessible to bare metal cores. Advanced ligand designs not only enhance photostability and efficiency but also enable hierarchical assembly and multifunctional catalysis.

Ligand engineering also enables higher-order organization of NCs. Jin et al. reported the atomically precise assembly of Au_{246}(p-MBT)$_{80}$ clusters into hierarchically ordered supercrystals [115]. The para-methylbenzenethiolate ligands self-organize on the curved NC surface, producing orientationally and translationally ordered lattices with unusually short interparticle separations. This work provided rare insight into ligand packing across atomic, molecular, and ensemble length scales, raising fundamental questions about how ligand symmetry and curvature govern self-assembly. Polymer–ligand complementarity further expands the design space for stable photocatalytic systems. Bera et al. grafted gold NCs and superclusters onto two-dimensional polydopamine supports, achieving enhanced photostability, reduced charge-transfer resistance, and significantly improved hydrogen evolution rates (Fig. 4(B)) [116]. Such hybrid architectures illustrate how ligand chemistry can be synergistically combined with functional supports to mitigate photodegradation. Despite these advances, ligand detachment and photochemical instability remain persistent challenges. Rational ligand design that balances strong binding, chemical robustness, and efficient electronic communication is therefore essential. In particular, the development of water-soluble and multifunctional ligands offers promising opportunities for uniform dispersion, enhanced stability, and sustainable photocatalytic applications such as water splitting. Continued innovation in surface ligand engineering will be pivotal for translating atomically precise NCs from model systems to practical, long-term photocatalytic technologies.

4.4. Heteroatom doping

While surface ligands regulate the external chemical environment of nanoclusters, heteroatom doping provides a complementary internal strategy, enabling direct manipulation of the electronic configuration and local atomic structure of the cluster framework itself [117]. Introducing heteroatoms into atomically precise metal NCs is a powerful strategy to modulate their electronic structures, photophysical behavior, and photocatalytic functions. Substitution with foreign metal atoms can alter optical gaps (E_g), excited-state dynamics, and charge-transfer pathways, thereby directly governing processes such as intersystem crossing (ISC), energy transfer (EnT), and single-electron transfer (SET). For instance, incorporation of Ir, Pt, or Rh into M@Au_{12} clusters was shown to enlarge Eg relative to Au_{13}, leading to enhanced quantum yields and prolonged excited-state lifetimes, which are favorable for singlet oxygen ($^1O_2$) generation. A representative example is provided by Wu et al. [118], who systematically investigated Cd-doped gold NCs—[$Au_{19}Cd_3$(p-MBT)$_{18}$]$^-$, $Au_{18}Cd_2$(p-MBT)$_{14}$(PPh_3)$_2$, and $Au_{25}Cd_1$(p-MBT)$_{17}$(PPh_3)$_2$—all featuring an icosahedral Au_{13} kernel with distinct shell structures. Synthesis process is shown in Fig. 4(C). These clusters exhibit optical gaps of 2.10, 1.94, and 1.92 eV, respectively, exceeding the thermodynamic threshold for $^1O_2$ generation. Notably, $Au_{25}Cd_1$ and $Au_{18}Cd_2$ display long-lived, oxygen-sensitive emissions (≈530 ns), characteristic of triplet-state phosphorescence, whereas $Au_{19}Cd_3$ shows a much shorter, oxygen-insensitive lifetime (≈40 ns), indicative of fluorescence. Importantly, increasing Cd content enlarges the singlet–triplet energy gap (ΔE_{ST}), which suppresses ISC and diminishes $^1O_2$ sensitization efficiency. The photocatalytic trends were validated through the $^1O_2$-mediated oxidation of secondary enaminones. Beyond peripheral doping, Li et al. reported a cobalt-centered icosahedral cluster, [$CoAu_{12}$(dppm)6]$^{2+}$, where the heteroatom occupies the core position [119]. Compared with [Au_{13}(dppm)$_6$]$^{5+}$, $CoAu_{12}$ exhibits superior photostability and markedly enhanced performance in visible-light-driven oxidative transformations involving $^1O_2$. Remarkably, $CoAu_{12}$ is also capable of generating superoxide radicals ($O_2^{\bullet-}$) via a SET pathway, enabling highly efficient green-light-driven oxidation of aldehydes to carboxylic acids with turnover numbers exceeding 18000.

Heteroatom effects are further amplified when NCs are integrated into hybrid photocatalytic systems. Wang et al. immobilized $M_1Ag_{24}(BT)_x$ (M = Ag, Pd, Pt, or Au) clusters onto UiO-66-NH_2 through electrostatic interactions [120]. Zeta potential measurements confirmed that negatively charged Mag_{24} clusters strongly interact with the positively charged MOF, forming Mag_{24}@UiO-66-NH_2 composites. These materials exhibit 5.6–6.4-fold enhancements in photocatalytic H_2 evolution relative to Ag nanoparticles or Ag_{25} clusters supported on the same framework. XPS analyses under dark and illuminated conditions revealed a Z-scheme charge-transfer mechanism between the NCs and the MOF, with $AuAg_{24}$@UiO-66-NH_2 achieving an apparent quantum efficiency of ~0.53% under 380 nm irradiation. In contrast, heteroatom doping can also be detrimental if energy-level alignment is unfavorable. For TiO_2-sensitized hydrogen evolution, all investigated NCs function as photosensitizers, yet doped clusters often show reduced activity [121]. XPS and UPS studies indicate staggered band alignment, where photoexcited electrons from higher unoccupied states (e.g., $LUMO^{+1}$) inject into the TiO_2 conduction band, while holes migrate to the NC HOMO. KS-orbitals and LUMO/HOMO orbitals of MAg_{24} nanoclusters achieved from DFT are shown in Fig. 4(D). Because heteroatom substitution shifts these frontier orbitals, Ag_{25} and $PtAg_{24}$ outperform $AuAg_{24}$ and $PdAg_{24}$. Similarly, Kurashige and co-workers [122] demonstrated that the spatial position of dopants is critical: Pd atoms located on the NC surface suppress water-splitting activity, whereas Pt atoms positioned at the NC–substrate interface significantly enhance performance.

Alloying Au clusters with Ag provides further insight into structure–property relationships. Qin et al. [123] synthesized $Au_8Ag_3(PPh_3)_7Cl_3$ clusters with precise Ag incorporation along the C_3 axis. Compared with Au_{11}, Ag doping dramatically reshapes the electronic structure, shifting emission from the near-infrared to the UV–visible region and improving photostability. These features translate into excellent activity for photocatalytic oxidation of benzylamine under light irradiation. Nevertheless, Liu et al. [121] showed that replacing the central atom of Ag_{25} with Pd, Pt, or Au leads to inferior photocatalytic behavior on TiO_2 due to energy-level mismatch, as corroborated by DFT calculations. These studies collectively emphasize that

heteroatom doping must be coupled with rational band engineering at the NC–semiconductor interface. Heteroatom doping enables atomic-level control over the electronic configuration, excited-state dynamics, and interfacial charge transfer of metal nanoclusters, offering a versatile handle to optimize photocatalytic reactions. While noble-metal dopants provide excellent activity and stability, incorporation of earth-abundant, non-noble metals is crucial for scalability and cost reduction. Among these, transition-metal dopants such as Co and Cd show particular promise by simultaneously tuning photophysics and reaction pathways, making them attractive candidates for large-scale solar-to-chemical energy conversion.

4.5. Cluster – semiconductor coupling

Coupling atomically precise metal NCs with semiconductor photocatalysts has emerged as a powerful strategy to overcome the intrinsic limitations of single-component systems, particularly inefficient charge separation and sluggish surface redox kinetics [125]. By judiciously integrating metal NCs as cocatalysts, both the interfacial electronic structure and reaction pathways of semiconductor photocatalysts can be fundamentally reprogrammed, leading to markedly enhanced photocatalytic performance. A wide range of metals have been explored in this context, spanning noble metals (Pt, Au, Ag, Pd) and earth-abundant alternatives (Cu, Bi, Ni). When metal NCs are immobilized on a semiconductor surface, TiO_2 being a prototypical example, the disparity between the semiconductor conduction band edge and the metal Fermi level drives spontaneous electron migration from the photoexcited semiconductor to the metal [126]. This interfacial charge redistribution establishes a Schottky junction, which selectively permits electron flow toward the metal cocatalyst while suppressing back transfer [127]. As a result, photogenerated electrons are efficiently harvested at the metal sites, prolonging carrier lifetimes and increasing the probability of surface redox reactions. The effectiveness of this electron-sink behavior is governed by the metal work function, with Pt widely recognized as a benchmark cocatalyst owing to its deep Fermi level and minimal overpotential for hydrogen evolution [128]. Progressive electron accumulation on the metal NCs shifts their Fermi level negatively, thereby thermodynamically favoring proton reduction during photocatalytic water splitting.

Beyond classical cocatalytic roles, certain metal NCs introduce additional light–matter interactions through localized surface plasmon resonance (LSPR) [129]. In plasmonic metals, collective oscillations of free electrons under light irradiation generate intense local electromagnetic fields and energetic “hot” carriers [130]. By tailoring particle morphology and size, strong absorption can be extended into the visible and near-infrared regions, substantially broadening the photoresponse of wide-band-gap semiconductors. Moreover, size-dependent electronic effects become increasingly pronounced at the nanocluster scale; smaller NCs often exhibit more negative effective Fermi levels, which accelerates interfacial proton reduction and enhances hydrogen evolution kinetics [131]. Recent studies illustrate how atomically precise NCs enable mechanistic control over photocatalytic reactions. Tian *et al.* anchored Au_{25} NCs onto BiOBr nanosheets, creating a composite with substantially improved CO_2 photoreduction activity [132]. The Au clusters promoted extended light absorption, efficient charge separation and facilitated proton-coupled electron transfer, while their anionic character strengthened CO_2 adsorption and activation. Density functional theory (DFT) calculations revealed that exposed Au sites lower the formation barriers for *COOH and *CO intermediates, resulting in nearly a threefold enhancement in CO generation (from 16.36 to 43.57 μmol g^{-1} h^{-1}). Silver nanoclusters provide another compelling example of structure–function synergy. Ag_{25} NCs, which uniquely combine molecule-like electronic discreteness with plasmonic features, exhibited almost quantitative selectivity toward methane during photocatalytic CO_2 reduction at elevated temperature (100 °C) [133]. DFT analysis confirmed favorable CO_2 adsorption energetics on Ag_{25}, while operando infrared spectroscopy identified a hydrogen-assisted multielectron reduction route involving formyl and formaldehyde intermediates that ultimately yield surface-bound CH_x species and methane. Complementing these findings, two polyoxometalate (POM)-protected silver clusters, $\{Ag_{27}(Si_2W_{18}O_{66})_3\}$ and $\{Ag_{24}(Si_2W_{18}O_{66})_3\}$, were synthesized via a solvothermal strategy using distinct organic ligands [134]. Single-crystal X-ray diffraction disclosed trefoil-like Ag_{24}^{14+} and Ag_{22}^{17+} cores stabilized by three C-shaped POM units, with delocalized valence electrons reinforcing argentophilic interactions. Ultrafast transient absorption spectroscopy verified rapid photoinduced charge transfer between the Ag cores and POM shells, and both clusters displayed selective CO_2-to-formic-acid conversion, representing the first example of CO_2 reduction activity in POM-stabilized Ag clusters.

Copper-based NCs further highlight the advantages of atomically defined cocatalysts, particularly for sustainable photocatalysis. Dong *et al.* reported a crystalline Cu–S–N cluster catalyst (Cu_6–NH) featuring protonated pyrimidine N–H groups that act as proximal proton relays [135]. This catalyst showed strong visible-light photoredox activity, excellent structural robustness, and near-unity selectivity toward CO formation. Integrated experimental and theoretical studies—including in situ DRIFTS and DFT calculations—demonstrated that the N–H functionalities significantly lower the energy barrier for *COOH formation, the rate-determining step, thereby accelerating CO_2 reduction. In parallel with conventional wide-band-gap oxides, emerging hybrid architectures underscore the versatility of NC–semiconductor coupling. Li *et al.* exploited reductive Ti vacancies in $Ti_{3-x}C_2T_\gamma$ MXene to construct a CdS/Au/MXene ternary system with a core–shell configuration [136]. Dual Schottky junctions formed at the CdS/Au and Au/MXene interfaces enabled cascade electron transfer, dramatically improving charge separation. Optimized composites achieved a hydrogen evolution rate of 5371 mmol g^{-1} h^{-1}, far surpassing bare CdS, with the apparent quantum efficiency increasing from 0.3% to 16.7% at 420 nm. In this system, Au NCs simultaneously functioned as photosensitizers and small-band-gap semiconductors, while the high conductivity of both Au and MXene facilitated rapid electron transport. Similarly, Wang *et al.* constructed a type-II photosystem by coupling TiO_2 with atomically precise $Ag_{44}(SR)_{30}$ NCs [124]. The hybrid photocatalyst delivered a hydrogen production rate of 7.4 mmol g^{-1} h^{-1}—an order of magnitude higher than pristine TiO_2—and maintained 83% of its activity after five cycles. Ultrafast transient absorption measurements revealed that Ag_{44} NCs act as visible-light absorbers and, under UV/vis

excitation, as small-band-gap semiconductors that promote charge separation and transport, thereby functioning as true cocatalysts rather than passive sensitizers.

Beyond fuel generation, NC–semiconductor heterostructures have demonstrated broad applicability in photocatalysis. Jin *et al.* employed Ag_{25} NCs for photo-driven CO_2 conversion with exclusive methane formation, while Au_{25} NCs integrated with TiO_2 nanocrystals enhanced visible-light-driven dye degradation by a factor of 1.6 [137]. In these systems, the narrow band gap of the NCs facilitated electron–hole separation across anatase and rutile TiO_2 phases, promoted the formation of reactive oxygen species such as •OH and singlet oxygen, and reinforced degradation pathways. Related Au NCs/TiO_2 nanotube heterostructures have been successfully applied in pollutant degradation, nitroarene reduction, and photocatalytic water splitting, underscoring the generality of this coupling strategy. Hence, cluster–semiconductor coupling offers a multifaceted approach to enhancing photocatalytic performance by simultaneously improving light harvesting, charge separation, and surface reaction kinetics. Atomically precise metal NCs enable fine control over interfacial energetics, active-site structure, and reaction pathways that are inaccessible in conventional nanoparticle systems. The integration of cocatalytic, plasmonic, and semiconductor-like functions within a single NC component maximizes catalytic efficiency while reducing material usage. Continued development of well-defined NC–semiconductor architectures is therefore essential for advancing solar-driven fuel production and CO_2 conversion technologies.

4.6. Pore confinement engineering

While cluster–semiconductor coupling governs interfacial charge separation and transport, spatial confinement within porous frameworks such as COFs and MOFs introduces an additional structural dimension**,** enabling precise control over cluster dispersion, accessibility, and microenvironmental effects [138]. Atomic-level control over catalytic environments is a central goal in photocatalysis and is well represented by metal NCs and reticular porous solids such as MOFs and COFs [139]. Metal NCs, composed of only a limited number of atoms, exhibit molecule-like electronic structures and pronounced size-dependent effects, enabling precise regulation of active sites and reaction energetics. Their adjustable nuclearity, composition, and surface coordination provide a powerful means to modulate catalytic pathways and selectivity [140]. However, their intrinsic instability, propensity to agglomerate, and weak interaction with conventional supports restrict their durability under catalytic conditions. Reticular frameworks offer a complementary strategy by providing crystalline, permanently porous matrices with programmable chemical environments [141]. Through rational selection of metal nodes and organic building units, MOFs and COFs allow systematic control over pore geometry, functionality, and spatial distribution of catalytic centers. MOFs benefit from diverse metal coordination motifs that directly participate in catalytic activation, whereas COFs leverage rigid covalent backbones and extended π-systems to enhance light absorption and charge migration [142]. Despite these advantages, limitations related to electrical conductivity, structural robustness, and complex product formation remain. Although NCs and reticular frameworks differ fundamentally in structural dimensionality, both embody the principle of precision catalysis through deliberate control of active-site structure and electronic properties [143]. Embedding atomically defined NCs within the confined pores of MOFs or COFs integrates the merits of both systems, offering a coherent platform to stabilize reactive species, tailor local reaction environments, and elucidate structure–activity correlations. This pore-confined hybrid approach represents a promising direction for advancing photocatalytic material design.

Zirconium- and transition-metal-based MOFs have become an adaptable scaffold for photocatalytic CO_2 reduction, as their robust frameworks permit precise regulation of pore chemistry, interfacial structure, and light–matter interactions [144]. Beyond intrinsic porosity and stability, catalytic performance is strongly dictated by the size, dispersion, and coordination environment of incorporated metal nanoclusters, which govern charge separation, adsorption strength, and reaction selectivity [145]. Through deliberate control of metal–ligand interactions, defect density, and cluster–framework coupling, MOF-based systems have been steered toward diverse reduction products, including CO, formate, hydrocarbons, and alcohols. For CO-selective pathways, tuning nanocluster environments within MOFs has proven particularly effective. Wang *et al.* showed that linker- and cluster-level defects in UiO-66-NH_2 reshape local electronic structures by adjusting light absorption and ligand-to-metal charge transfer energies, with missing-linker defects delivering a 2.2-fold enhancement in CO formation relative to missing-cluster analogues [146]. In another study, Li *et al.* integrated Pt nanoclusters into a Ni-MOF, where the complementary roles of small Pt clusters for H_2 activation and open Ni sites for CO_2 adsorption enabled efficient long-wavelength activity, achieving 9.57% CO_2 conversion at 940 nm and promoting CO and CH_4 formation through hydrogen spillover (Fig. 5(A)) [147]. Size-dependent accessibility of active sites and interfacial synergy were central to this performance. Fang *et al.* further demonstrated that dispersing UiO-66 in a soluble form preserves framework integrity while maximizing exposure of active domains, leading to a CO evolution rate of 30.6 μmol h^{-1} from only 5.0 mg of catalyst—approximately 1.5 times higher than the insoluble counterpart [148]. Collectively, these studies highlight that nanocluster size, distribution, and confinement within MOF architectures critically influence photocatalytic CO_2 reduction reaction. Rational modulation of these parameters provides a viable route to optimize charge transfer and reaction kinetics, underscoring the importance of cluster-level engineering in next-generation MOF-based photocatalysts.

The ultrasmall dimensions of metal NCs impart high densities of accessible active sites and favorable quantum effects, yet these same features often compromise structural robustness under photocatalytic conditions [149]. Porous hosts provide an effective route to regulate NC size, spatial distribution, and interfacial interactions, thereby mitigating sintering and deactivation [150]. Among them, MOFs are particularly attractive because their chemically programmable architectures enable deliberate positioning and immobilization of NCs at the molecular level. A representative example was reported by Yao *et al.*, who anchored Au_{25}(L-Cys)$_{18}$ NCs within UiO-66-NH_2 through the formation of covalent amide linkages between the cluster ligands and framework amino groups [151]. This chemically bonded configuration markedly outperformed physically blended UiO-

66-NH_2/$Au_{25}(PET)_{18}$ systems, highlighting the importance of controlled cluster–support coupling. The covalent hybrid delivered a hydrogen evolution rate approximately 90 times higher than bare UiO-66-NH_2 and maintained its activity over repeated cycles, whereas the mechanically mixed analogue suffered rapid performance decay. Such improvements were attributed to strengthened metal–support interactions that stabilize the cluster size and geometry, promote interfacial charge transfer, and suppress carrier recombination. This example underscores how precise confinement and fixation of NCs within MOFs can preserve size- and shape-dependent reactivity while simultaneously enhancing durability, reinforcing the critical role of cluster-scale engineering in photocatalyst design.

Beyond stabilizing nanoclusters within porous hosts, an emerging strategy is to directly integrate atomically precise clusters as structural nodes, thereby translating their intrinsic size- and geometry-dependent properties into long-range ordered frameworks. Using this concept, Xu *et al.* synthesized a well-defined copper nanocluster, $Cu_8(SN)_4(tBuS)_4$ (SN = 4-(4-pyridinyl)thiazole-2-thiol), and employed it as a metal node to construct a Cu-based MOF [152]. In this design, the SN ligand functions as a Janus linker: the thiolate group stabilizes the Cu_8 core, while the pyridyl moiety directs framework formation, thereby preserving the cluster size and geometry within an ordered porous lattice. The resulting Cu-MOF exhibited efficient photocatalytic hydrogen evolution when operated with fluorescein as a photosensitizer and triethylamine as a sacrificial donor. Importantly, the framework retained its activity over multiple cycles, indicating that incorporation into a crystalline network effectively suppresses cluster degradation. Transient photocurrent measurements revealed a pronounced enhancement upon addition of fluorescein, confirming rapid electron injection into the Cu-MOF and efficient migration of photogenerated charges. Relative to isolated $Cu_8(SN)_4(tBuS)_4$ units, the periodic and porous architecture of the MOF enables improved charge transport and utilization of the size-defined clusters, leading to superior photocatalytic performance.

Precisely engineered organic frameworks provide an important reference point for evaluating the role of nanocluster size and interfacial architecture in hybrid photocatalysts. Fu *et al.* reported a metal-free azine-linked COF (N3-COF) capable of driving CO_2 reduction to methanol using water as the sole reductant under visible light, without sacrificial agents [153]. The catalyst delivered a methanol yield of 13.7 μmol g^{-1} over 24 h and maintained appreciable activity even at 1% CO_2 concentration. Its crystallinity and performance were preserved over multiple cycles, underscoring the intrinsic robustness of the ordered COF backbone. Compared with g-C_3N_4 under similar conditions, azine-linked COFs exhibited markedly higher activity, establishing them as efficient metal-free photocatalysts for solar fuel generation. Building on this platform, Ning *et al.* coupled N3-COF with MoS_2 nanodomains to form a hybrid system that leverages size- and interface-dependent charge transfer effects [154]. The introduction of MoS_2, with well-defined nanoscale dimensions, enabled efficient CO_2 reduction even in the presence of oxygen. At an O_2 concentration of 20%, comparable to ambient air, the hybrid achieved a CO evolution rate of 28 μmol g^{-1} h^{-1}, exceeding that obtained under oxygen-free conditions. These studies highlight how integrating COFs with nanoscale cocatalysts of controlled size and morphology can unlock new reaction environments and enhance photocatalytic efficiency, even in metal-free or low-metal systems.

4.7. Vacancies and defects

Point defects, particularly vacancies, are central to tailoring the electronic structure and catalytic behavior of supported metal clusters. Beyond serving as anchoring sites, such defects can modulate charge redistribution at the metal–support interface, thereby promoting reactant activation. A representative example was reported by Wei *et al.* [155], who showed that oxygen-vacancy–rich TiO_2 profoundly alters the behavior of supported Pt nanoclusters. In their system, oxygen vacancies induce an unusual dual effect, namely reversed electron transfer from the oxide to Pt and accelerated hydrogen spillover, which together markedly enhance hydrogen evolution kinetics. Spectroscopic and theoretical analyses (XPS, PDOS calculations, DFT, and in situ Raman spectroscopy) confirmed that the presence of oxygen vacancies renders Pt electron-rich, modifying its adsorption energetics. Simultaneously, the defective TiO_2 surface facilitates hydrogen migration from Pt to the support, further accelerating reaction turnover. As a result, VO-rich Pt/TiO_2 exhibits a mass activity 16.7 times higher than that of VO-poor Pt/TiO_2 and 58.8 times greater than commercial Pt/C. This study highlights how deliberate defect engineering in supports can regulate interfacial charge transfer and reaction pathways, offering a powerful strategy for designing high-performance hydrogen evolution catalysts through precise control of vacancy chemistry.

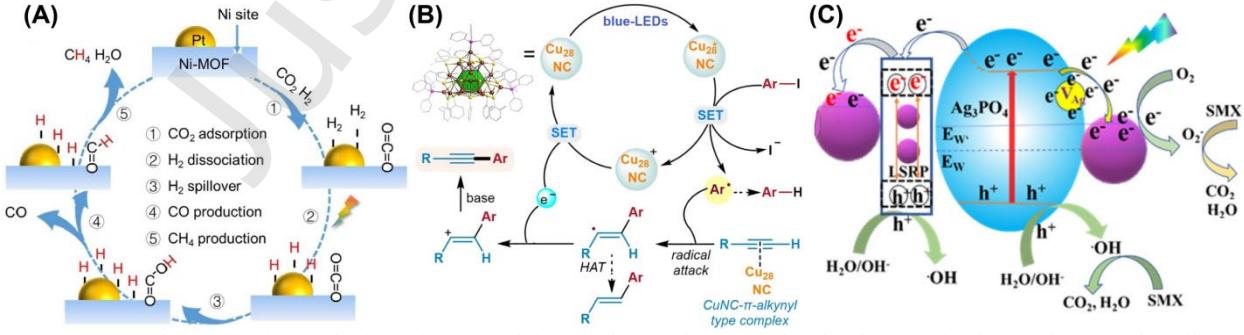

Figure 5. (A) Proposed CO_2 reduction mechanism using Pt NCs/Ni-MOF photocatalyst. Reproduced with permission from Ref. [147], John Wiley & Sons 2023. (B) Proposed mechanism for increased photocatalytic performance. Reproduced with permission from Ref. [156], John Wiley & Sons 2023. (C) Charge separation and migration mechanism of Ag/Ag_3PO_4–V_{Ag}. Reproduced with permission from Ref. [157], Elsevier B.V 2023.

Defect engineering at the atomic scale has emerged as an effective strategy to tailor the electronic configuration, surface reactivity, and light–matter interaction of metal nanoclusters. In

particular, well-defined vacancies can serve as catalytically active centers while simultaneously modulating charge transport and adsorption behavior, making them highly attractive for photocatalytic applications. In this context, Nematulloev *et al.* reported a gram-scale, one-pot synthesis of defective $[Cu_{28}H_{10}(C_7H_7S)_{18}(TPP)_3]$ nanoclusters (Cu_{28}), in which a surface vacancy was precisely identified at one vertex of the tetrahedral framework [156]. Structural and optical analyses revealed that this atomic-level defect plays a decisive role in governing the catalytic properties. The defective Cu_{28} clusters exhibited high activity and selectivity toward visible-light-driven C–C cross-coupling reactions (Fig. 5(B)). Beyond their catalytic performance, these atomically defined defective clusters provide an ideal platform for correlating structure–property relationships, offering valuable insight into how surface defects in nanoclusters and nanoparticles govern catalytic behavior. A complementary example was reported by Liu *et al.*, who synthesized Ag/Ag_3PO_4 composites containing Ag vacancies (V_{Ag}) via a facile in situ reduction strategy [157]. The introduction of Ag nanoclusters not only suppressed the intrinsic photocorrosion of Ag_3PO_4 but also induced a localized surface plasmon resonance effect, enhancing light absorption and charge separation. Meanwhile, V_{Ag} sites strengthened H_2O adsorption and promoted electron accumulation (Fig. 5(C)), collectively accelerating photocatalytic reactions. As a result, Ag/Ag_3PO_4–V_{Ag} achieved complete degradation of sulfamethoxazole (20 mg L^{-1}) within 15 min, with a reaction rate constant far exceeding those of pristine Ag_3PO_4 and Ag/Ag_3PO_4. Notably, the catalyst maintained high activity in natural water matrices, highlighting its practical potential. Together, these studies demonstrate that precisely engineered vacancies in metal nanoclusters and cluster-modified semiconductors are powerful tools for regulating charge dynamics and catalytic reactivity, offering a rational pathway toward high-performance photocatalysts.

Defect engineering combined with rational cluster loading offers a powerful route to simultaneously regulate charge dynamics and surface reaction pathways in photocatalysts. By tailoring the electronic structure of the host and introducing catalytically active nanoclusters, both bulk carrier behavior and interfacial kinetics can be synergistically optimized. Along this line, Hou *et al.* developed a stepwise strategy to address carrier recombination and sluggish surface reactions in polymeric carbon nitride (CN) [158]. Nitrogen vacancies were first introduced to construct defect-rich CN (N_vCN), which effectively modulated the electronic structure and promoted charge separation. Subsequently, CoOx nanoclusters with strong oxygen affinity were anchored onto N_vCN, serving as highly active sites for interfacial reactions. Experimental results and theoretical calculations revealed that the vacancies facilitated interfacial charge transfer, while CoO_x clusters enhanced O_2 adsorption and lowered the energy barrier for *OOH formation, thereby accelerating the two-electron oxygen reduction pathway toward H_2O_2. As a result, the optimized CoO_x–N_vCN system delivered a H_2O_2 production rate of 244.8 μmol L^{-1} h^{-1}, together with an apparent quantum efficiency of 5.73% at 420 nm and a solar-to-chemical conversion efficiency of 0.47%, outperforming most reported CN-based photocatalysts. This work underscores the effectiveness of combining vacancy engineering with cluster modification, providing a general design principle for constructing highly efficient photocatalysts with enhanced charge utilization and surface reactivity.

5. Applications

Atomically precise metal NCs have attracted growing attention as photocatalysts because their optoelectronic properties, redox behavior, and stability can be deliberately tailored while avoiding the toxicity concerns often associated with conventional metals. Their uniform nuclearity, large fraction of exposed surface atoms, flexible structural motifs, and abundant low-coordination sites make NCs ideal model systems for correlating catalytic function with atomic structure. In contrast to bulk metals, NCs exhibit discrete, molecule-like electronic states, and subtle changes in cluster size, shape, or composition can induce pronounced shifts in energy levels and reactivity. The emergence of nonmetallic characteristics at this ultrasmall scale further differentiates their catalytic behavior from that of larger nanoparticles. From a photocatalytic perspective, these size- and shape-dependent electronic features directly govern light harvesting, charge excitation, and carrier separation, which are central to reaction efficiency. Consequently, NC-based architectures have become an important platform for designing high-performance photocatalysts with tunable activity and selectivity. This section surveys representative cluster-integrated systems across key photocatalytic transformations, including hydrogen evolution, carbon dioxide reduction, organic synthesis, pollutant degradation, hydrogen peroxide generation, and nitrogen fixation, with particular emphasis on how cluster size and geometry dictate interfacial charge dynamics and reaction pathways.

5.1. CO_2 reduction

Photocatalytic CO_2 reduction offers a sustainable pathway for transforming CO_2 into value-added chemicals such as CO, formate, methane, methanol, and higher-order carbon products using solar energy [159]. Despite its conceptual appeal and mild reaction conditions, the process remains kinetically and thermodynamically challenging due to the linear geometry and high bond strength of CO_2, as well as competition from the hydrogen evolution reaction in aqueous systems [160]. Effective activation typically requires stabilization of key surface-bound intermediates, while controlling product selectivity, particularly toward multicarbon products, demands precise regulation of active-site structure and electronic properties [161]. MOFs provide a tunable scaffold for addressing these challenges, as both metal nodes and organic linkers can be engineered to host size-defined metal nanoclusters and modulate their local environments. In a seminal study, Jiang *et al.* introduced an N-heterocyclic carbene (NHC)-assisted nucleation strategy to immobilize ultrasmall Au nanoclusters within UiO-68-NHC, achieving uniform dispersion and strong covalent anchoring for the first time [29]. The NHC linkers suppress cluster aggregation, in stark contrast to amine- or imidazolium-functionalized analogues, which yield large Au particles on external surfaces. The confined Au nanoclusters exhibit pronounced local surface plasmon resonance effects, resulting in a CO evolution rate of 57.6 mmol g^{-1} h^{-1}, over four times higher than that of UiO-68-NH_2/Au composites lacking NHC stabilization. This system demonstrates how precise control over nanocluster size, dispersion, and interfacial bonding within MOFs directly translates into enhanced

activity, durability, and photostability in CO_2 reduction. More broadly, it establishes metal–NHC motifs as a versatile platform for probing structure–reactivity relationships of ultrasmall clusters in heterogeneous photocatalysis and for extending nanocluster design principles into ordered porous solids.

The fabrication of heterogeneous catalysts typically begins with the precise synthesis of metal NCs using protective ligands, followed by their immobilization onto a support. While ligands ensure atomic precision, they often hinder catalytic activity by blocking reactant access and modifying the electronic structure of the NCs. Consequently, selective ligand removal, preserving cluster nuclearity, is critical for maintaining both activity and stability. Kawawaki *et al.* investigated the ligand desorption behavior of 2-phenylethanethiolate (PET)-protected Au_{25} NCs ($[Au_{25}(PET)_{18}]$) supported on metal oxides (Fig. 6(A)) [30]. Using multiple experimental techniques, they elucidated a multistep process: dissociation of ligands from the Au NC surface, adsorption of byproducts onto the support, and eventual desorption as volatile species such as styrene or CO_2. For Au_{25}(PET, p-MBA)$_{18}$/$BaLa_4Ti_4O_{15}$, calcination at 300 °C removed most ligands while preserving cluster size, though trace organics and S oxides remained even at 500 °C (Fig. 6(B)). In systems incorporating a Cr_2O_3 interlayer, immediate light irradiation post-calcination was necessary to form a protective layer, preventing cluster aggregation. When irradiation followed within minutes, Au NCs were stabilized at ~1.5 nm, enabling long-term high activity in water splitting. This work underscores the importance of controlling cluster size, shape, and interfacial chemistry in heterogeneous photocatalysts. By carefully balancing ligand removal, support interactions, and protective coatings, it is possible to preserve the structural integrity of ultrasmall NCs, maximizing their catalytic efficiency and durability.

The design of structurally novel silver clusters has increasingly leveraged polyoxometalates (POMs) as multifunctional components. POMs can act as anionic templates, form intercluster salts with cationic Ag clusters, or serve as multidentate ligands stabilizing lacunary clusters. Beyond structural roles, the redox-active nature of POMs enables strong electronic coupling with Ag clusters, potentially enhancing photocatalytic CO_2 reduction through synergistic interactions. Feng *et al.* synthesized two atomically precise POM-stabilized Ag clusters, $\{Ag_{27}(Si_2W_{18}O_{66})_3\}$ and $\{Ag_{24}(Si_2W_{18}O_{66})_3\}$, via a one-pot solvothermal method using distinct organic ligands (Fig. 6(C)) [31]. Single-crystal X-ray analysis revealed trefoil-propeller-shaped Ag cores stabilized by three C-shaped $\{Si_2W_{18}O_{66}\}$ units. Delocalized valence electrons (~10 per cluster) induce strong argentophilic interactions, while femtosecond and nanosecond transient absorption spectroscopy confirmed rapid charge transfer between the POM ligands and the Ag cores. Photocatalytic tests demonstrated highly selective CO_2-to-formate conversion, placing these clusters among the most efficient systems reported. This work highlights how careful control of cluster nuclearity, geometry, and POM interface can tune electronic structure, facilitate ultrafast charge dynamics, and enhance photocatalytic performance. Moreover, it establishes a versatile strategy for expanding the family of atomically precise Ag clusters and exploring their applications in solar-driven CO_2 reduction and carbon-neutral energy conversion.

Copper(I) nanoclusters (Cu NCs), owing to their atomic precision, serve as ideal platforms for probing structure–property relationships and guiding rational design in photocatalysis. The synthesis of high-nuclear Cu(I) NCs often relies on templating strategies, including the use of polyoxomolybdates, which govern both cluster nuclearity and surface architecture. Fang *et al.* employed $(NH_4)_2Mo_4O_{13}$ or $(NH_4)_6Mo_7O_{24}$ as polyoxomolybdate templates, modulated reaction acidity, and introduced diphenylmethylsilane as a mild reducing agent to construct five atomically precise Mo–Cu NCs: $Mo_{14}Cu_{42}$, Mo_5Cu_{36}, $Mo_{16}Cu_{36}$-1, $Mo_{16}Cu_{36}$-2, and $Mo_{22}Cu_{30}$ [41]. Single-crystal X-ray diffraction revealed that the polymerization state of the molybdate templates dictated the encapsulation pattern of the Cu shell, thereby tuning the number and accessibility of catalytic sites. These Mo–Cu NCs exhibited remarkable activity and selectivity in photocatalytic CO_2 reduction. Without sacrificial agents or photosensitizers, $Mo_{30}Cu_{22}$, $Mo_{14}Cu_{42}$, and $Mo_{16}Cu_{36}$-1 achieved >99.9% selectivity for CO formation under Xe irradiation, with rates of 160.8, 97.8, and 133.6 μmol g^{-1} h^{-1}, respectively, surpassing that of Mo_5Cu_{36}. In the presence of a photosensitizer and sacrificial agent, $Mo_{22}Cu_{30}$ and $Mo_{16}Cu_{36}$-1 reached CO production rates of 7370.8 and 5672.1 μmol g^{-1} h^{-1} with selectivities of 90.6% and 90.3%. Structural analyses confirmed exposed Mo–O–Cu sites on the cluster surfaces, facilitating synergistic activation of CO_2, while in situ DRIFTS identified *COOH as a key reaction intermediate. This study underscores the importance of cluster size, shape, and template-mediated surface engineering in defining active-site accessibility and optimizing photocatalytic performance, providing a blueprint for designing next-generation Cu NC–based CO_2 reduction catalysts.

The encapsulation of high-nuclearity cobalt clusters presents a compelling platform for exploring structure–property relationships due to their unique geometries and rich catalytic, electronic, and magnetic features. Guo *et al.* reported a series of atomically precise core–shell Co–PONb clusters with diverse shapes and nuclearities, ranging from the 50-nuclearity octahedral $Co_{12}Nb_{38}$ to 54-nuclearity basket-shaped $Co_{20}Nb_{34}$, 62-nuclearity sphere-shaped $Co_{26}Nb_{36}$, and 87-nuclearity barrel-shaped $Co_{33}Nb_{54}$ [58]. These assemblies were achieved through judicious use of $NaBO_3$ as an oxidant and phosphates to regulate reaction basicity, demonstrating a versatile strategy for constructing high-

nuclearity TM–PONb core–shell clusters.Notably, $Co_{26}Nb_{36}$ and $Co_{33}Nb_{54}$ represent the largest Co-PONb clusters reported to date, incorporating the highest-nuclearity cobalt cores within polyoxometalates. These clusters exhibit exceptional visible-light-driven photocatalytic CO_2 reduction, highlighting their potential as molecular models for cluster-based photocatalysis. The well-defined inorganic cores provide precise atomic and geometric information, serving as molecular analogues for amorphous core–shell metal oxide nanoparticles. In particular, the encapsulated cobalt oxide cores offer scalable models for investigating the electronic and magnetic properties of bulk cubic-spinel Co_3O_4. This work underscores how controlling cluster nuclearity and shape can guide the design of core–shell materials with tailored properties, opening avenues for applications in catalysis, electronics, photonics, and magnetism.

Optimizing photocatalytic CO_2 reduction toward C_2 products requires catalysts that combine high adsorption capacity for CO_2 and H_2O, electron-rich surface regions, and synergistic interactions among multiple active sites. Duan *et al.* developed a tandem photocatalyst, Pd_{SA+NCs}/CeO_2, integrating Pd single atoms (Pd_{SA}), Pd nanoclusters (Pd_{NCs}), and CeO_2 with abundant oxygen vacancies (Ov), achieving a C_2H_6 production rate of 14.7 μmol g^{-1} h^{-1} and an electron consumption rate of 206.3 μmol g^{-1} h^{-1}, which was 17.2 and 11.3 times higher than Pd_{SA}/CeO_2 and Pd_{NCs}/CeO_2, respectively [109]. Femtosecond transient absorption spectroscopy (fs-TAS) and density functional theory (DFT) calculations (Fig. 6(D)) revealed that Ov on CeO_2 act as CO_2 adsorption sites and facilitate electron-driven activation. Pd_{SA} promotes water activation, generating high-energy H* species, whereas Pd_{NCs} regulate CO* intermediate binding and create electron-rich "islands" on the surface through hybridized orbital

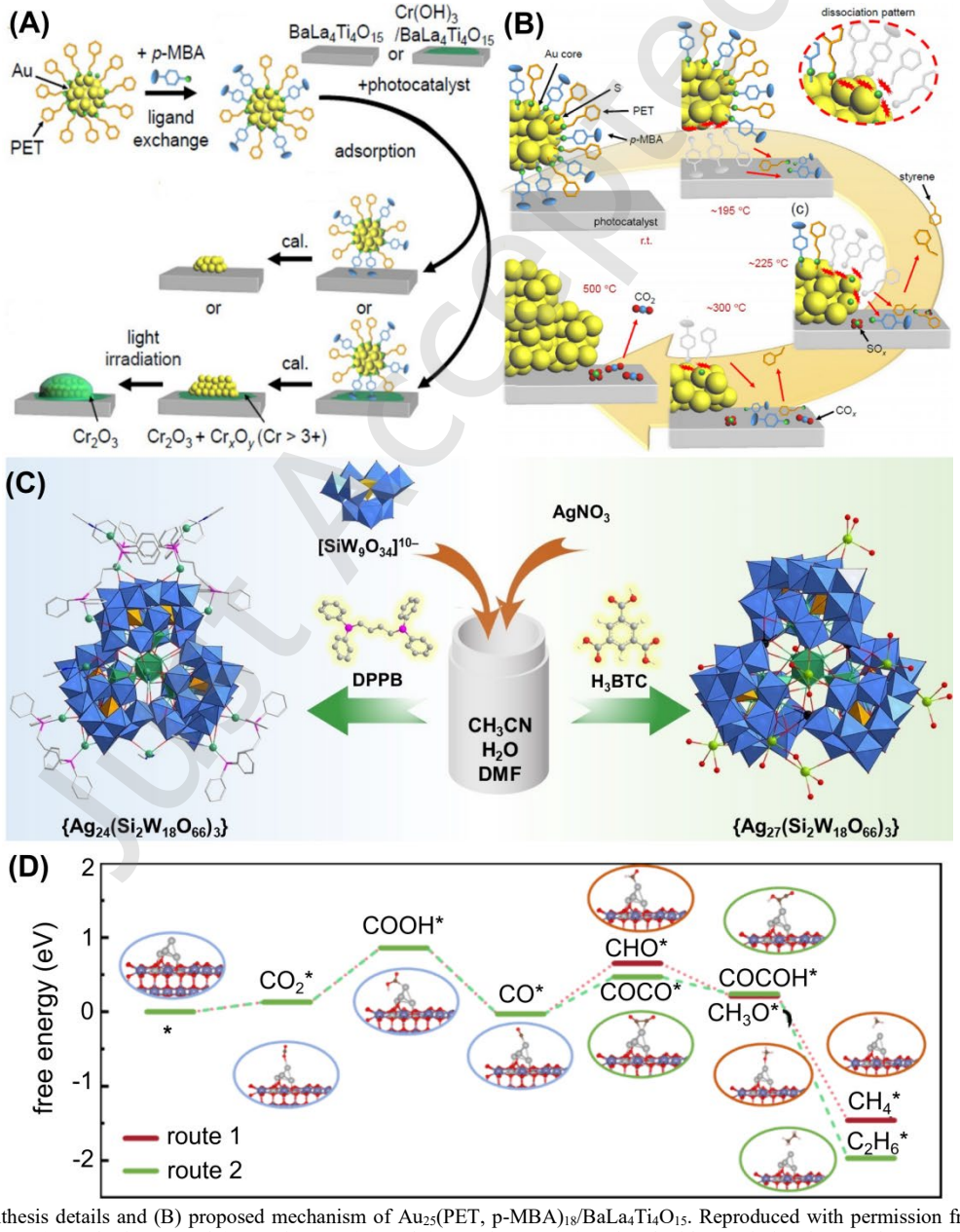

Figure 6. (A) Synthesis details and (B) proposed mechanism of Au_{25}(PET, p-MBA)$_{18}$/$BaLa_4Ti_4O_{15}$. Reproduced with permission from Ref. 30, John Wiley & Sons 2021. (C) Synthesis route of $\{Ag_{27}(Si_2W_{18}O_{66})_3\}$ and $\{Ag_{24}(Si_2W_{18}O_{66})_3\}$. Printed with permission from Ref. [31], John Wiley & Sons 2024. (D) free energy illustration for CO_2 reduction over Pd_{SA+NCs}/CeO_2. Reproduced with permission from Ref. [109], America Chemical Society 2025.

overlap, enhancing CO* coupling and CO–CO* protonation. The combined effect of these three synergistic centers significantly improves both the selectivity and activity toward C_2H_6 formation. This work demonstrates that integrating noble metals at different scales can strategically reconstruct the electron spatial density on a catalyst surface, thereby promoting critical coupling steps in CO_2 reduction. It provides a conceptual framework for designing multiscale, multi-active-site photocatalysts that achieve high efficiency and selectivity in complex carbon-conversion reactions.

5.2. H_2 evolution

Green hydrogen (H_2), owing to its high energy density and near-zero carbon footprint, has emerged as a promising alternative to fossil fuels, offering a sustainable pathway to address energy crises and climate change [22]. Among various H_2 production strategies, solar-driven seawater splitting stands out for its potential to harness abundant solar energy. Realizing efficient solar-to-hydrogen conversion necessitates semiconductor photocatalysts with suitable band gaps, efficient charge-carrier mobility, and rapid surface reaction kinetics [23]. The integration of cocatalysts has proven an effective strategy to enhance surface kinetics by providing active sites with lower overpotentials, selectively trapping photogenerated charges, and suppressing recombination [26]. Cocatalyst design has therefore become a central focus in improving photocatalytic performance. Notably, Jiang et al. anchored Ir nanoclusters onto a mesoporous TiO_2 matrix via a two-step method (Fig. 7(A)) [42]. These nanoclusters are homogeneously dispersed across the (101) facets of 1% Ir/TiO_2, which act as electron sinks, creating a negatively charged surface layer that selectively adsorbs H^+ while repelling Cl^-, thus mitigating salt-induced corrosion. Concurrent electron transfer from Ir to TiO_2 generates Ti^{3+} defects, elevating surface energy and providing additional active sites to accelerate H_2 evolution. Optical properties are significantly enhanced after Ir loading, particularly in the visible and near-infrared regions. The local surface plasmon resonance (LSPR) of Ir nanoclusters under illumination produces hot electrons, which are injected into the TiO_2 conduction band, further increasing charge-carrier density. As a result, the 1% Ir/TiO_2 catalyst exhibits a hydrogen evolution rate of 46.0 mmol g^{-1} h^{-1}, an apparent quantum yield (AQY) of 8.5% at 365 nm, and a turnover frequency (TOF) of 1163.38 h^{-1} in simulated seawater under full-spectrum irradiation. Remarkably, the catalyst retains 92.6% of its activity after ten cycles over 90 days. Density functional theory calculations reveal a lowered hydrogen adsorption-free energy (ΔGH*) upon Ir loading, with Ir and Ti^{3+} sites favoring H^+ adsorption while resisting Cl^- corrosion (Fig. 7(B)). Overall, 1% Ir/TiO_2 exemplifies a synergistic approach combining efficient charge separation, selective ion adsorption, and Cl^- tolerance, offering a robust platform for sustainable seawater hydrogen production. These results underscore the transformative potential of metal-cluster modification in advancing solar-driven H_2 generation.

Heterometallic lanthanide–transition-metal (4f–3d) clusters, as noble-metal-free molecular entities, combine well-defined crystal structures with multiple metal centers containing 4f and 3d electrons [16]. Such clusters offer a unique platform for synergistic effects, positioning them as promising candidates for efficient molecular photocatalysts. For example, Chen et al. synthesized four isomorphic 4f–3d clusters, $Ln_{52}Ni_{56}$ (Ln = Eu, Pr, Nd, Gd), and anchored them onto CdS, significantly enhancing photocatalytic H_2 evolution [26]. Among these, the $Eu_{52}Ni_{56}$@xCd_x/CdS-3 composite displayed the highest activity, achieving 25,353 mmol h^{-1} g^{-1}. This remarkable performance is attributed to multipath charge transfer mediated by Eu^{2+} centers, which facilitates efficient electron–hole separation (Fig. 7(C)) and synergistic interactions between the lanthanide and transition-metal sites. This study highlights a rational strategy to boost hydrogen evolution by precisely assembling atomically defined 4f–3d clusters on semiconductor surfaces. By leveraging the unique electronic interactions and structural precision of heterometallic clusters, this approach provides a versatile blueprint for designing next-generation photocatalysts with high activity and tunable properties.

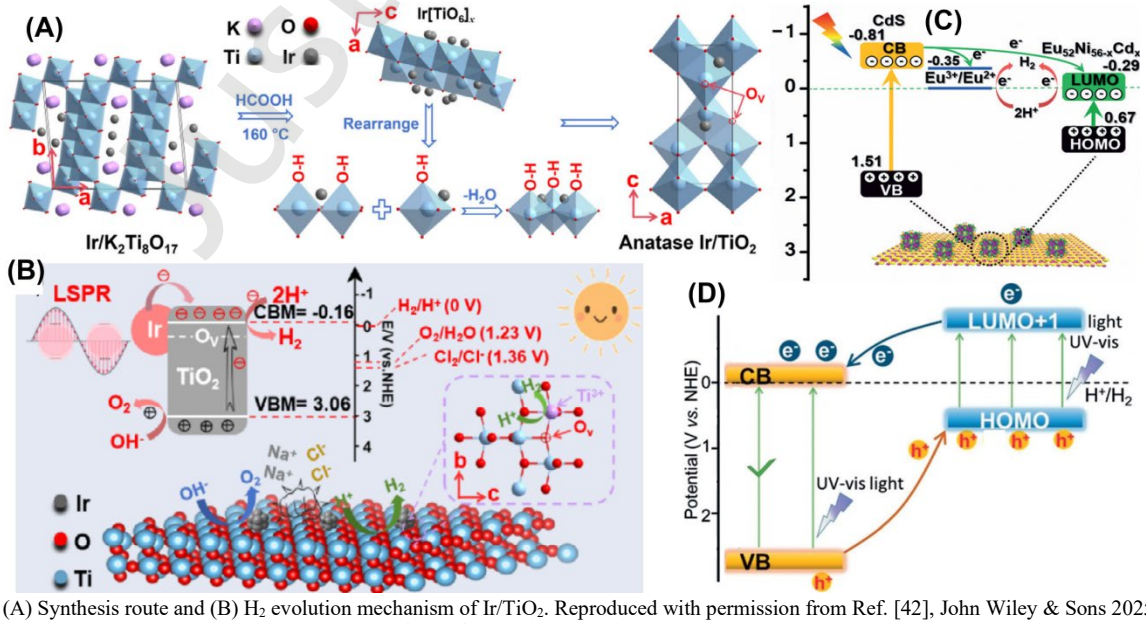

Figure 7. (A) Synthesis route and (B) H_2 evolution mechanism of Ir/TiO_2. Reproduced with permission from Ref. [42], John Wiley & Sons 2025. (C) Charge separation and migration mechanism of $Eu_{52}Ni_{56}$@xCd_x/CdS-3 for H_2 evolution. Printed with permission from Ref. [26], John Wiley & Sons 2018. (D) Type II charge trasnfer mechanism of $Ag_{44}(SR)_{30}$/TiO_2. Reproduced with permission from Ref. 57, John Wiley & Sons 2020.

Bimetallic PdPt nanoclusters have demonstrated superior photocatalytic performance compared to monometallic Pt catalysts, owing to their unique crystalline structure and synergistic effects. Chang et al. synthesized 2D ordered mesoporous TiO_2 nanosheets (mTSs) with tunable thickness and pore size via a monomicelle assembly process [23]. Ultrasmall, highly dispersed PdPt nanoclusters were incorporated onto the mTSs through a stepwise reduction strategy, yielding the mTSs-$Pd_{0.5}Pt1$ catalyst. The material retained a well-defined 2D hexagonal (p6mm) mesoporous structure with a large pore size (~23 nm), high specific surface area (~157 $m^2\ g^{-1}$), and substantial pore volume (~0.27 $cm^3\ g^{-1}$). The mTSs-$Pd_{0.5}Pt1$ catalyst exhibited remarkable photocatalytic H_2 evolution, achieving 17.4 mmol $g^{-1}\ h^{-1}$ with excellent stability. This performance arises from a synergistic combination of structural and electronic features: the ordered mesoporous architecture provides abundant active sites and enhances light harvesting; oxygen vacancy (O_V) engineering introduces defect states below the conduction band, narrowing the bandgap and extending visible-light absorption; and PdPt nanoclusters act as electron sinks, promoting charge separation while optimizing the Gibbs free energy (ΔGH*) for H_2 adsorption and desorption. The dual functionalization of mTSs with OV and bimetallic clusters enables efficient photogenerated electron–hole utilization and accelerates surface hydrogen evolution. This study highlights how the integration of structural engineering with surface modification in bimetallic nanoclusters provides a versatile strategy to design high-performance photocatalysts. By synergistically tuning mesoporous architecture, defect states, and bimetallic active sites, such catalysts offer a robust platform for sustainable hydrogen production and energy conversion.

The size of metal nanoparticles (NPs) critically influences their function in photocatalytic systems. Smaller NPs exhibit higher energy levels, but once these exceed the conduction band (CB) of the semiconductor, their ability to extract electrons is lost. Conversely, overly large NPs provide lower surface area and can act as recombination centers by capturing both electrons and holes [7]. Atomically precise metal nanoclusters (NCs), with discrete energy levels, combine multiple absorptions across the UV/Vis/IR spectrum with intrinsic catalytic activity, enabling them to serve simultaneously as light absorbers and cocatalysts. For example, Wang et al. deposited $Ag_{44}(SR)_{30}$ (1, SR = thiolate) NCs onto TiO_2 and investigated photocatalytic H_2 production [57]. By tuning excitation from visible light to the full solar spectrum, the charge-transfer pathway could be controlled, establishing a type II photocatalytic mechanism (Fig. 7(D)). The NCs not only extend light absorption but also synergistically enhance charge separation and transport, achieving a H_2 evolution rate of 7.4 mmol $h^{-1}\ g^{-1}$, tenfold higher than pristine TiO_2. Under visible-light irradiation, the NCs function primarily as light absorbers, while under full-spectrum illumination, they act as a small-band-gap semiconductor to facilitate efficient electron–hole separation. This dual functionality demonstrates that NCs can operate as true cocatalysts rather than simple photosensitizers, highlighting their potential in designing highly efficient photocatalytic systems. This study illustrates how atomically precise metal NCs provide a versatile platform for integrating light absorption and catalytic activity, offering a rational route for advancing solar-driven hydrogen evolution.

All-inorganic polyoxometalates (POMs) with multidentate O-donating sites have recently emerged as effective protective ligands for Ag nanoclusters [28]. The reversible proton storage, redox activity, and photochemical properties of POMs endow the encapsulated Ag nanoclusters with unique catalytic and photoluminescent behaviors. Chi et al. synthesized three structurally novel Ag nanoclusters encapsulated by bowl-like POM ligands, namely $\{Ag_{14}(Sb_3W_{30})_2\}$-1, $\{Ag_{14}(Sb_3W_{30})_2\}$-1a, and $\{Ag_{14}(Sb_3W_{30})_2\}$-2, via a one-pot solvothermal approach [71]. Single-crystal X-ray analyses revealed structural isomerism of the $\{Ag_{14}\}^{10+}$ core, likely induced by distinct O-atom distributions in the coordinating $\{Sb_3W_{30}\}$ ligands. Density functional theory calculations identified $\{Ag_{14}(Sb_3W_{30})_2\}$-1 as a 4-electron superatom with a Jahn-Teller distorted $\{Ag_{14}\}$ core ($1S^21P^2$), whereas $\{Ag_{14}(Sb_3W_{30})_2\}$-2 behaves as a 4-electron supermolecule ($1s_g^21s_u^2$) isoelectronic to the van der Waals dimer He_2. These differing electronic structures underpin their distinct physicochemical properties: $\{Ag_{14}(Sb_3W_{30})2\}$-1 exhibits efficient photothermal conversion, while $\{Ag_{14}(Sb_3W_{30})2\}$-2 shows strong photoluminescence. Both clusters demonstrate excellent photocatalytic H_2 evolution, achieving TONs of ~24,117 and ~22,233 after 6 hours, respectively. This activity arises from the synergistic cooperation between the redox-active $\{Sb_3W_{30}\}$ ligands and Ag active sites, highlighting the potential of POM-encapsulated nanoclusters in solar-driven hydrogen generation. This work not only expands the structural diversity of Ag-POM nanoclusters but also provides insights into isomer-dependent properties in atomically precise clusters.

Encapsulation of metal nanoclusters (NCs) within crystalline porous metal–organic frameworks (MOFs) offers an effective strategy to stabilize NCs and construct high-performance photocatalytic systems. The confinement within MOFs suppresses migration and aggregation of NCs, while their discrete, molecule-like electronic structure imparts semiconductor-like behavior, enabling the formation of heterojunction photocatalysts that extend the lifetime of photoexcited charge carriers. Wang et al. reported the incorporation of four MAg_{24} (M = Ag, Pd, Pt, Au) NCs into the visible-light-responsive MOF UiO-66-NH_2 via electrostatic interactions, forming MAg_{24}@UiO-66-NH_2, differing only by the single-atom metal at the cluster core [63]. Ag_{25}@UiO-66-NH_2 exhibited exceptional hydrogen evolution, with a rate ~5.6 times higher than AgNPs@UiO-66-NH_2 and ~6.4 times higher than Ag_{25} supported on UiO-66-NH_2, while maintaining remarkable stability. Introducing heteroatom metals at the cluster core further enhanced activity in the order Ag_{25} < $PdAg_{24}$ < $PtAg_{24}$ < $AuAg_{24}$, with $AuAg_{24}$@UiO-66-NH_2 reaching 3.6 mmol $g^{-1}h^{-1}$, ~4.8 times higher than Ag_{25}@UiO-66-NH_2. Femtosecond transient absorption spectroscopy revealed that encapsulation significantly prolongs charge carrier lifetimes, consistent with the observed photocatalytic trends. In situ X-ray photoelectron spectroscopy (XPS) confirmed the formation of a Z-scheme heterojunction, facilitating efficient charge separation. This represents the first demonstration of a Z-scheme photocatalytic system based on metal NC–MOF composites. The MOF confinement ensures excellent photocatalytic stability and recyclability, while the central heteroatom dictates activity by modulating charge transfer and the electronic state of surface Ag sites. Overall, MAg_{24}@UiO-66-NH_2 composites highlight how precise heteroatom doping and MOF encapsulation

synergistically enhance photocatalytic hydrogen production, offering a blueprint for the design of structurally precise, tunable heterogeneous photocatalysts.

5.3. H_2O_2 production

Hydrogen peroxide (H_2O_2) is a green, nonpolluting, and multifunctional oxidant with broad applications in chemical synthesis, medical disinfection, and environmental remediation [3]. Developing environmentally benign, cost-effective, and efficient strategies for H_2O_2production is therefore of significant interest. Compared to the conventional anthraquinone process, photocatalytic production of H_2O_2 from seawater offers advantages of abundant feedstock, simple operational requirements, and an environmentally friendly process [13]. Au NCs, with tunable optical properties, are ideal for converting solar energy into chemical energy and have shown promise as photocatalysts [28]. However, their practical application is limited by short carrier lifetimes, intrinsic instability, and poorly understood charge transfer mechanisms. Enhancing interfacial charge transfer kinetics has been recognized as an effective approach to overcome these limitations. Li et al. synthesized Au NCs decorated with three aminophenol isomers—p-Aminophenol (p-Au), m-Aminophenol (m-Au), and o-Aminophenol (o-Au), via a one-step heat treatment and employed them as photocatalysts for H_2O_2 production [139]. The interfacial kinetics of these systems were systematically investigated using transient photovoltage (TPV), transient potential scanning (TPS), and photo-induced current (TPC) measurements. Although TPC confirmed a common reaction pathway for all three catalysts and the conduction band positions were similar under working conditions, m-Au and p-Au exhibited higher surface effective charges than o-Au. Additionally, m-Au demonstrated stronger O_2 adsorption and faster oxygen reduction reaction (ORR) kinetics, leading to superior H_2O_2 photoproduction over 36 h. Using the Butler–Volmer equation, the specific rate ratios for H_2O_2 formation were calculated, revealing that ORR rates are governed primarily by surface effective charges and O_2 adsorption, with conduction band position playing a secondary role. This study provides a detailed understanding of how catalyst structure, surface properties, and interfacial kinetics collectively dictate photocatalytic performance, offering valuable guidance for the rational design of efficient Au NC-based photocatalysts.

Schiff-base-derived catechol COFs are prone to decomposition, limiting their reusability. In contrast, COFs adopting keto conformations exhibit narrower photoresponsive band gaps and enhanced structural stability, making them attractive for improving photocatalytic efficiency and durability. Stabilized confined metal clusters can further facilitate electron transfer, promoting the separation of photogenerated electron-hole pairs and enhancing photocatalytic performance. For example, Zhou et

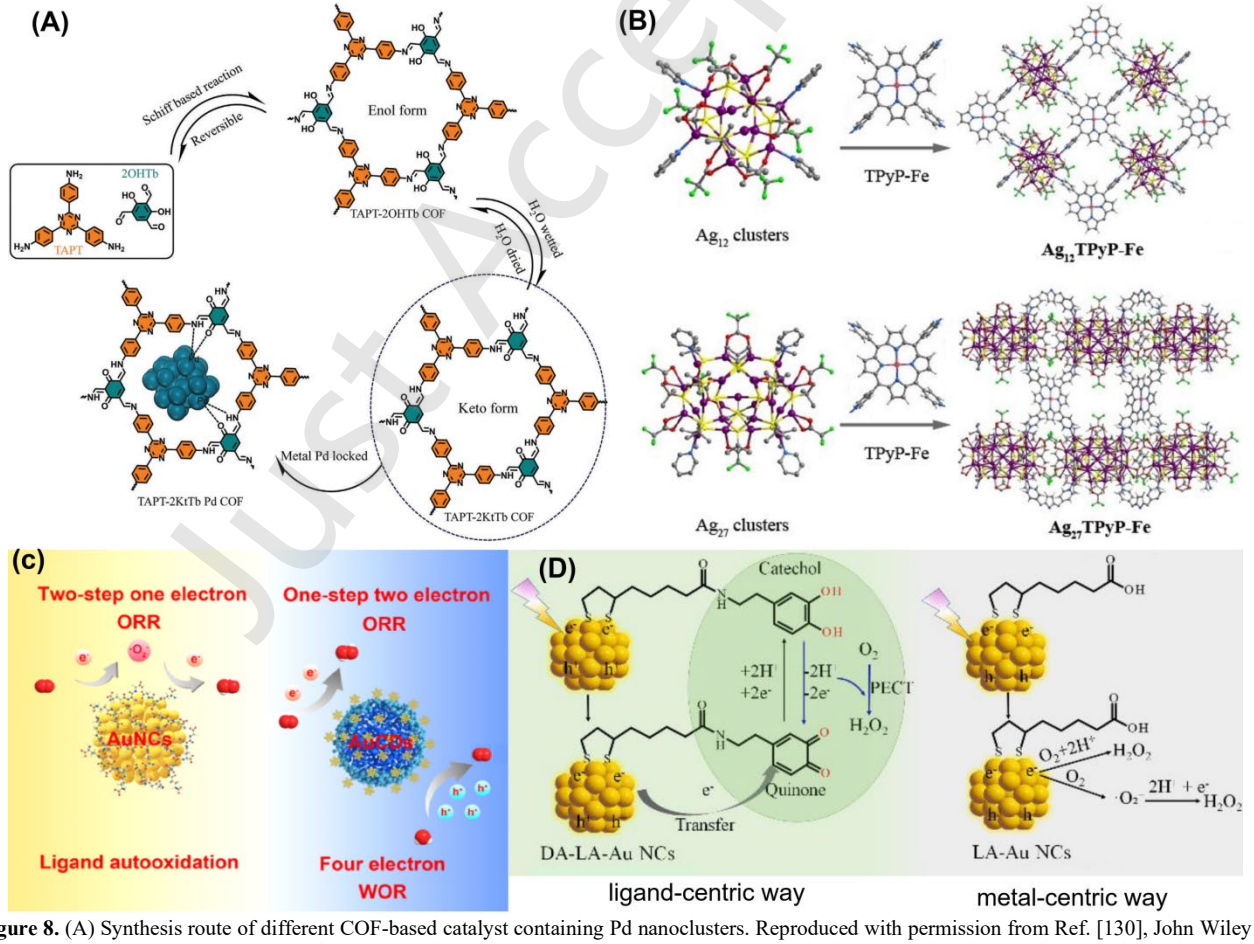

Figure 8. (A) Synthesis route of different COF-based catalyst containing Pd nanoclusters. Reproduced with permission from Ref. [130], John Wiley & Sons 2025. (B) Preparation process and structures of Ag12TPyP-Fe and Ag27TPyP-Fe. Printed with permission from Ref. [59], John Wiley & Sons 2024. (C) Proposed mechanism of Au NCs and Au CDs. Reproduced with permission from Ref. [162], Elsevier B.V 2025. (D) Synthesis route of DA-LA-Au NCs and LA-Au NCs. Reproduced with permission from Ref. [163], Elsevier B.V 2025.

al. reported a general strategy to construct two novel COF-based photocatalysts: TAPT-2KtTb Pd COF, containing Pd nanoclusters, and TAPT-2OHTb COF, lacking Pd (Fig. 8(A)) [130]. The confined Pd nanoclusters stabilize the keto form, significantly boosting photocatalytic H_2O_2 production. Solid-state ^{13}C NMR and FTIR analyses confirm the Pd clusters efficiently convert enol to ketone structures, while PXRD characterization indicates that the stabilized keto configuration reduces photocatalyst degradation. Theoretical studies suggest that confined Pd clusters enhance the transport of photogenerated carriers. The COFs' photophysical and electrochemical properties facilitate energy-level matching with reaction precursors, enabling effective H_2O_2 generation from water or seawater under visible light. Experimental data show that locking the keto structure via Pd nanoclusters enhances photocatalytic activity by 106–164%. H_2O_2 is generated via direct $2e^-$ water oxidation and indirect $2e^-$ oxygen reduction pathways under visible irradiation. Under O_2-rich conditions, TAPT-2OHTb COF and TAPT-2KtTb Pd COF produce 1566.4 and 3231.7 μmol g^{-1} h^{-1} in pure water, decreasing to 1011.9 and 2676.3 μmol g^{-1} h^{-1} in seawater, respectively. This strategy, utilizing enol-based COFs to confine Pd nanoclusters and lock the keto form, not only enhances structural stability but also markedly improves photocatalytic H_2O_2 production. These findings offer valuable insights for the design of robust, high-performance photocatalysts suitable for complex aqueous environments.

Achieving liquid-phase H_2O_2 production requires catalytic sites capable of simultaneously reducing CO_2 and O_2 generated from water oxidation in artificial photosynthesis systems. Iron porphyrinates are promising candidates, as they provide well-established sites for both CO_2 and O_2 reduction. For example, Chen et al. demonstrated that the assembly of plasmonic Ag(I) clusters with iron porphyrinates within a MOF enables the construction of a high-performance, stable photocatalyst for coupled CO_2 reduction and pure H_2O_2 generation [59]. Using reticular chemistry, isolated, high-density Ag(I) clusters were successfully incorporated into two robust MOF photocatalysts (Fig. 8(B)), and their performance and mechanistic behaviors were systematically compared. The combination of multinuclear Ag(I) clusters and Fe porphyrinates within MOFs facilitates efficient CO_2 reduction and H_2O_2 synthesis without the need for photosensitizers or sacrificial electron donors. Mechanistic studies reveal that Ag(I) clusters serve as the photosensitive unit and water oxidation site, whereas Fe porphyrinates function as the CO_2/O_2 reduction centers. The system benefits from favorable redox potentials, efficient charge transfer between Ag(I) clusters and Fe porphyrinates, the plasmonic enhancement of Ag(I), and CO_2 capture capability. Collectively, these features enable highly efficient artificial photosynthesis with superior performance relative to previously reported systems. This work provides valuable insights for designing next-generation artificial photosynthesis platforms that integrate light absorption, water oxidation, and dual-electron reduction processes for H_2O_2 production.

Considerable efforts have focused on understanding photocatalytic H_2O_2 production and developing highly efficient catalysts. Strategies typically involve tuning material band gaps or regulating catalyst–reactant interactions, while advanced techniques such as transient absorption spectroscopy, in-situ FTIR, and in-situ Raman spectroscopy are employed to track intermediate formation. Li et al. reported two types of gold nanoclusters: thiol-stabilized Au NCs and carbon-dot-stabilized Au CDs [162], providing a platform to investigate interfacial kinetics of photocatalytic H_2O_2 generation. Three quasi in-situ techniques, namely transient photovoltage (TPV), transient potential scanning (TPS), and transient photocurrent (TPC), were applied to probe charge transfer and distribution under operational conditions. TPV revealed differences in illumination-induced charge transfer between Au NCs and Au CDs, whereas TPS and TPC highlighted variations in interfacial charge dynamics, electron transfer numbers, and reactant adsorption. Incorporation of carbon dots alters hole consumption from ligand oxidation to four-electron water oxidation, stabilizing active sites and promoting efficient O_2 reduction. Remarkably, the oxygen reduction reaction (ORR) shifts from a two-step one-electron pathway to a one-step two-electron process (Fig. 8(C)). This integrated operando approach enables a detailed understanding of ligand dynamics, interfacial charge separation, reactant activation, and electron transfer pathways at the nanoscale. The study demonstrates both a strategy for synthesizing stable metal clusters and a comprehensive methodology for probing photocatalytic kinetics, offering valuable insights for the design of high-performance, durable photocatalysts.

Conventional nanocluster (NC) designs primarily exploit the metal core for catalysis, while ligands act merely as stabilizers, underutilizing their chemical potential. This limits both reaction selectivity, such as the inability to suppress $^{\bullet}O_2^-$ formation, and activity, due to restricted reactant access to metal sites. Liu et al. addressed this challenge through bioinspired ligand engineering [163]. Drawing inspiration from catechol oxidase enzymes, which employ organic cofactors like tyrosine quinone motifs for selective O_2 activation, they developed dopamine-grafted lipoic acid-protected Au NCs (DA-LA-Au NCs) as ligand-centric photocatalytic nanozymes for H_2O_2 production via O_2 reduction (Fig. 8(D)). This contrasts with conventional LA-Au NCs, where catalysis is metal-centered. This strategy integrates three innovations: (1) translocation of the active site from the Au core to redox-active DA ligands, repurposing the metal as an electron reservoir; (2) biomimetic pathway gating through DA's catechol/quinone interconversion, enabling proton-coupled electron transfer (PCET) and directing photogenerated electrons exclusively toward $2e^-$ O_2 reduction (H_2O_2 selectivity near 100%), bypassing $^{\bullet}O_2^-$ formation; (3) ligand-engineered nanoenvironments, where the dense DA layer acts as an "O_2 funnel," enhancing reactant–catalyst collisions (validated by molecular dynamics). Integration of enzyme-inspired control with ultrasmall NC size enabled a record H_2O_2 production of 1198 μmol/L and a solar-to-chemical conversion efficiency of 0.39%, 3.9 times higher than that of natural plants. DA ligands function as molecular switches, promoting PCET, enhancing visible-light absorption, and improving electron transfer kinetics. Encapsulation within ZIF-8 (DA-LA-Au NCs@ZIF-8) further stabilizes the system, maintaining high performance without sacrificial agents. This ligand-centric design merges enzyme-like precision with NC functionality, establishing a versatile platform for selective photocatalysis and sustainable oxidant production.

5.4. Organic synthesis

Visible-light photoredox catalysis has become an essential strategy in modern organic synthesis, enabling a wide range of bond-forming reactions under exceptionally mild conditions [164]. In these systems, photoexcited metal complexes or organic dyes mediate single-electron or energy-transfer events, allowing reactions to proceed at ambient temperature without harsh radical initiators [165]. A major advantage of photoredox chemistry is its compatibility with diverse cocatalysts, including Brønsted acids, enzymes, and transition-metal complexes, which can intercept reactive radical intermediates and expand synthetic scope [166]. Recently, atomically precise metal NCs have attracted increasing attention as photocatalysts because their well-defined atomic structures and strong quantum confinement effects impart unique photophysical and redox properties. Among the reactive oxygen species generated under light irradiation, singlet oxygen ($^1O_2$) plays a particularly important role in driving selective oxidative transformations [167]. Metal NCs are especially effective in producing $^1O_2$, making them attractive platforms for photocatalytic organic synthesis. A representative example was reported by Kamachi and co-workers, who constructed a surface-exposed Au–Ag alloy nanocluster stabilized within a ring-shaped polyoxometalate, $[P_8W_{48}O_{184}]^{40-}$ [33]. In this system, Au^+ ions selectively replaced electron-rich Ag atoms in a preformed Ag nanocluster, yielding a well-defined $\{Au_8Ag_{26}\}$ alloy with a core–shell configuration (Fig. 9(B)). Comprehensive structural and electronic characterization using single-crystal X-ray diffraction, elemental analysis, ADF-STEM, XPS, and X-ray absorption spectroscopy confirmed the successful formation of the alloy cluster. Photocatalytic studies demonstrated that the Au–Ag nanocluster exhibits markedly higher activity and stability than the parent Ag cluster during aerobic oxidation reactions. Under visible-light irradiation, the alloy cluster efficiently generated $^1O_2$, enabling the selective oxidation of various organic substrates in an oxygen atmosphere. Importantly, incorporation of Au not only enhanced photocatalytic efficiency but also significantly improved structural robustness within the polyoxometalate framework. These results highlight the advantages of alloying strategies for tuning the photophysical and catalytic properties of atomically precise nanoclusters. More broadly, they demonstrate that integrating well-defined metal clusters with inorganic hosts represents a powerful approach for constructing next-generation photocatalysts. Such hybrid systems are expected to play an increasingly important role in organic synthesis by offering precise control over electronic structure, reactivity, and stability, thereby expanding the scope of visible-light-driven transformations.

Copper nanoclusters (Cu NCs) have emerged as attractive photocatalysts owing to the natural abundance of copper, its rich redox chemistry, and the favorable photophysical properties imparted by ultrasmall cluster sizes. Their strong absorption in the visible region and relatively long-lived excited states make Cu NCs particularly well suited for photocatalytic organic transformations. A representative example was reported by Bodiuzzaman and co-workers, who developed a structurally well-defined Cu_{13} nanocluster stabilized by naphthalene thiolate and triphenylphosphine ligands ($Cu_{13}N_{ap}$) (Fig. 9(A)) [75]. The cluster features a Cu_{13} core constructed from stacked triangular Cu_3 motifs and displays remarkable catalytic efficiency in the visible-light-driven decarboxylation of carboxylic acids across a broad substrate range. Notably, $Cu_{13}N_{ap}$ significantly outperformed its isostructural analogue Cu_{13}DCBT, highlighting the decisive influence of ligand identity on catalytic behavior. Detailed spectroscopic analysis and density functional theory (DFT) calculations revealed that the superior activity of $Cu_{13}N_{ap}$ originates from its enhanced light-harvesting ability and prolonged excited-state lifetime, both arising from strong electronic interactions between the copper core and the naphthalene-based ligands. These features promote efficient energy transfer to the substrate rather than direct metal–substrate coordination. Consistent with this interpretation, mechanistic studies indicated that the reaction proceeds predominantly through an outer-sphere energy-transfer pathway, while the conventional inner-sphere copper-mediated route is disfavored due to a high activation barrier. The catalytic consequence of this ligand-induced modulation is striking: $Cu_{13}N_{ap}$ delivers up to 90% yield in decarboxylative oxygenation reactions under visible light, compared with only 28% for Cu_{13}DCBT. These findings clearly demonstrate how subtle changes in ligand architecture can dramatically alter excited-state dynamics and reactivity. Overall, this study underscores the critical role of surface ligands in tailoring the photocatalytic performance of copper nanoclusters and highlights ligand engineering as a powerful strategy for designing efficient photocatalysts for organic synthesis.

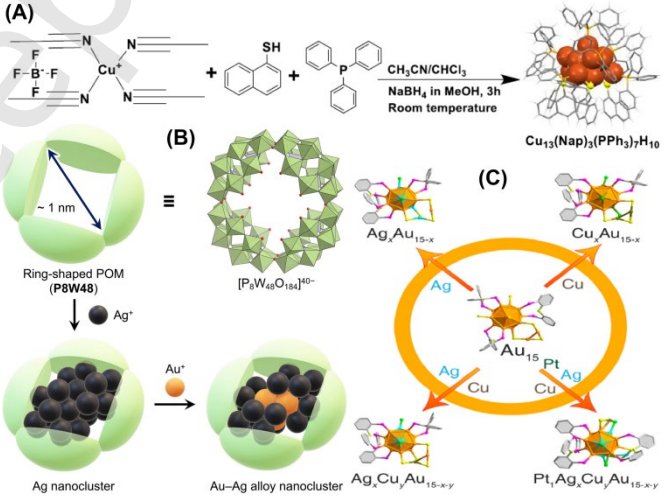

Figure 9 (A) Preparation process of Cu13Nap. Reproduced with permission from Ref. [75], America Chemical Society 2024. (B) Preparation route of Au-Ag alloy C+NCs within the cavity of a ring shaped POM P8 W48. Reproduced with permission from Ref. [33], John Wiley & Sons 2024. (C) Heteroatom alloying of Au15 NCs. Reproduced with permission from Ref. [77], America Chemical Society 2024.

Establishing clear structure–property relationships in metal nanoclusters remains a central challenge for the rational design of photocatalysts. Addressing this issue, Zhu and co-workers constructed a systematic M_{15} cluster platform through controlled alloying of a parent Au_{15} nanocluster, affording a series of heterometallic derivatives with precisely defined compositions, including $Pt_1Ag_xCu_yAu_{15-x-y}$, $Ag_xCu_yAu_{15-x-y}$, Ag_xAu_{15-x}, and Cu_xAu_{15-x} clusters (Fig. 9(C)) [77]. The availability of atomically resolved structures enabled a direct correlation between cluster composition, photophysical behavior, and catalytic performance. Among this family, the Cu_xAu_{15-x} nanoclusters exhibited the most pronounced phosphorescence and the highest efficiency for singlet oxygen generation under blue-light irradiation. This enhanced photoreactivity translated into excellent catalytic

performance in the oxidation of silyl enol ethers, affording α,β-unsaturated ketones and aldehydes with high efficiency. Systematic photocatalytic studies further demonstrated the broad applicability of these clusters, including reactions involving diverse enol ethers, biologically relevant substrates, and multiple oxidation transformations. Mechanistically, the superior activity of Cu-doped clusters was attributed to optimized electronic structures that favor intersystem crossing and efficient energy transfer to molecular oxygen. The clear dependence of photocatalytic performance on atomic composition highlights the importance of precise structural control in tuning excited-state dynamics. Overall, this work establishes a compelling structure–function paradigm for metal nanocluster photocatalysts and provides a blueprint for the rational development of cluster-based systems with tailored photoredox activity for organic synthesis.

Heterostructure engineering that integrates metal NCs with transition-metal chalcogenides (TMCs) has emerged as an effective strategy to regulate charge migration and enhance photocatalytic efficiency [168]. By combining complementary components, such hybrid systems benefit from reduced activation barriers, promoted directional charge transfer, and increased densities of accessible active sites [169]. As a result, cocatalyst-assisted NC/TMC architectures have shown markedly improved charge separation and utilization under light irradiation. A representative example was reported by Yan and co-workers, who constructed a hierarchically organized GR/Ag_x NCs/CdS heterostructure via a facile cascade self-assembly route under ambient conditions [140]. In this system, glutathione-protected Ag_x nanoclusters were first immobilized onto CdS nanosheets, followed by electrostatic assembly with graphene (GR), yielding a three-component architecture with well-defined interfacial contact. Within the heterostructure, Ag_x NCs serve as light-harvesting centers and act as charge-transfer bridges between CdS and GR owing to their favorable band alignment. The outer graphene layer further promotes electron extraction and transport, thereby suppressing charge recombination. This rational spatial arrangement enables efficient charge separation and directional electron flow, resulting in markedly enhanced visible-light photocatalytic performance. The GR/Ag_x NCs/CdS system exhibits high activity toward selective organic transformations, including anaerobic reduction of aromatic nitro compounds and oxidation of aromatic alcohols to aldehydes. Mechanistic investigations clarified the distinct functions of each component, confirming the synergistic role of NCs in mediating interfacial charge transfer. Overall, this work highlights the power of heterostructure design in maximizing the catalytic potential of atomically precise metal nanoclusters. By integrating NCs with conductive and semiconducting supports, such architectures provide an effective platform for directing charge flow and improving photocatalytic efficiency, offering valuable guidance for the development of advanced photocatalysts for organic synthesis and solar energy conversion.

Sulfones constitute an important class of compounds in pharmaceuticals and functional materials, yet their conventional synthesis often relies on harsh conditions or stoichiometric reagents, limiting functional-group tolerance. Although copper-based photocatalysts offer a more sustainable alternative, many reported systems suffer from narrow substrate scope, high metal loading, or reliance on UV irradiation. Addressing these limitations, Alotaibi and co-workers reported a uniquely structured Cu_{19} nanocluster that enables efficient visible-light-driven sulfonylation reactions under mild conditions [141].The Cu_{19} cluster features an unusual Cu_{13}-centered Ino decahedral core with partially exposed metal sites, generated by incorporating bromide ions during synthesis in CH_2Br_2. This unshielded metallic core plays a decisive role in photocatalysis, enabling efficient single-electron transfer to aryl halides (Br or Cl) and generating aryl radicals that subsequently undergo C–S bond formation with sulfinates. Unlike conventional systems, the Cu_{19} catalyst operates without additional ligands or harsh additives and displays broad substrate tolerance toward both aryl and alkyl sulfinates. Mechanistic studies supported by DFT calculations revealed that the exposed copper surface facilitates direct interaction with sulfinate anions, thereby lowering the barrier for SET and promoting efficient radical generation. The structural accessibility of the Cu_{19} core is therefore key to its high catalytic activity. Notably, the nanocluster functions as a heterogeneous photocatalyst and can be recycled multiple times without loss of activity, highlighting its robustness. This work demonstrates how deliberate exposure of metal cores within atomically precise nanoclusters can unlock new reactivity patterns. The Cu_{19} system exemplifies a promising strategy for designing next-generation photocatalysts that combine structural precision, operational simplicity, and high efficiency for C–S bond formation under mild conditions, further expanding the scope of nanocluster-enabled organic synthesis.

Cross-coupling reactions are central to modern synthetic chemistry, and their photoinduced variants have attracted growing interest as sustainable routes to C–C, C–N, and C–S bond formation. In this context, nanocluster-based photocatalysts offer unique advantages by combining light harvesting with efficient charge separation. A representative example was reported by Tirumala and co-workers, who developed Pd nanoclusters supported on quasi-spherical Cu_2O nanoparticles as an efficient photocatalytic platform for visible-light-driven C–C coupling reactions under ambient conditions [142]. Compared with bare Cu_2O, the Pd-decorated hybrid exhibited markedly enhanced catalytic activity. Transient reflection spectroscopy revealed that this improvement originates from efficient charge separation across the Cu_2O–Pd interface. Specifically, a Schottky junction forms between Cu_2O and Pd, enabling directional electron transfer from photoexcited Cu_2O to the Pd nanoclusters, while suppressing hole migration. Density functional theory calculations corroborated these observations, showing strong electronic coupling between the Cu_2O conduction band and the empty Pd states, as well as favorable interaction with the adsorbed aryl substrates. Importantly, photothermal contributions were ruled out, confirming that the catalytic enhancement arises from true photoinduced charge transfer rather than thermal effects. The transferred electrons activate C–H bonds of the adsorbed substrates via a Mars–van Krevelen–type mechanism, thereby promoting efficient C–C bond formation. The superior performance of the Cu_2O–Pd system relative to Cu_2O alone highlights the critical role of nanocluster–semiconductor interfaces in controlling charge dynamics. Beyond demonstrating an effective strategy for photocatalytic cross-coupling, this work underscores how rational nanoscale design can enable solar-

driven organic transformations, offering a viable pathway toward sustainable synthesis powered by renewable energy.

5.5. Pollutant removal

Emerging organic contaminants have become a growing threat to aquatic environments and human health. Among them, organohalides represent a particularly hazardous class due to their extensive use in industrial manufacturing, agrochemicals, flame retardants, and water disinfection [170]. These compounds are characterized by highly stable carbon–halogen bonds (C–F: 485 kJ mol^{-1}; C–Cl: 330 kJ mol^{-1}; C–Br: 276 kJ mol^{-1}), which severely hinder natural degradation processes [171]. Despite their typically trace-level occurrence in surface waters (10^{-3}–10^{-6} mg L^{-1}), organohalides exhibit pronounced aquatic toxicity, endocrine-disrupting behavior, and genotoxicity, posing long-term ecological and public health risks. Photocatalytic oxidation has emerged as a promising strategy for the complete mineralization of organohalides into CO_2, H_2O, and halide ions under mild conditions [172]. However, conventional oxidation systems often suffer from limited selectivity, particularly in complex water matrices where target pollutants are present at concentrations orders of magnitude lower than coexisting organic species [3]. This challenge has stimulated growing interest in nanostructured photocatalysts capable of coupling selective adsorption with efficient oxidation. Recent advances in Au-based nanocluster photocatalysts have demonstrated notable progress in this direction. Teng *et al.* reported a catalyst composed of atomically dispersed Au and sub-nanometer Au clusters (≈3–10 atoms) anchored on crystalline potassium-incorporated poly(heptazine imide) (K-PHI) [43]. This architecture enables synergistic photocatalytic behavior under visible-light irradiation. Specifically, Au single atoms serve as highly active sites for water oxidation, promoting the generation of hydroxyl radicals (•OH), while adjacent Au nanoclusters act as photoinduced Lewis acid centers that preferentially adsorb organohalide molecules. Spectroscopic analyses and theoretical calculations revealed that incorporation of Au nanoclusters introduces Au 6s orbitals into the electronic structure of K-PHI, facilitating hole accumulation and strengthening substrate–catalyst interactions. This spatially confined configuration creates a localized oxidation microenvironment enriched with both reactive •OH species and adsorbed organohalides, thereby greatly enhancing reaction selectivity and mineralization efficiency. As a result, the AuSA–NC/K-PHI system achieves rapid and selective degradation of persistent organohalides even in the presence of high concentrations of competing substances. Notably, a fixed-bed photoreactor constructed with this catalyst demonstrated efficient removal of refractory organohalides from real tap and groundwater at a throughput of 2 L h^{-1}, exhibiting over threefold improvement in logarithmic degradation efficiency compared with conventional advanced oxidation processes. This work highlights the importance of spatially coupled adsorption–oxidation sites in photocatalyst design and underscores the potential of metal nanocluster engineering for selective pollutant removal. Hence, the integration of atomically precise metal clusters with tailored semiconductor supports represents a powerful strategy for overcoming selectivity limitations in photocatalytic water treatment. Such approaches not only advance sustainable remediation technologies but also provide new insights into the rational design of catalytic systems for complex chemical transformations.

Compared with monometallic clusters, alloyed Au nanoclusters introduce an additional degree of structural and electronic tunability. Their optical response and electronic configuration are highly sensitive to the identity, concentration, and spatial distribution of the dopant metal. Moreover, because a large fraction of atoms reside at the surface, ligand coordination plays a decisive role in governing both atomic arrangement and catalytic behavior. In this context, Liu *et al.* reported a family of thiolate-protected Au–Ag alloy nanoclusters synthesized via a one-pot strategy using adamantanethiol (HS-Adm) as the capping ligand. Mass spectrometric analysis identified the products as $[Au_{23}–xAg_x(S\text{-}Adm)_{15}]$ (x = 0–11) [54], while single-crystal X-ray diffraction unambiguously resolved the structures for x = 4–7. These nanoclusters consist of an icosahedral $Au_{13}–xAg_x$ core (x = 3–6) surrounded by one AgS_3 unit and three $Au_3(SR)_4$ staple motifs. Notably, the steric bulk of the adamantanethiol ligand induces a distinct rearrangement of surface motifs and dictates the preferred incorporation sites of Ag atoms. Density functional theory calculations revealed that Ag incorporation narrows the HOMO–LUMO gap to approximately 1.5 eV, with Ag_4Au_{19} identified as the most thermodynamically stable composition within the series. This electronic modulation translates directly into improved photocatalytic performance. When supported on TiO_2, the Au–Ag alloy clusters exhibit significantly enhanced activity for the visible-light-driven degradation of RhB and phenol compared with their monometallic Au_{23} counterparts. These results highlight how precise alloying and ligand engineering can cooperatively tailor the geometric and electronic structures of metal nanoclusters. Such control enables improved light absorption, charge separation, and catalytic efficiency, underscoring the promise of alloy nanoclusters as tunable building blocks for advanced photocatalytic systems aimed at environmental remediation.

A persistent limitation in Au nanocluster–based photocatalysts lies in their insufficient structural stability when immobilized on conventional oxide or silica supports, particularly under prolonged photoirradiation. This instability significantly restricts their practical application. To address this issue, Deng *et al.* developed a robust anchoring strategy by integrating Au nanoclusters into a thiol-functionalized covalent organic framework (COF-S-SH), thereby achieving enhanced stability and photocatalytic efficiency (Fig. 10(A)) [55]. The COF support features uniform micropores (~2.8 nm), which effectively confine nanocluster growth while simultaneously preventing aggregation. More importantly, thiol groups introduced into the framework serve dual functions: they act as anchoring sites for Au species through strong Au–S interactions and facilitate electronic coupling between the metal clusters and the COF matrix. This design enables the construction of a Z-scheme photocatalytic system (Fig. 10(B)), which significantly improves charge separation efficiency. Specifically, the COF was synthesized from 2,5-divinylterephthalaldehyde and 1,3,5-tris(4-aminophenyl)benzene, producing a vinyl-functionalized framework amenable to post-synthetic thiol modification. Subsequent in situ reduction of $HAuCl_4$ using glutathione generated uniformly dispersed Au nanoclusters with an average

size of approximately 1.8 ± 0.2 nm. The resulting Au@COF composite exhibited excellent photostability under visible-light irradiation (>420 nm) for extended operation. Photoelectrochemical measurements and binding energy calculations confirmed that the Au–S–COF linkage establishes an efficient Z-scheme charge-transfer pathway, enabling rapid electron–hole separation and suppressing recombination. This study demonstrates that combining spatial confinement with strong chemical anchoring offers a powerful strategy for stabilizing metal nanoclusters while enhancing photocatalytic performance. The COF–Au hybrid architecture provides a versatile platform for designing durable, high-efficiency photocatalysts and offers valuable insights for the rational development of next-generation materials for pollutant degradation.

The in situ generation of Bi nanoclusters on semiconductor surfaces offers an effective strategy for constructing intimate interfacial contacts and facilitating directional charge transport. Such an approach not only strengthens interfacial coupling through covalent interactions but also promotes efficient migration of photogenerated charge carriers, thereby enhancing overall catalytic performance. In this context, Cheng *et al.* reported a Bi-modified $BiVO_4$ (Bi–BVO) system prepared via $NaBH_4$-assisted in situ reduction and systematically investigated its piezo-photocatalytic degradation behavior toward tetracycline hydrochloride (TC-HCl) [173]. Detailed spectroscopic and theoretical analyses revealed that the introduction of Bi nanoclusters induces lattice distortion in BVO, as evidenced by shortened V–O bond lengths observed in IR and Raman spectra. This structural perturbation facilitates the formation of oxygen vacancies, which act as electron traps and contribute to improved

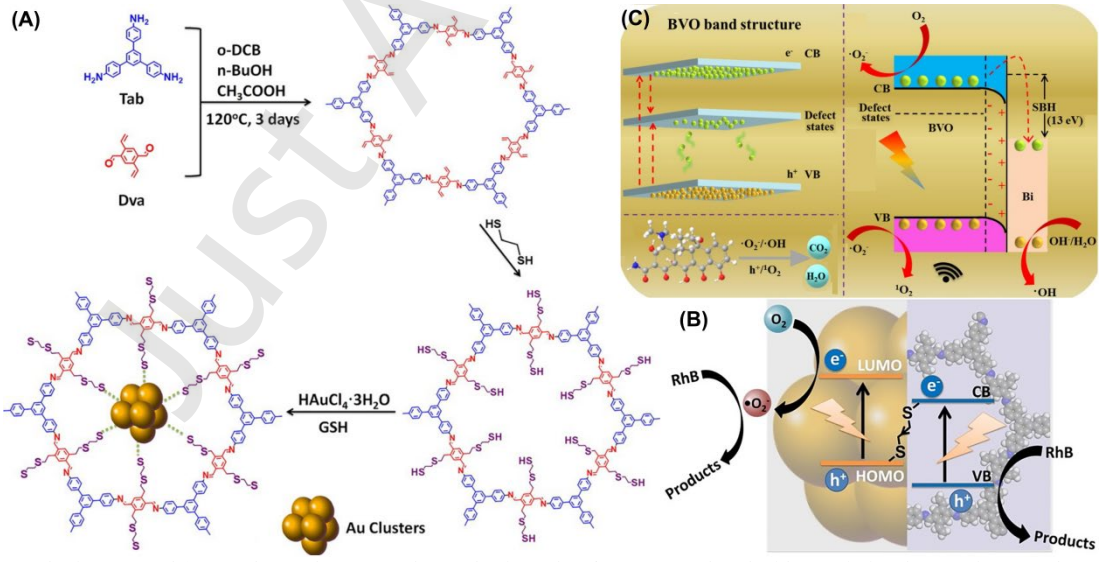

Fig. 10. (A) Synthesis route and (B) Z-scheme charge trasnfer mechanism of Au/COF. Reproduced with permission from Ref. [55], John Wiley & Sons 2020. (C) Proposed mechanism of Bi NCs/$BiVO_4$. Reproduced with permission from Ref. [173], Elsevier B.V 2025.

charge separation. Simultaneously, the deposited Bi nanoclusters form a conductive surface layer, enabling rapid electron transport and establishing a Schottky junction at the Bi–BVO interface. Although the metallic Bi layer partially suppresses the intrinsic piezoelectric response of BVO by providing an alternative conduction pathway, the synergistic coupling of piezoelectric polarization and photocatalytic excitation results in markedly enhanced catalytic activity. The optimized Bi–BVO catalyst exhibited a TC-HCl removal efficiency of 84.03% within 30 min, which was attributed to the reduced Schottky barrier height (Φ_{SB} ≈ 13 eV) and the coexistence of radical- and non-radical-mediated reaction pathways (Fig. 10(C)). Density functional theory calculations further confirmed the structural stability of Bi nanoclusters on the BVO surface and their role in modulating interfacial electronic states. This study highlights the dual function of metal nanoclusters and oxygen vacancies in regulating charge transport and catalytic reactivity, offering valuable insights into the rational design of high-performance piezo-photocatalysts for environmental remediation.

Structured design has emerged as a key strategy to address challenges in adsorbent–photocatalyst recovery and practical deployment. The inherent cementitious properties of geopolymer (GP) make it an ideal candidate for fabricating inorganic membranes and 3D-printed architectures, enabling precise spatial control of functional components. Jin *et al.* demonstrated a structural–functional design of a GP/DCN adsorbent–photocatalyst via an in situ geopolymerization approach [171]. By tuning precursor ratios, GP nanoclusters were uniformly deposited on DCN surfaces, creating nanoscale separation between adsorption and photocatalytic sites. The strong adsorption capacity of GP allows rapid capture of trace tetracycline (TC) under dynamic conditions, while the photogenerated electrons from DCN are efficiently transferred to GP, facilitating enhanced photocatalytic degradation. Hydroxide ions released from GP further contribute to ·OH radical formation, synergistically boosting oxidative processes. This close matching of adsorption and degradation kinetics enables remarkable performance: in static tests, 0.5CG achieved 94.7% removal of 10 mg/L TC within 5 min, while dynamic degradation of trace TC (400 μg/L, 1000 mL) reached 89.4% under the same timeframe. Furthermore, 3D-printed GP/DCN structures exhibited 64.1% removal of trace TC, demonstrating practical application potential. Mechanistic studies indicated that h^+, $\bullet O_2^-$, and •OH species participate in photocatalytic processes, with GP-derived OH^- ions promoting •OH generation. This work highlights the dual role of

GP as both an adsorbent and an electron mediator, providing a scalable strategy for the low-cost fabrication of structured adsorbent–photocatalysts and offering guidance for the dynamic capture and degradation of antibiotics with multiple pKa values.

Given the high cost of noble metal nanoclusters, the exploration of earth-abundant alternatives as semiconductor co-catalysts for dehalogenation is highly desirable. Copper (Cu), with its rich electronic configuration and inherent affinity for halogen atoms, has emerged as a promising candidate for promoting reductive dehalogenation of persistent organohalides such as decabromodiphenyl ether and chlorinated biphenyls. Wang *et al.* reported the synthesis of Cu cluster-modified flower-like $ZnIn_2S_4$ photocatalysts and demonstrated their application in the visible-light-driven dechlorination of PCB 209 [172]. The study revealed that a Cu loading of 0.1 wt% on $ZnIn_2S_4$ achieved the highest dechlorination rate (0.054 min^{-1}), with photogenerated electrons identified as the primary active species. PCB 209 exhibited site-selective dechlorination, preferentially at para- and meta-positions, which was rationalized by density functional theory calculations showing electron-rich Cu nanoclusters stabilizing these sites and elongating the corresponding C–Cl bonds. Modification with Cu nanoclusters also enhanced visible-light absorption, improved charge separation, and increased reduction capability, resulting in a 99.5% PCB 209 removal within 90 min. Solvent effects were notable, with DMF facilitating electron migration and achieving the fastest dechlorination. Importantly, the Cu/$ZnIn_2S_4$ composite displayed excellent stability and recyclability, retaining over 83% degradation efficiency after five cycles. These findings underscore the potential of Cu nanocluster–modified semiconductors as cost-effective, efficient photocatalysts for the selective dehalogenation of persistent organohalides. This work highlights the importance of tuning electronic structure and interface engineering in metal-cluster-based photocatalysts and suggests promising avenues for translating laboratory designs to practical environmental remediation.

5.6. Methane conversion

Methane (CH_4), the primary component of natural gas and a byproduct of oil extraction, is a potent greenhouse gas, nearly 25 times more impactful than CO_2 [21]. Transforming CH_4 into value-added chemicals such as ethanol ethane (C_2H_6), (CH_3CH_2OH), methanol (CH_3OH), and ethylene (C_2H_4) has gained considerable attention due to its potential for sustainable energy utilization and environmental mitigation [21]. Designing green, selective oxidation processes is critical to reduce greenhouse gas emissions while efficiently exploiting natural gas resources. Photocatalytic approaches powered by solar energy offer a promising route for such transformations [25]. Partial oxidation of CH_4 to liquid methanol is particularly attractive, as it stores energy in a convenient form while avoiding overoxidation to CO_2. However, CH_4 activation is kinetically challenging due to its strong C–H bond and the thermodynamic preference for complete oxidation. Xu et al. addressed this challenge by developing a biomimetic photocatalyst, Fe SA-NC/C_3N_4, comprising graphitic carbon nitride (g-C_3N_4) supporting iron oxide nanoclusters (Fe NC) and satellite iron single atoms (Fe SA) (Fig. 11(A)) [39]. Upon light irradiation, photoexcited electrons from Fe_2O_3 were transferred to Fe SA, facilitating O_2 activation and driving the proton-coupled electron transfer (PCET) process. This cooperative mechanism enabled efficient CH_4 activation via in situ generated •OH intermediates and the formation of (Fe–O–Fe) moieties, resulting in selective CH_3OH production with 98.5% selectivity and a rate of 5.02 mmol g^{-1} h^{-1} at room temperature—outperforming most reported photocatalysts. Mechanistic studies revealed that the binuclear Fe sites formed by Fe SA and Fe NC act synergistically to activate O_2 and CH_4, while •OH radicals promote selective oxidation to methanol. The work demonstrates that rationally engineered metal clusters and single-atom sites can effectively lower activation barriers, offering a blueprint for designing advanced photocatalysts for CH_4 valorization and solar-to-chemical energy conversion.

The activity of noble metal nanoclusters in photocatalysis is strongly influenced by their size, shape, atomic composition, and chemical environment. Smaller clusters often exhibit superior catalytic activity compared to bulk metals, and certain species, such as Au nanoclusters, can extend the visible-light response of photocatalysts. Kaipanchery et al. demonstrated that TiO_2 nanoclusters, with band gaps aligned to the solar spectrum, efficiently drive the photocatalytic conversion of methane to ethane [24]. Mechanistic studies, including calculations of reaction energies (ΔE) and activation barriers (E_a), reveal that methane C–H activation proceeds comparably on bare TiO_2 and Au_6–TiO_2 clusters. Interestingly, the second C–H activation is facilitated by the Au_6–TiO_2 system, while the incorporation of Au_6 clusters lowers the energy barrier for C–C coupling, promoting ethane formation. Electron donation from Au_6 weakens the C–H bond, enhancing activation, and the transition states of C–H and C–C bond formation exhibit carbanion character, which drives the reaction toward ethane with higher selectivity and yield. Moreover, methane activation can occur in the gas phase via reactive oxygen species generated on the photocatalyst surface, and the gold cocatalyst further improves overall efficiency. The final desorption energy of ethane is lower on Au_6–TiO_2 than on bare TiO_2, indicating enhanced product release. These insights into the key catalytic steps provide a framework for designing TiO_2-based nanocluster photocatalysts optimized for high-efficiency methane-to-ethane conversion with minimal byproduct formation.

The design of dual-active cocatalysts with complementary oxidation and reduction functions is critical for the simultaneous activation of O_2 and CH_4 in photocatalytic partial oxidation of methane (POM). Random distribution of oxidation and reduction sites, however, limits the coupling of generated redox intermediates, while carriers with uncontrolled migration enhance electron–hole recombination, reducing overall catalytic efficiency. Engineering adjacent dual active sites at the interface of cocatalysts offers a promising strategy to overcome these

limitations, enabling bimolecular activation and enhanced POM performance. Si et al. reported an oxygen-vacancy-mediated interfacial space-charge layer comprising $Au^{\delta+}$–Ov–W^{5+} on WO_{3-x}/TiO_2 for high-efficiency CH_4 photo-oxidation to C_1 liquid oxygenates [174]. The Au–WO_{3-x}/TiO_2 catalyst achieved reaction rates up to 11,698 μmol g^{-1} with 99% selectivity, outperforming individual Au/TiO_2 and WO_3/TiO_2 systems. Mechanistic studies revealed that electron-deficient $Au^{\delta+}$ sites lower the initial C–H dissociation energy, whereas electron-rich Ov–W^{5+} sites preferentially adsorb O_2 in a terminal configuration, promoting formation of •OOH rather than excess •OH. The $Au^{\delta+}$–Ov–W^{5+} interface also facilitates conversion of $*CH_3OH$ to HCOOH, suppressing overoxidation to gaseous products (Fig. 11(B)). This study exemplifies the effectiveness of interfacial dual active sites in improving carrier separation and enabling selective adsorption and activation of reactants, offering a rational blueprint for designing highly efficient photocatalysts for methane oxidation.

Controlling the formation of reactive oxygen species (ROS) at the molecular level is crucial for selective CH_4 oxidation, as the

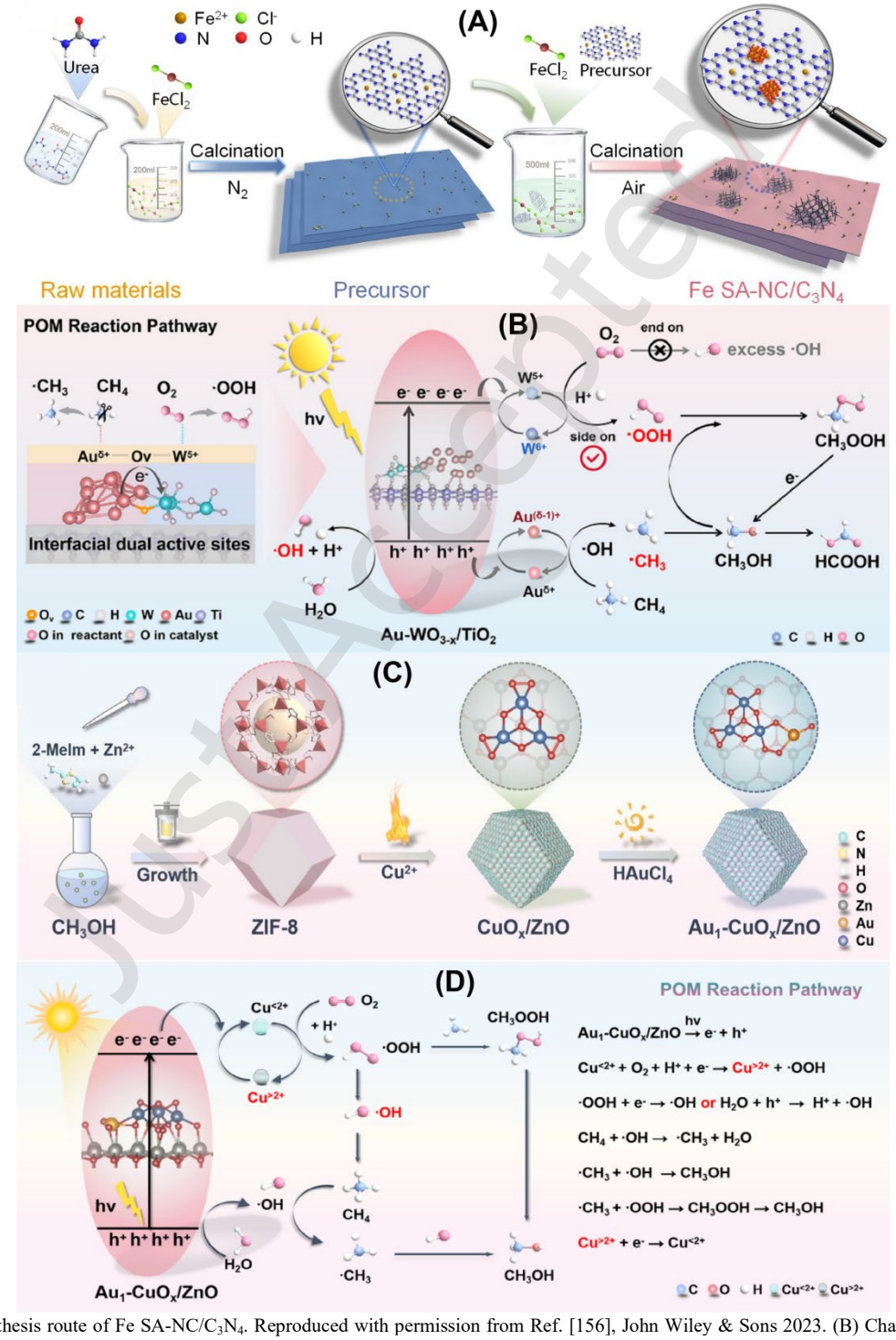

Fig. 11. (A) Synthesis route of Fe SA-NC/C_3N_4. Reproduced with permission from Ref. [156], John Wiley & Sons 2023. (B) Charge separation and migration mechanism of Au–WO_{3-x}/TiO_2 for methane conversion. Reproduced with permission from Ref. [174], Elsevier B.V 2025. (C) Synthesis route and (D) charge trasnfer mechanism of Au_1-CuO_x/ZnO for methane conversion. Reproduced with permission from Ref. [175], John Wiley & Sons 2025.

interplay between active-site electronic structure and ROS intermediates strongly dictates photocatalytic activity and selectivity. To address this challenge, Si et al. engineered the ROS pathways and types by tailoring the electronic environment of

Table 1 performance comparison of different nanoclusters based photocatalysts for different applications.

Reaction	Catalyst	Performance	Stability	Ref.
H_2 evolution	TMCs QDs	440 μmol g^{-1} h^{-1}	8 h	[22]
	$PdPt/TiO_2$	17.4 mmol g^{-1} h^{-1}	18	[23]
	$Ln_{52}Ni_{56-x}Cd_x/CdS$	25353 μmol g^{-1} h^{-1}	40 h	[26]
	Ir/TiO_2	46.0 mmol g^{-1} h^{-1}	25 h	[42]
	$Ag_{44}(SR)_{30}/TiO_2$	7.4 mmol g^{-1} h^{-1}	36 h	[57]
	Ag_{25}@UiO-66-NH_2	3.6 mmol g^{-1} h^{-1}	18 h	[63]
	$\{Ag_{24}(Si_2W_{18}O_{66})_3\}$	98.5 μmol	106 h	[71]
	$Ag/g\text{-}C_3N_4$	1439.77 μmol g^{-1} h^{-1}	24 h	[76]
	Pt-$Cd_xZn_{1-x}S$	270.6 mmol g^{-1} h^{-1}	12 h	[86]
	AuNCs@PDA	3.2 mmol g^{-1} h^{-1}	8 h	[129]
	Pt/TiO_2	45.28 A mg^{-1}	n/a	[155]
Water splitting	$Pt/KCa_2Nb_3O_{10}$	H_2+O_2 (90 μmol)	30 h	[44]
CO_2 reduction	$\{Ag_{27}(Si_2W_{18}O_{66})_3\}$	HCOOH (23.2 μmol)	n/a	[31]
	Co-PONbs	CO/H_2 (21.41/12.99 μmol h^{-1})	15 h	[58]
	Ag_{27}TPyP-Fe	CO (36.5 μmol g^{-1} h^{-1})	150 h	[59]
	CuAu-SAPNPs-TiO_2	CH_4 (748.8 μmol g^{-1} h^{-1})	168 h	[36]
	Fe SA-NC/C_3N_4	CH_3OH (5.02 μmol g^{-1} h^{-1})	900 h	[39]
	$Mo_{22}Cu_{30}$	CO (7370.8 μmol g^{-1} h^{-1})	29 h	[41]
	Au NCs/metal cations	CO (3.45 μmol g^{-1} h^{-1})	9 h	[82]
	Au/MOF	CH_4+H_2 (154.3 μmol g^{-1} h^{-1})	12 h	[29]
	Pd/CeO_2	C_2H_4 (206. 3 μmol g^{-1} h^{-1})	14 h	[109]
	Pt_3Co/Mo_2C	CO (3.68 μmol g^{-1} h^{-1})	25 h	[127]
	111-nuclear $\{Ni_{48}La_{63}\}$	CO (4800 μmol g^{-1} h^{-1})	20 h	[131]
	m-Aminophenol/Au	CO (2645.3 μmol g^{-1} h^{-1})	n/a	[139]
	$(AgCu)_{44}/TiO_2$	CH_4+CO (122.86 μmol g^{-1} h^{-1})	n/a	[144]
	Ag_{44}/CdS	CO (197.02 μmol g^{-1} h^{-1})	12 h	[154]
	MIL-125-NH_2-Au_{25}/g-C_3N_4	CH_3OH (200.2 μmol g^{-1} h^{-1})	24 h	[161]
	Pd/Py-bTDC	CO (17.75 μmol g^{-1} h^{-1})	20 h	[166]
pollutant removal	AuSA-NC/K-PHI	90% in 60 min	100 h	[43]
	Au_{23}@xAg_x(S-Adm)$_{15}$	100% in 19 min	n/a	[54]
	Au/COF	90% in 30 min	5 runs (2.5 h)	[55]
	GP/g-C_3N_4	94.71% in 5 min	5 runs (25 min)	[171]
	$Cu/ZnIn_2S_4$	99.5% in 90 min	5 runs (4.5 h)	[110]
	Ag/Ag_3PO_4	100% in 15 min	3 runs (45 min)	[157]
	CuO/TiO_2	78.42% in 60 min	5 runs (5 h)	[170]
	$Bi/BiVO_4$	84.03% in 30 min	5 runs (2.5 h)	[173]
H_2O_2 production	CsDs/Au	285.4 μmol L^{-1}	12 h	[162]
	DA-LA-Au NCs	1198 μmol L^{-1}	3 h	[163]
	Ag_{27}TPyP-Fe	H_2O_2 (35.9 μmol g^{-1} h^{-1})	-	[59]
	TAPT-2KtTb Pd COF	2676.3 μmol g^{-1} h^{-1}	15 h	[130]
	CoO_x/CN	244.8 μmol g^{-1} h^{-1}	40 h	[158]
CH_4 conversion	Au-WO_3/TiO_2	11698 μmol g^{-1}	10 h	[174]
	Au_1-CuO_x/ZnO	16856 μmol g^{-1}	16 h	[175]
	MoO_x/TiO_2	3.8 mmol g^{-1}	12 h	[176]
	Au-CoO_x/TiO_2	50.8 μmol	20 h	[177]

active sites, breaking the conventional trade-off between activity and selectivity in CH_4 photooxidation to CH_3OH [175]. They designed Au single atoms (SAs) anchored on CuO_x NCs supported on dodecahedral ZnO (Au_1-CuO_x/ZnO) via in situ transformation of a microporous metal-organic framework (MOF) (Fig. 11(C)). This catalyst exhibited remarkable CH_3OH production (~16,856 μmol g^{-1}) with 100% selectivity at room temperature. In situ characterizations and DFT calculations revealed that Au SAs induced an asymmetric electronic structure in Cu centers, causing a rearrangement of Cu 3d orbitals and an upshift of the d-band center. This enhanced the hybridization between Cu sites and the key *OOH intermediate, particularly via d_z^2–p_z and d_{xz}/d_{yz}–p_x orbitals, promoting O–O cleavage to generate *OH rather than direct *OOH desorption, thereby controlling the type of ROS formed. The asymmetric electronic environment also polarized CH_4 molecules, lowering the first C–H dissociation energy and facilitating activation (Fig. 11(D)). Consequently, the generated •OH radicals effectively drive CH_4 oxidation to CH_3OH with exceptional selectivity. This work highlights the pivotal role of orbital engineering in modulating ROS formation and guiding selective intermediate cleavage, establishing a blueprint for designing highly selective photocatalysts for partial methane oxidation.

The volatility of active Mo species at high temperatures (≥500 °C) has limited the practical deployment of Mo-based catalysts in thermocatalytic CH_4 oxidation. Photocatalysis under ambient conditions offers a promising solution. Wu et al. demonstrated that subnanometric MoO_x clusters anchored on TiO_2 can fully expose Mo active sites for selective CH_{44}oxidation with O_2. [176] AC HAADF-STEM and X-ray absorption spectroscopy confirmed the presence of tetrahedral [MoO_4] hexavalent MoO_x clusters, uniformly dispersed on TiO_2. In situ EPR, XPS, and NMR studies revealed a distinct photocatalytic cycle: photogenerated electron–hole pairs are captured by Mo^{6+} sites to form Mo^{4+}/Mo^{5+} centers, which reduce adsorbed O_2 to surface peroxides (Mo–OO). This species promotes CH_4 physisorption and C–H activation while suppressing •OH and O_2•$^-$ formation, thus preventing overoxidation. DFT calculations corroborated that Mo–OO is the reactive site for initial C–H bond cleavage. Consequently, MoO_x–TiO_2 achieved a high C_1 oxygenates yield of 3.8 mmol g^{-1} with nearly 100% selectivity within 2 h of irradiation, corresponding to a 13.3% apparent quantum yield at 365 nm. Long-term tests (1800 min) demonstrated sustained productivity and selectivity (>95%). These findings highlight the role of MoO_x cocatalysts in enhancing carrier separation and directing selective oxidation, providing a rational blueprint for designing efficient, non-noble-metal photocatalysts for CH_4 valorization.

A key limitation of wide-bandgap photocatalysts for CH_4 oxidation is their tendency to overoxidize oxygenated products via highly reactive hydroxyl radicals (•OH) generated from water photo-oxidation. Developing stable photocatalysts that suppress overoxidation while maintaining high selectivity toward oxygenates is therefore crucial. Song et al. reported a dual-cocatalyst system in which TiO_2 was modified with nanometals (Au, Pd, Ag, Pt) and CoO_x NCs for room-temperature CH_4 oxidation to CH_3OH with O_2 [177]. Under light irradiation, nanometals enhance electron–hole separation and promote O_2 reduction, while CoO_x modulates the oxidative sites of the photocatalyst, preventing direct water oxidation to •OH. This strategy effectively suppresses overoxidation of CH_3OH to HCHO and CO_2. The Au–CoO_x/TiO_2 catalyst achieved a maximum yield of CH_3OOH and CH_3OH of 2,540 μmol g^{-1} h^{-1} with 95% selectivity, among the highest reported for low-temperature CH_4 conversion systems. This work demonstrates the potential of dual-cocatalyst design to control reactive oxidative species and stabilize primary oxygenated products, providing a blueprint for selective CH_4 photooxidation under mild conditions.

6. Conclusion and future perspective

Metal NCs embedded within MOFs and COFs have emerged as a transformative class of photocatalytic materials that synergistically combine the precision of molecular clusters with the structural tunability of extended frameworks. Over the past three years, these hybrid systems have demonstrated exceptional promise in light-driven applications, ranging from CO_2 reduction and H_2 evolution, H_2O_2 generation, CH_4 conversion, organic synthesis, and pollutant degradation, Table 1. The integration of atomically defined NCs into porous, highly ordered frameworks enables precise control over electronic states, active-site distribution, and substrate accessibility, providing a versatile platform for tailoring reaction selectivity, energy efficiency, and long-range charge transport. From a synthetic standpoint, significant progress has been achieved in constructing NC–framework hybrids with controlled composition, spatial confinement, and chemical environment. Covalent anchoring of clusters onto functional linkers or nodes, in situ growth of NCs within framework cavities, post-synthetic ion exchange, and encapsulation strategies have all demonstrated the ability to suppress aggregation, enhance stability, and preserve the intrinsic reactivity of NCs. Confinement within well-defined pores not only mitigates sintering but also allows fine-tuning of substrate orientation and diffusion, offering a level of structural control difficult to achieve in unsupported nanoclusters. Simultaneously, engineering the framework itself, through linker modification, defect introduction, topology selection, and electronic tuning, has proven essential for optimizing light absorption, interfacial charge transfer, and mass transport. These complementary strategies collectively provide a modular toolbox for constructing hybrid photocatalysts with tunable function at both local and extended length scales. Despite these advances, several critical challenges remain before NCs–MOF/COF hybrids can reach their full potential [178-180]. Reproducibility of synthetic procedures is a persistent concern, as minor variations in reaction conditions often result in heterogeneous materials with divergent catalytic performance. The long-term stability of these hybrids under operational conditions is another key limitation, with photodegradation of ligands, cluster agglomeration, and framework instability compromising sustained activity. Furthermore, the ultrafast dynamics of photoexcited nanoclusters, including charge separation, recombination, and energy transfer, remain poorly understood, limiting the ability to rationally design systems with predictable performance. The development of robust, high-resolution characterization methods capable of capturing structural and electronic changes under real reaction conditions is therefore essential.

Looking forward, mechanistic insight will be central to advancing the field. Combining advanced operando techniques, such as ultrafast spectroscopy, in situ electron microscopy, X-ray absorption, and synchrotron-based diffraction, with theoretical modeling and machine learning approaches, can provide a detailed understanding of charge migration, active-site evolution, and ligand dynamics during catalysis. Such insight will allow for the rational tuning of NC electronic states, framework conductivity, and interfacial coupling, ultimately leading to systems in which light absorption, charge separation, and catalytic turnover are precisely coordinated. Computational and data-driven strategies can further accelerate materials discovery, helping to identify optimal cluster–framework combinations and predict their performance in diverse photocatalytic reactions.

Expanding the chemical and functional scope of NCs–framework photocatalysts represents another major opportunity. Current applications are predominantly limited to well-established reactions, such as singlet-oxygen-mediated oxidation. Extending NC-catalyzed photocatalysis to more demanding transformations, including C–H activation, selective CO_2 reduction to multi-carbon products, and asymmetric synthesis, will require the development of clusters with high-energy triplet states, enhanced redox potentials, and well-defined stereochemical environments. In particular, enantiopure or chiral NCs integrated into frameworks offer an untapped potential for asymmetric photocatalysis, combining light-driven activation with stereocontrol in a single material.

Sustainability considerations will also play a decisive role in the future development of these hybrids. Most current NC–framework systems rely heavily on noble metals such as Au, Pt, and Ag, which are expensive and scarce, limiting large-scale applications. Moving toward earth-abundant metals, multimetallic alloys, and heteroatom-doped clusters is crucial to reduce costs while maintaining or enhancing photocatalytic efficiency. Equally important is the design of water-compatible, ligand-stabilized NCs, which can improve dispersion, stability, and catalytic performance under aqueous conditions relevant to solar fuel production and environmental remediation. Scalable and reproducible synthetic protocols are essential to translate laboratory discoveries into practical technologies, and efforts should focus on methods that allow precise control over cluster size, stoichiometry, and spatial arrangement while remaining economically viable.

Finally, the integration of NCs with reticular frameworks offers unique opportunities to address long-standing limitations in photocatalysis. By combining atomic-level precision with long-range structural order, these hybrids can simultaneously optimize local electronic effects and macroscopic charge and mass transport. This dual control provides a pathway for designing robust, multifunctional photocatalysts capable of operating under realistic conditions with high efficiency and selectivity. The convergence of advanced synthesis, in situ characterization, and computational design is poised to accelerate the development of these materials, ultimately enabling practical applications in energy conversion, environmental remediation, and synthetic chemistry.

In conclusion, NC–MOF/COF hybrids represent a frontier in photocatalyst design, offering a platform where molecular precision meets structural sophistication. Continued progress will rely on coordinated advances in material synthesis, mechanistic understanding, and performance optimization. By addressing stability, scalability, and sustainability challenges, future research can unlock the full potential of these hybrid systems, paving the way for high-performance, durable, and versatile photocatalysts that meet the demands of energy and environmental technologies.

Acknowledgements

We thank financial support from the National Natural Science Foundation of China (No. 22172167).

Declaration of competing interest

The authors have no competing interests to declare that are relevant to the content of this article.

Author contribution statement

The manuscript was written through contributions of all authors.

References

1. Sanwal, P.; Raza, A.; Miao, Y.; Lumbers, B.; Li, G. Recent advances in coinage metal nanoclusters: From synthesis strategies to electrocatalytic performance. Polyoxometalates 2024, 3, 9140057.
2. Gu, X.; Zhang, J.; Guo, S.; Zhang, Y.; Xu, L.; Jin, R.; Li, G. Tiara Ni Clusters for Electrocatalytic Nitrate Reduction to Ammonia with 97% Faradaic Efficiency. J. Am. Chem. Soc. 2025, 147, 22785.
3. Ahmad, I.; Li, H.; Ahmed, S. B.; Alotaibi, M.T.; Li, G. Shedding light on unprecedented spatial confinement of metal clusters by metal/covalent organic frameworks for photocatalysis. Appl. Phys. Rev. 2025, doi:10.1063/5.0285638.
4. Zhang, J.; Zhang, Y.;. Qin, Z.; Li, Z.; Tong, Z.; Zhao, Z.; Gascón, J. A.; Li, G. How Carbene Ligands Transform AuAg Alloy Nanoclusters for Electrocatalytic Urea Synthesis. Angew. Chem. Int. Ed. 2025, 64, e202420993.
5. Li, Q.; Zhang, Y.; Xu, L.; Chen, H.; Zhang, L.; Khalid, M.S.; Li, Z.; Li, Z.; Li, G. 0D/1D p-n heterostructured composite of bismuth ferrite perovskite clusters on sodium titanate nanotube arouse exceptional blue-light-driven photooxidation. Appl. Catal. B 2025, 361, 124706.
6. Zhang, J.; Gu, X.; Li, G. Robust Metal Nanoclusters for Electrocatalytic Synthesis. Chin. J. Struct. Chem. 2025, 44, 100650.
7. Xiong, Q.; Shi, Q.; Li, Z .; Wang, B.; Baiker, A .;Li, G. Facet-induced reduction directed AgBr/Ag0/TiO2{100} Z-scheme heterojunction for tetracycline removal. Chin. J. Catal., 2025, 75, 164.
8. Ahamd, I.; Babar, Z.; Zhang, Y.; Al-Qattan, A.; Ahmed, S.B.; Li, G. Unlocking sunlight driven photocatalysis: synthesis, diversity, and applications of COF-based S-scheme heterojunction photocatalysts. J. Mater. Chem. A 2025, 13, 15517.
9. Zhang, J.; Zhou, W.; Zhao, J.; Xu, L.; Jiang, X.; Li, Z.; Peng, Y.; Li, G. Intrareticular Exciton Effects Regulate Photocatalytic Activity in Donor–Acceptor Olefin-Linked Covalent Organic Frameworks. Small 2024, 20, 2408324.
10. Ahamd, I.; Li, G.; Abduljawad, M. M.; Alfaifi, M. Q.; Alrashed, Y. I.; Albaqi, F. M. Shedding light on covalent organic framework photocatalysts: Concept, design strategies, and applications-A review. Green Chem. 2025, 27, 7042.
11. Ahmad, I.; Zhang, Y.; Al-Qattan, A.; AlFaify, S. Li, G. Unlocking the Engineering of Solar-driven ZnO Composites: From fundaments to multifield tuning strategies toward sustainable and eco-friendly chemical energy. Chin. J. Struct. Chem. 2025, 44, 100700.
12. Xu, S.; Wang, P.; Zhang, B.; Wang, C.; Low, J.; Ivanov, V. K.; Zhang, Z. Nickel-substituted polyoxometalate-CdS single-cluster photocatalysts for efficient plastic waste degradation coupled with H2 production. *Polyoxometalates* 2025, 4, 9140096.
13. Guo, S.; Pan, C.; Hou, M.; Hou, Y.; Yao, S.; Lu, T.; Zhang, Z. Dual Regulation of Sensitizers and Cluster Catalysts in Metal‐Organic Frameworks to Boost H2 Evolution. Angew. Chem. Int. Ed. 2025, 64, e202420398.

14. Deng, W.; Zhu, Z.; Sun, Y.; Xu, H.; Liu, S; Wen, H. Recent advances in {P4Mo6}-based polyoxometalates. Polyoxometalates 2024, 3, 9140071.
15. Li, Z.; Xie, Y.; Han, Y.; Wang, H.; Gao, J.; Chen, L.; Xu, L,; Lu, L.; Zhao, Y.; Wang, E.; G. Li, Unraveling the Significance of FeN4 and Fe3S4 Active Species for Sustained Direct Ammonia Fuel Cells and Zinc-Air Batteries. Nano Res. Energy 2025, 4, e9120169.
16. Zhang, J.; Busari, F. K.; Zhang, Y.; Guo, S.; Zhao, Y.; Wang, B.; Zeng, Q.; Zhao, Z.; Li, G. RuOx Clusters Anchored on Self-Assembled SnO2 Cubic Nanocage for Boosting Sustainable Acidic Water Oxidation. Nano Res. Energy 2025, 4, e9120140.
17. Zeng, Q.; Zhang, J.; Jadhav, S. M.; Wang, Y.; Li, Z.; Xiao, D.; Li, G. Unraveling the role of MoOx clusters in ternary Mo/Co3NiOx for boosting acidic oxygen-evolution performance. Adv. Sci. 2025, e11456.
18. Zhang, J.; Guo, S.; Li, T.; Zhang, Y.; Zeng, Q.; Sanwal, P.; Xu, L.; G. Li, Unravelling the High-Valence Iridium Single-Atoms on MnCoOx Clusters for Proton Exchange Membrane Water Electrolyzer. Appl. Catal. B 2025, 361, 125518.
19. Li, Z.; Zhang, J.; Qin, Z.; Li, Z.; H.; Tong, Gascón, J. A.; Li, G. Symmetry Breaking in chiral gold nanoclusters by ansa-metallamacrocycles strain. Aggregate 2025, doi: 10.1002/agt2.70168..
20. Ziarati, A.; Gotfredsen, H.; Rosspeintner, A.; Zhao, J.; Anderson, H. L.; Bürgi, T. Encapsulation of an Au_{25} nanocluster inside a porphyrin nanoring enhances singlet oxygen generation and photo-electrocatalytic CO_2 reduction. *Angew. Chem. Int. Ed.* 2025, *64*, e202414908.
21. Liu, L.; Corma, A. Metal catalysts for heterogeneous catalysis: From single atoms to nanoclusters and nanoparticles. *Chem. Rev.* 2018, *118*, 4981.
22. Jin, R.; Li, G.; Sharma, S.; Li, Y.; Du, X. Toward Active-Site Tailoring in Heterogeneous Catalysis by Atomically Precise Metal Nanoclusters with Crystallographic Structures. Chem. Rev. 2021, 121, 567.
23. Sanwal, P.; Zhang, J.; Wang, H.; Babar, Z.; Zhang, Y.; Peng, X.; Li, G. Simultaneous activity and stability gains in PEM electrolyzer via targeted Cr3+ occupation in spinel Co3O4 octahedral lattices. Nano Res. doi: 10.26599/NR.2025.94908133.
24. Gu, X.; Guo, S.; Zhang, Y.; Zhang, J.; Sanwal, P.; Xu, L.; Zhao, Z.; Jin, R.; Li, G. Boosting Oxygen Evolution Performance Over Synergistic Tiara Nickel Clusters and Thin Layered Double Hydroxides. Nano Res. Energy 2024, 3, e9120134.
25. Li, S.; Nagarajan, A. V.; Du, X.; Li, Y.; Liu, Z.; Kauffman, D. R.; Mpourmpakis, G.; Jin, R. Dissecting critical factors for electrochemical CO_2 reduction on atomically precise Au nanoclusters. *Angew. Chem.* 2022, *134*, e202211771.
26. Qin, Z.; Lakra, A.; Somni, R. R.; Peng, W.; Li, G.; Hu, G.; Tong, Z. A Robust Atomically Precise Nanocluster Catalyst for Simultaneously C-O and C-C Bond Cleavage in Lignin Models. ACS Catal. 2025, 15, 20270.
27. Zhang, J.; Xu, L.; Guo, S.; Zhang, Y.; Zhao, Y.; Wu, G.; Li, G. Amorphous MnRuOx Containing Microcrystalline for Enhanced Acidic Oxygen-Evolution Activity and Stability. Angew. Chem. Int. Ed. 2024, 63, e202405641.
28. Irie, T.; Sasaki, K.; Das, S.; Negishi, Y. Materials innovation and the changing face of photocatalytic and electrocatalytic carbon dioxide reduction research: From metal nanoclusters to extended frameworks. *Angew. Chem. Int. Ed.* 2025, e202515667.
29. Jiang, Y.; Yu, Y.; Zhang, X.; Weinert, M.; Song, X.; Ai, J.; Han, L.; Fei, H. N-Heterocyclic carbene-stabilized ultrasmall gold nanoclusters in a metal–organic framework for photocatalytic CO_2 reduction. *Angew. Chem. Int. Ed.* 2021, *60*, 17388.
30. Sanwal, P.; Gu, X.; Zhang, Y.; Li, G. The Tiara Nickel Cluster Story from Theory to Catalytic Applications. Prec. Chem. 2025, 3, 157.
31. Zhang, Y.; Gu, X.; Li, Z.; Miao, Y.; Li, G. Unravelling the Complex Causality behind Sulphur-Ligated Gold Clusters in Acetylene Hydrochlorination. J. Phys. Chem. Lett. 2025, 16, 2314.
32. Isozaki, K.; Iseri, K.; Saito, R.; Ueda, K.; Nakamura, M. Dual catalysis of gold nanoclusters: Photocatalytic cross-dehydrogenative coupling by cooperation of superatomic core and molecularly modified staples. *Angew. Chem. Int. Ed.* 2024, *63*, e202312135.
33. Kamachi, M.; Yonesato, K.; Okazaki, T.; Yanai, D.; Kikkawa, S.; Yamazoe, S.; Ishikawa, R.; Shibata, N.; Ikuhara, Y.; Yamaguchi, K.; Suzuki, K. Synthesis of a gold–silver alloy nanocluster within a ring-shaped polyoxometalate and its photocatalytic property. *Angew. Chem. Int. Ed.* 2024, *63*, e202408358.
34. Hada, A. M.; Zetes, M.; Focsan, M.; Astilean, S.; Craciun, A. M. Photoluminescent histidine-stabilized gold nanoclusters as efficient sensors for fast and easy visual detection of Fe ions in water using paper-based portable platform. *Int. J. Mol. Sci.* 2022, *23*, 12410.
35. Zetes, M.; Hada, A. M.; Todea, M.; Gaina, L. I.; Astilean, S.; Craciun, A. M. Dual-emissive solid-state histidine-stabilized gold nanoclusters for applications in white-light generation. *Nanoscale Adv.* 2023, *5*, 5810.
36. Xie, Z.; Li, L.; Gong, S.; Xu, S.; Luo, H.; Li, D.; Chen, H.; Chen, M.; Liu, K.; Shi, W.; Xu, D. Clustering-resistant Cu single atoms on porous Au nanoparticles supported by TiO_2 for sustainable photoconversion of CO_2 into CH_4. *Angew. Chem. Int. Ed.* 2024, *63*, e202410250.
37. Shang, Y.; Gao, H.; Li, L.; Ma, C.; Gu, J.; Zhu, C.; Yang, Z.; Wang, C.; Zhang, Y.; Chen, G. Green synthesis of fluorescent Ag nanoclusters for detecting Cu^{2+} ions and its "switch-on" sensing application for GSH. *J. Spectrosc.* 2021, 8829654.
38. Saleh, S. M.; El-Sayed, W. A.; El-Manawaty, M. A.; Gassoumi, M.; Ali, R. An eco-friendly synthetic approach for copper nanoclusters and their potential in lead ions sensing and biological applications. *Biosensors* 2022, *12*, 197.
39. Piracha, S.; Gu, X.; Zhang, Y.; Miao, Y.; Li, G. Unlocking New Frontiers in Ultrasmall-Seized Metal Nanoclusters for Boosting Electrochemical Energy Conversions. Chem. Phys. Rev. 2025, 6, 021302.
40. Chen, L.; Chen, G.; Gong, C.; Xing, Z.; Li, J.; Zhang, Y.; Xu, G.; Li, G.; Peng, Y. Unveiling Low-valence Platinum Single Atoms in Sulfur-Containing Covalent Organic Frameworks for Exceptional Photocatalytic Hydrogen Evolution. Nat. Commun. 2024, 15, 10501.
41. Li, Z.; Zhang, J.; Li, G.; Puddephatt, R. J. Self-assembly of the smallest and tightest molecular trefoil knot. Nat. Commun. **2024**, 15, 154.
42. Li, Z.; Xu, M.; Wang, J.; Zhang, Y.; Liu, W.; Gu, X.; Han, Z.; Ye, W.; Li, G. Boosting up Electrosynthesis of Urea with Nitrate and Carbon Dioxide via Synergistic Effect of Metallic Iron Cluster and Single-Atom. Small 2024, 20, 2400036.
43. Zhang, Y.; Gu, X.; Busari, F. K.; Barkaoui, S.; Han, Z.; Baiker, A.; Zhao, Z.; Li, G. Size hierarchy of gold clusters in nanogold-catalyzed acetylene hydrochlorination. Nano Res. **2024**, 17, 9594.
44. Busari, F. K.; Babar, Z.; Raza, A.; Li, G. Unlocking New Frontiers: Boosting up Electrochemical Catalysis with Metal Clusters and Single-Atoms. Sust. Mater. Technol. 2024, 40, e00958.
45. Wang, Y. X.; Zhang, J.; Su, H. F.; Cui, X.; Wei, C. Y.; Li, H.; Zhang, X. M. Photochemical synthesis of atomically precise Ag nanoclusters. *ACS Nano* 2023, *17*, 11607.
46. Wang, Y. X.; Zhang, F. Q.; Qi, Z.; Zhao, X.; Zhang, N.; Li, H.; Li, H.; Zhang, X. M. Photochemical synthesis of $Ag_{12}Cu_7$ nanocluster with cuprophilicity-related long-lived phosphorescence. *Aggregate* 2025, *6*, e675.
47. Fan, J. Q.; Cen, K.; Xu, H. J.; Wang, H. Y.; Yang, Y.; Zhu, Z. M.; Liu, H.; Chen, D.; Fan, W.; Li, M. B. Photochemical synthesis of group 10 metal nanoclusters for electrocatalysis. *Nanoscale* 2023, *15*, 19079.
48. Ferlazzo, A.; Bonforte, S.; Florio, F.; Petralia, S.; Sorace, L.; Muzzi, B.; Caneschi, A.; Gulino, A. Photochemical eco-friendly synthesis of photothermal and emissive copper nanoclusters in water: Toward sustainable nanomaterials. *Mater. Adv.* 2024, *5*, 8034.
49. Zhang, P.; Wang, T.; Chang, X.; Zhang, L.; Gong, J. Synergistic cocatalytic effect of carbon nanodots and Co_3O_4 nanoclusters for the photoelectrochemical water oxidation on hematite. *Angew. Chem.* 2016, *128*, 5945.
50. Li, Z.; Xu, L.; Babar, Z.; Raza, A.; Zhang, Y.; Gu, X.; Miao, Y.; Zhao, Z.; Li, G. Fabrication of MXene-Bi2WO6 heterojunction by Bi2Ti2O7 hinge for extraordinary LED-light-driven photocatalytic performance. Nano Res. 2024, 17, 4729.
51. Li, Z.; Zhang, J.; Li, G. Dynamic assembly of chiral golden knots. Chin. J. Struct. Chem. 2024, 43, 100300.
52. Kang, J.; Gao, P.; Zhang, G.; Shi, L.; Zhou, Y.; Wu, J.; Shuang, S.; Zhang, Y. Rapid sonochemical synthesis of copper nanoclusters with

red fluorescence for highly sensitive detection of silver ions. *Microchem. J.* 2022, *178*, 107370.
53. Liu, W.; Guo, F.; Long, J.; Feng, G.; Huang, M.; Lu, Z. H. Ultrasound-assisted synthesis of highly dispersed nickel nanoclusters on MXene for efficient dehydrogenation of hydrazine borane. *Surf. Interfaces* 2025, *56*, 105563.
54. Zhang, J.; Raz, A.; Zhao, Y.; Guo, S.; Babar, Z.; Xu, L.; Cao, C.; G. Li, Intrinsically Robust Cubic MnCoOx Solid Solution: Achieving High Activity for Sustainable Acidic Water Oxidation. J. Mater. Chem. A 2023, 11, 25345.
55. Shi, Q.; Zhang, X.; Li, Z.; Raza, A.; Li, G. Plasmonic Au Nanoparticle of a Au/TiO2−C3N4 Heterojunction Boosts up Photooxidation of Benzyl Alcohol Using LED Light. ACS Appl. Mater. Interfaces 2023, 15, 30161.
56. Zhang, J.; Wang, H.; Zhang, Y.; Li, Z.; Yang, D.; Zhang, D.; Tsukuda, T.; Li, G. A Revealing insight into gold cluster photocatalysts: Visible versus (vacuum) ultraviolet lights. J. Phys. Chem. Lett. 2023, 14, 4179.
57. Zhang, Y.; Zhang, J.; Li, Z.; Qin, Z.; Sharma, S.; Li, G. Atomically precise copper dopants in metal clusters boost up stability, fluorescence, and photocatalytic activity. Commun. Chem. 2023, 6, 24.
58. Qin, Z.; Li, Z.; Sharma, S.; Peng, Y.; Jin, R.; Li, G. Self-Assembly of silver Clusters into One- and Two-Dimensional Structures and Highly Selective Methanol Sensing. Research 2022, 0018.
59. Qin, Z.; Wang, J.; Sharma, S.; Malola, S.; Wu, K.; Häkkinen, H.; Li, G. Photo-Induced Cluster-to-Cluster Transformation of $[Au_{37-xAgx}(PPh_3)_{13}Cl_{10}]^{3+}$ into $[Au_{25-y}Ag_y(PPh_3)_{10}Cl_8]^{+}$: Fragmentation of A Trimer of 8-Electron Superatoms by Light. J. Phys. Chem. Lett. **2021**, 12, 10920.
60. Qin, Z.; Zhang, J.; Wan, C.; Liu, S.; Abroshan, H.; Jin, R.; Li, G. Atomically Precise Nanoclusters with Reversible Isomeric Transformation for Rotary Nanomotors. Nat. Commun. 2020, 11, 6019.
61. Tan, L.; Li, Y.; Lv, Q.; Gan, Y.; Fang, Y.; Tang, Y.; Wu, L.; Fang, Y. Development of soluble UiO-66 to improve photocatalytic CO_2 reduction. *Catal. Today* 2023, *410*, 282.
62. Shen, H.; Xu, J.; Fu, Z.; Wei, X.; Kang, X.; Shi, W.; Zhu, M. Photoluminescence quenching of hydrophobic Ag_{29} nanoclusters caused by molecular decoupling during aqueous phase transfer and emission recovery through supramolecular recoupling. *Angew. Chem.* 2024, *136*, e202317995.
63. Wang, H.; Zhang, X.; Zhang, W.; Zhou, M.; Jiang, H. L. Heteroatom-doped Ag_{25} nanoclusters encapsulated in metal–organic frameworks for photocatalytic hydrogen production. *Angew. Chem.* 2024, *136*, e202401443.
64. Gu, Y.; Tang, S.; Liu, X.; Liang, X.; Zhu, Q.; Wu, H.; Yang, X.; Jin, W.; Chen, H.; Liu, C.; Zhu, Y. Stability prediction of gold nanoclusters with different ligands and doped metals: Deep learning and experimental tests. *J. Mater. Chem. A* 2024, *12*, 4460.
65. Wang, Y.; Liu, S.; Lile, P.; Norwood, S.; Hernandez, A.; Manna, S.; Mueller, T. Accelerated prediction of atomically precise cluster structures using on-the-fly machine learning. *npj Comput. Mater.* 2022, *8*, 173.
66. Mastracco, P.; González-Rosell, A.; Evans, J.; Bogdanov, P.; Copp, S. M. Chemistry-informed machine learning enables discovery of DNA-stabilized silver nanoclusters with near-infrared fluorescence. *ACS Nano* 2022, *16*, 16322–16331.
67. Rugma, T. P.; Pillay, M. N.; Liu, C. W. Recent developments in atomically precise metal nanocluster-based photocatalysts for hydrogen production. *Dalton Trans.* 2025.
68. Tang, L.; Wang, L.; Wang, B.; Pei, Y.; Wang, S. Discovery of atomically precise metal nanoclusters by high-throughput synthesis platform. *Chem. Eur. J.* 2024, *30*, e202302602.
69. Mao, X.; Wang, L.; Xu, Y.; Wang, P.; Li, Y.; Zhao, J. Computational high-throughput screening of alloy nanoclusters for electrocatalytic hydrogen evolution. *npj Comput. Mater.* 2021, *7*, 46.
70. Chen, Z. L.; Zhu, C.; Zhao, R.; Lu, L.; Li, F.; Zhou, M.; Kang, X.; Xuan, J.; Zhu, M. Nanoclusters as deep-red light-absorbing photocatalysts for laser- or LED-driven Povarov cyclization. *Angew. Chem.* 2025, e19781.
71. Liu, Z.; Qin, Z.; Cui, C.; Luo, Z.; Yang, B.; Jiang, Y.; Lai, C.; Wang, Z.; Wang, X.; Fang, X.; Li, G.; Wang, F.; Xiao, C.; Yang, X. In-Situ Generation and Global Property Profiling of Metal nanoclusters by Ultraviolet Laser Dissociation-Mass Spectrometry. Sci. China Chem. 2022, 65, 1196.
72. Piracha, S.; Batool, S.; Zhang, Y.; Miao, Y.; Li, G.; Hasan, M. Unfolding the Significance of Metal Oxides for Photocatalytic Sustainable Water Splitting Combined with Organic Pollutants. J. Mater. Sci. 2025, 60, 5721.
73. Ahmad, I.; Zhang, J.; Alfaifi, M. Q.; Ahmed, S. B.; Li, G. Solar-driven conversions of plastic waster to valuable chemicals with green hydrogen production. Int. J. Hydrogen Energy, 2025, 149, 150149.
74. Zhang, Y.; Ahmad, I.; Khalid, M. S.; Li, H.; Miao, Y.; Li, G. Zhen Zhao, Type II heterojunction of spinel ferrite-anchored titanate nanotubes for blue-light-driven photocatalytic oxidation. J. Alloys Comp. 2025, 1010, 184012.
75. Shi, H.; Shi, Q.; Pirach, S.; Li, G. Stannum Vacancies at Precise Interface of 2D/2D g-C3N4/SnS S-Scheme Heterojunction Boost up Photocatalysis. J. Mater. Chem. A 2024, 12, 20270.
76. Xie, Z.; Wang, C.; Wu, F.; Hu, R.; Zhang, J.; Du, H.; Zhang, S.; Zhou, Y. Loading silver nanoclusters onto g-C_3N_4 by formamide-assisted in situ strategy to achieve efficient photocatalytic water splitting for hydrogen production. *J. Photochem. Photobiol. A* 2025, *462*, 116275.
77. Zhang, Y.; Li, Z.; Zhang, J.; Xu, L.; Han, Z.; Baiker, A.; Li, G. Nanostructured Ni-MoCx: An Efficient Non-Noble Metal Catalyst for the Chemoselective Hydrogenation of Nitroaromatics. Nano Res. **2023**, 16, 8919.
78. Li, S.; Du, X.; Liu, Z.; Li, Y.; Shao, Y.; Jin, R. Size effects of atomically precise gold nanoclusters in catalysis. *Precision Chem.* 2023, *1*, 14.
79. Busi, K. B.; Majji, M.; Krishna, A. M. S.; Ball, W. B.; Dalapati, G. K.; Motapothula, M. R.; Chakrabortty, S. Effect of surface ligands on the photocatalytic hydrogen production of Cu nanoclusters. *Int. J. Hydrogen Energy* 2025, *116*, 279.
80. Shi, Q.; Zhang, Y.; Li, Z.; Han, Z.; Xu, L.; Baiker,A.; G. Li, Morphology Effects in MnCeOx solid solution-catalyzed NO reduction with CO: active sites, water tolerance, and reaction pathway. Nano Res. **2023**, 16, 6951.
81. Li, S.; Nagarajan, A. V.; Du, X.; Li, Y.; Liu, Z.; Kauffman, D. R.; Mpourmpakis, G.; Jin, R. Dissecting critical factors for electrochemical CO_2 reduction on atomically precise Au nanoclusters. *Angew. Chem.* 2022, *134*, e202211771.
82. Liu, X.; Zhang, Y.; Li, Z.; Li, G.; Taherkhani, F. Surface ligand engineering on the optical properties of atomically precise AuAg nanoclusters. Chin. J. Struct. Chem. 2023, 42, 100154.
83. Xu, C.; Pan, Y.; Wan, G.; Liu, H.; Wang, L.; Zhou, H.; Yu, S.-H.; Jiang, H.-L. Turning on visible-light photocatalytic C–H oxidation over metal–organic frameworks by introducing metal-to-cluster charge transfer. *J. Am. Chem. Soc.* 2019, *141*, 19110.
84. Yu, C.; Li, G.; Kumar, S.; Kawasaki, H.; Jin, R. Stable $Au_{25}(SR)_{18}/TiO_2$ composite nanostructure with enhanced visible-light photocatalytic activity. *J. Phys. Chem. Lett.* 2013, *4*, 2847.
85. Alotaibi, M. F.; Sagadevan, A.; Yuan, P.; Bodiuzzaman, M.; Murugesan, K.; Zhou, R.; Yin, J.; Thomas, S.; Huang, R. W.; Halappa, M. N.; Dong, C. Unshielded ino-decahedral core copper nanoclusters enable efficient photocatalytic sulfonylation of aryl halides. *J. Am. Chem. Soc.* 2025, *147*, 28932.
86. Liu, F.; Wang, Y.; Zhang, C.; Li, Z.; Ma, X.; Liu, M. Pt sub-nanoclusters on ZIF-derived ultrafine $Cd_xZn_{1-x}S$ solid solution: High-performance photoreforming lactic acid to H_2 and value-added chemicals. *Electron.* 2025, e70024.
87. Yamazaki, Y.; Tomoyasu, Y.; Kawawaki, T.; Negishi, Y. Activation of photocatalytic CO_2 reduction by loading hydrophobic thiolate-protected Au_{25} nanocluster cocatalyst. *Nanoscale Adv.* 2025, *7*, 1518.
88. Zhao, J.; Ziarati, A.; Rosspeintner, A.; Bürgi, T. Anchoring of metal complexes on Au_{25} nanocluster for enhanced photocoupled electrocatalytic CO_2 reduction. *Angew. Chem. Int. Ed.* 2024, *63*, e202316649.
89. Liu, Z.; Wang, Y.; Ji, W.; Ma, X.; Gianopoulos, C. G.; Calderon, S.; Ma, T.; Luo, L.; Mazumder, A.; Kirschbaum, K.; Dickey, E. C. Generalizable organic-to-aqueous phase transfer of a Au_{18} nanocluster with luminescence enhancement and robust photocatalysis in water. *ACS Nano* 2025, *19*, 9121.
90. Zhao, H.; Zhang, C.; Han, B. L.; Mahato, P.; Yang, C. Z.; Yu, P. X.; Wang, Z.; Tung, C.-H.; Sun, D. Gram-scale synthesis of an ultrastable 38-nuclei copper(I) alkynide nanocluster for unraveling bifunctional photocatalysis. *Nano Lett.* 2025, in press.

91. Li, P.; Zhao, Z.; Tian, L.; Liu, R.; Wang, X.; Yang, W.; Cui, Y. S.; Humphrey, M. G.; Zhang, C.; Hu, K. Harnessing the potent excited-state reductive power of pyrene-modified N-heterocyclic carbene-stabilized Au_{13} nanoclusters for four-electron nitroarene reduction with unity selectivity. *J. Am. Chem. Soc.* 2025, in press.
92. Higaki, T.; Liu, C.; Morris, D. J.; He, G.; Luo, T. Y.; Sfeir, M. Y.; Zhang, P.; Rosi, N. L.; Jin, R. $Au_{130-x}Ag_x$ nanoclusters with non-metallicity: A drum of silver-rich sites enclosed in a Marks-decahedral cage of gold-rich sites. *Angew. Chem. Int. Ed.* 2019, *58*, 18798.
93. Biswas, S.; Das, S.; Negishi, Y. Progress and prospects in the design of functional atomically precise Ag(I)-thiolate nanoclusters and their assembly approaches. *Coord. Chem. Rev.* 2023, *492*, 215255.
94. Negishi, Y.; Iwai, T.; Ide, M. Continuous modulation of electronic structure of stable thiolate-protected Au_{25} cluster by Ag doping. *Chem. Commun.* 2010, *46*, 4713.
95. Bootharaju, M. S.; Joshi, C. P.; Parida, M. R.; Mohammed, O. F.; Bakr, O. M. Templated atom-precise galvanic synthesis and structure elucidation of a $[Ag_{24}Au(SR)_{18}]^-$ nanocluster. *Angew. Chem.* 2016, *128*, 934.
96. Zheng, Z. H.; Xiao, F. X.; Xu, Y. J. Atomically precise alloy nanoclusters steering photocatalysis. *Small* 2025, *21*, 2505282.
97. Chen, A.; Yin, B.; Huang, B.; Liu, Y.; Chen, S.; Pei, Y.; Zhu, M. Insight into the mechanism of single-metal-atom tailoring on the surface of Au–Cu alloy nanoclusters. *J. Phys. Chem. Lett.* 2022, *13*, 4139.
98. Li, X.; Ajmal, S.; Fang, P.; Zhou, X.; Lu, M.; Li, S.; Chen, P.; Li, P.; Zhu, M. Ultrafine low-loading AgCu nanoclusters supported on defective ZIF-8 for the click reaction with high stability. *New J. Chem.* 2024, *48*, 13859.
99. Liu, L. J.; He, J. Atomically precise coinage metal nanocluster photocatalysts: Recent advances in organic synthesis. *Aggregate* 2025, e70226.
100. Zheng, K.; Zhang, J.; Zhao, D.; Yang, Y.; Li, Z.; Li, G. Motif-mediated $Au_{25}(SPh)_5(PPh_3)_{10}X_2$ nanorods with conjugated electron delocalization. *Nano Res.* 2019, *12*, 501.
101. Kwak, K.; Choi, W.; Tang, Q.; Kim, M.; Lee, Y.; Jiang, D. E.; Lee, D. A molecule-like $PtAu_{24}(SC_6H_{13})_{18}$ nanocluster as an electrocatalyst for hydrogen production. *Nat. Commun.* 2017, *8*, 14723.
102. Hirai, H.; Takano, S.; Nakashima, T.; Iwasa, T.; Taketsugu, T.; Tsukuda, T. Doping-mediated energy-level engineering of $M@Au_{12}$ superatoms (M = Pd, Pt, Rh, Ir) for efficient photoluminescence and photocatalysis. *Angew. Chem. Int. Ed.* 2022, *61*, e202207290.
103. Mymoona, P.; Rival, J. V.; Nonappa; Shibu, E. S.; Jeyabharathi, C. Platinum-grafted twenty-five atom gold nanoclusters for robust hydrogen evolution. *Small* 2024, *20*, 2308610.
104. Shen, H.; Mizuta, T. An atomically precise alkynyl-protected $PtAg_{42}$ superatom nanocluster and its structural implications. *Chem. Asian J.* 2017, *12*, 2904.
105. Chiu, T. H.; Liao, J. H.; Gam, F.; Chantrenne, I.; Kahlal, S.; Saillard, J. Y.; Liu, C. W. All-selenolate-protected eight-electron platinum/silver nanoclusters. *Nanoscale* 2021, *13*, 12143–12148.
106. Lin, X.; Sun, K.; Fu, X.; Ren, X.; Yang, Y.; Liu, C.; Huang, J. Correlating kernel–shell structures with optical properties of Pt_1Ag_{24} and Pt_1Ag_{14} nanoclusters. *J. Phys. Chem. C* 2021, *125*, 2194–2201.
107. Wang, M.; Li, S.; Tang, X.; Zuo, D.; Jia, Y.; Guo, S.; Guan, Z. J.; Shen, H. One-step preparation of Pt/Ag nanoclusters for CO_2 transformation. *Phys. Chem. Chem. Phys.* 2023, *25*, 30373–30380.
108. Du, X. L.; Wang, X. L.; Li, Y. H.; Wang, Y. L.; Zhao, J. J.; Fang, L. J.; Zheng, L. R.; Tong, H.; Yang, H. G. Isolation of single Pt atoms in a silver cluster: Forming highly efficient silver-based cocatalysts for photocatalytic hydrogen evolution. *Chem. Commun.* 2017, *53*, 9402–9405.
109. Zhang, X.; Li, Z.; Pei, W.; Li, G.; Liu, W.; Du, P.; Wang, Z.; Qin, Z.; Qi, H.; Liu, X.; Zhou, S.; Zhao, J.; Yang, B.; Shen, W. Crystal Phase Mediated Restructuring of Pt on TiO2 with Tunable Reactivity: Redispersion versus Reshaping. ACS Catal. 2022, 12, 3634.
110. Raza, A.; Rafi, A. A.; Hassan, J.; Rafiq, A.; Li, G. Rational design of 2D heterostructured photo- & electro-catalysts for hydrogen evolution reaction: A Review. Appl. Surf. Sci. Adv. 2023, 15, 100402.
111. Wang, S.; Tang, L.; Cai, B.; Yin, Z.; Li, Y.; Xiong, L.; Kang, X.; Xuan, J.; Pei, Y.; Zhu, M. Ligand modification of Au_{25} nanoclusters for near-infrared photocatalytic oxidative functionalization. *J. Am. Chem. Soc.* 2022, *144*, 3787–3792.
112. Isozaki, K.; Ueno, R.; Ishibashi, K.; Nakano, G.; Yin, H.; Iseri, K.; Sakamoto, M.; Takaya, H.; Teranishi, T.; Nakamura, M. Gold nanocluster functionalized with peptide dendron thiolates: Acceleration of the photocatalytic oxidation of an amino alcohol in a supramolecular reaction field. *ACS Catal.* 2021, *11*, 13180–13187.
113. Isozaki, K.; Iseri, K.; Saito, R.; Ueda, K.; Nakamura, M. Dual catalysis of gold nanoclusters: Photocatalytic cross-dehydrogenative coupling by cooperation of superatomic core and molecularly modified staples. *Angew. Chem. Int. Ed.* 2024, *63*, e202312135.
114. Liu, Y.; Wierzbicka, E.; Springer, A.; Pinna, N.; Wang, Y. Influence of the electronic properties of the ligand on the photoelectrochemical behavior of Au_{25} nanocluster-sensitized TiO_2 photoanode. *J. Phys. Chem. C* 2022, *126*, 1778–1784.
115. Zeng, C.; Chen, Y.; Kirschbaum, K.; Lambright, K. J.; Jin, R. Emergence of hierarchical structural complexities in nanoparticles and their assembly. *Science* 2016, *354*, 1580–1584.
116. Bera, D.; Mahata, S.; Biswas, M.; Kumari, K.; Rakshit, S.; Nonappa; Ghosh, S.; Goswami, N. Efficient photocatalytic hydrogen production using in situ polymerized gold nanocluster assemblies. *Small* 2025, *21*, 2406551.
117. Gong, X.; Shi, Q.; Zhang, X.; Li, J.; Ping, G.; Xu, H.; Ding, H.; Li, G. Synergistic Effects of PtFe/CeO2 Catalyst afford high Catalytic Performance in selective hydrogenation of cinnamaldehyde. J. Rare Earths 2023, 41, 233e239.
118. Zhou, Y.; Gu, W.; Wang, R.; Zhu, W.; Hu, Z.; Fei, W.; Zhuang, S.; Li, J.; Deng, H.; Xia, N.; He, J. Controlled sequential doping of metal nanoclusters. *Nano Lett.* 2024, *24*, 2226–2233.
119. Liu, H.; Li, K.; Li, F.; Zhao, Y.; Fan, W.; Pei, Y.; Li, M. B. Cobalt-kernelled icosahedral gold nanocluster. *Chin. Chem. Lett.* 2025, 111230.
120. Wang, H.; Zhang, X.; Zhang, W.; Zhou, M.; Jiang, H. L. Heteroatom-doped Ag_{25} nanoclusters encapsulated in metal–organic frameworks for photocatalytic hydrogen production. *Angew. Chem.* 2024, *136*, e202401443.
121. Liu, Y.; Long, D.; Springer, A.; Wang, R.; Koch, N.; Schwalbe, M.; Pinna, N.; Wang, Y. Correlating heteroatoms doping, electronic structures, and photocatalytic activities of single-atom-doped $Ag_{25}(SR)_{18}$ nanoclusters. *Solar RRL* 2023, *7*, 2201057.
122. Wu, G.; Mo, Q. L.; Xiao, Y.; Wang, K.; Ge, X. Z.; Xu, S. R.; Li, J. L.; Shao, Y. Q.; Xiao, F. X. Alloy metal nanocluster: A robust and stable photosensitizer for steering solar water oxidation. *Inorg. Chem.* 2022, *62*, 520–529.
123. Qin, Z.; Zhao, D.; Zhao, L.; Xiao, Q.; Wu, T.; Zhang, J.; Wan, C.; Li, G. Tailoring the stability, photocatalysis and photoluminescence properties of Au_{11} nanoclusters via doping engineering. *Nanoscale Adv.* 2019, *1*, 2529–2536.
124. Y. Wang, X.-H. Liu, Q. Wang, M. Quick, S. A. Kovalenko, Q.-Y. Chen, N. Koch and N. Pinna, Angew. Chem., Int. Ed., 2020, 59, 7748–7754.
125. Hassan, J.; Zaheer, A.; Raza, A.; Li, G. Au-Based Heterostructure Composites for Photo and Electro Catalytic Energy Conversions. Sust. Mater. Technol. 2023, 36, e00609.
126. Shi, Q.; Zhang, X.; Liu, X.; Xu, L.; Liu, B.; Zhang, J.; Xu, H.; Han, Z.; Li, G. In-situ exfoliation and assembly of 2D/2D g-C3N4/TiO2(B) hierarchical microflower: Enhanced photo-oxidation of benzyl alcohol under visible light. Carbon 2022, 195, 401.
127. Shi, Q.; Ping, G.; Wang, X.; Xu, H.; Li, J.; Cui, J.; Abroshan, H.; Ding, H.; Li, G. CuO/TiO2 Heterojunction Composite: An Efficient Photocatalyst for Selective Oxidation of Methanol to Methyl Formate. J. Mater. Chem. A 2019, 7, 2253.
128. Darkwah, W. K.; Appiagyei, A. B.; Kofie, S. N.; Twum Akrofi, S.; Anang, D. A.; Teye, G. K.; Puplampu, J. B. Single-atom and

nanocluster photocatalysts for hydrogen peroxide synthesis under visible light. *ACS Eng. Au* 2025, *5*, 70–88.
129. Bera, D.; Mahata, S.; Biswas, M.; Kumari, K.; Rakshit, S.; Nonappa; Ghosh, S.; Goswami, N. Efficient photocatalytic hydrogen production using in situ polymerized gold nanocluster assemblies. *Small* 2025, *21*, 2406551.
130. Zhou, J.; Chen, J.; Li, N.; Gou, F.; Yang, Z.; Zeng, M.; Shao, M. Covalent organic frameworks with constrained palladium nanoclusters lock the enol–keto tautomerism enhancing hydrogen peroxide photosynthesis. *Small* 2025, *21*, 2409006.
131. Bai, K. P.; Wu, C.; Lu, J. T.; Chen, W. P.; Cui, M. D.; Zheng, Y. Z. Assembling giant nanoclusters as heterogeneous catalysts for effectively converting CO_2 to CO under visible light. *Small* 2025, *21*, 2412630.
132. Tian, J.; Zhong, K.; Zhu, X.; Yang, J.; Mo, Z.; Liu, J.; Dai, J.; She, Y.; Song, Y.; Li, H.; Xu, H. Highly exposed active sites of Au nanoclusters for photocatalytic CO_2 reduction. *Chem. Eng. J.* 2023, *451*, 138392.
133. Xiong, Y.; Chen, H.; Hu, Y.; Yang, S.; Xue, X.; He, L.; Liu, X.; Ma, J.; Jin, Z. Photodriven catalytic hydrogenation of CO_2 to CH_4 with nearly 100% selectivity over Ag_{25} clusters. *Nano Lett.* 2021, *21*, 8693–8700.
134. Feng, Y.; Fu, F.; Zeng, L.; Zhao, M.; Xin, X.; Liang, J.; Zhou, M.; Fang, X.; Lv, H.; Yang, G. Y. Atomically precise silver clusters stabilized by lacunary polyoxometalates with photocatalytic CO_2 reduction activity. *Angew. Chem. Int. Ed.* 2024, *63*, e202317341.
135. Dong, J. P.; Xu, Y.; Zhang, X. G.; Zhang, H.; Yao, L.; Wang, R.; Zang, S. Q. Copper–sulfur–nitrogen cluster providing a local proton for efficient carbon dioxide photoreduction. *Angew. Chem.* 2023, *135*, e202313648.
136. Li, Z.; Huang, W.; Liu, J.; Lv, K.; Li, Q. Embedding CdS@Au into ultrathin $Ti_{3-x}C_2T_y$ to build dual Schottky barriers for photocatalytic H_2 production. *ACS Catal.* 2021, *11*, 8510–8520.
137. Yu, C.; Li, G.; Kumar, S.; Kawasaki, H.; Jin, R. Stable $Au_{25}(SR)_{18}/TiO_2$ composite nanostructure with enhanced visible-light photocatalytic activity. *J. Phys. Chem. Lett.* 2013, *4*, 2847–2852.
138. Qi, X.; Xie, Y. L.; Niu, J. Y.; Zhao, J. W.; Li, Y. M.; Fang, W. H.; Zhang, J. Application of hard and soft acid–base theory to construct heterometallic materials with metal–oxo clusters. *Angew. Chem. Int. Ed.* 2025, *64*, e202417548.
139. Li, L.; Li, Z.; Li, J.; Wang, J.; Xu, H.; Yu, H.; Lin, Q.; Huang, H.; Liu, Y.; Kang, Z. Isomer effects of aminophenol-decorated gold nanoclusters for H_2O_2 photoproduction via two-step one-electron oxygen reduction reaction. *Small* 2025, *21*, 2410843.
140. Yan, X.; Zheng, B. X.; Zhu, J. R.; Li, Y. B.; Xiao, F. X. Spatially confining atomically precise metal nanoclusters steers photoredox organic transformation. *Inorg. Chem.* 2025, *64*, 3572–3581.
141. Alotaibi, M. F.; Sagadevan, A.; Yuan, P.; Bodiuzzaman, M.; Murugesan, K.; Zhou, R.; Yin, J.; Thomas, S.; Huang, R. W.; Halappa, N. M.; Dong, C. Unshielded ino-decahedral core copper nanoclusters enable efficient photocatalytic sulfonylation of aryl halides. *J. Am. Chem. Soc.* 2025, *147*, 28932–28942.
142. Addanki Tirumala, R. T.; Gyawali, S.; Le, T.; Kumar, S.; Tan, S.; Wang, B.; Bristow, A. D.; Andiappan, M. Visible-light-driven photocatalytic carbon–carbon coupling reaction under atmospheric temperature and pressure conditions using hybrid Cu_2O–Pd nanostructures. *ACS Appl. Mater. Interfaces* 2025, *17*, 26651–26660.
143. Ueda, K.; Saito, R.; Iseri, K.; Sekiya, S.; Nakamura, M.; Isozaki, K. Accelerated catalysis of atomically precise thiolate-protected gold nanoclusters by supramolecular ligand engineering. *ACS Catal.* 2025, *15*, 12260–12268.
144. Liu, Y.; Zheng, X.; Liu, X.; Gao, T.; Pinna, N.; Wang, Y. Copper doping enhances the activity and selectivity of atomically precise Ag_{44} nanoclusters for photocatalytic CO_2 reduction. *Adv. Funct. Mater.* 2025, e03708.
145. Xu, H.; Liu, X.; Zhou, G.; Bi, C.; Liu, Q.; Jiang, W.; Wang, B.; Zhu, X.; Chu, P. K.; Wang, X. Controlled photocatalytic reduction of CO_2 by precise atomic-level interface modification and engineering of silver nanoclusters. *Adv. Sci.* 2025, e16096.
146. Wang, S. Q.; Wang, X.; Cheng, X. M.; Ma, J.; Sun, W. Y. Tailoring defect-type and ligand-vacancies in Zr(IV) frameworks for CO_2 photoreduction. *J. Mater. Chem. A* 2022, *10*, 16396–16402.
147. Ma, W.; Sun, J.; Yao, S.; Wang, Y.; Chen, G.; Fan, G.; Li, Y. Synergistic interplay of dual active sites on metallic Ni-MOFs loaded with Pt for thermal–photocatalytic conversion of atmospheric CO_2 under infrared light irradiation. *Angew. Chem. Int. Ed.* 2023, *62*, e202313784.
148. Tan, L.; Li, Y.; Lv, Q.; Gan, Y.; Fang, Y.; Tang, Y.; Wu, L.; Fang, Y. Development of soluble UiO-66 to improve photocatalytic CO_2 reduction. *Catal. Today* 2023, *410*, 282–288.
149. Rakshitha, R.; Sinchana, H. C.; Pallavi, N. Assessing the effectiveness of coprecipitation-assisted ZnS/C nanoclusters in the photocatalytic decomposition of 2,4-dichlorophenoxyacetic acid herbicide. *World J. Environ. Biosci.* 2025, *14*, 1–9.
150. Ke, J.; Jiang, L.; Sun, Q.; Wu, S.; Zheng, H.; Ye, J.; Zheng, H.; Zhong, Y.; Huang, D.; Wu, Y.; Wang, B. BPEI-stabilized photocatalytic Au/TiO_2 nanoclusters with enhanced antimicrobial activity for wound healing applications. *Int. J. Nanomedicine* 2025, 11197–11210.
151. Yao, A.; Du, Y.; Han, M.; Wang, Y.; Hu, J.; Zhu, Q.; Sheng, H.; Zhu, M. Covalence-bridged atomically precise metal nanocluster–metal–organic framework hybrids for enhanced photostability and photocatalysis. *Nano Res.* 2023, *16*, 1527–1532.
152. Xu, Y.; Dong, Q. G.; Dong, J. P.; Zhang, H.; Li, B.; Wang, R.; Zang, S. Q. Assembly of copper clusters into a framework: enhancing structural stability and photocatalytic HER performance. *Chem. Commun.* 2023, *59*, 3067–3070.
153. Fu, Y.; Zhu, X.; Huang, L.; Zhang, X.; Zhang, F.; Zhu, W. Azine-based covalent organic frameworks as metal-free visible-light photocatalysts for CO_2 reduction with H_2O. *Appl. Catal. B: Environ.* 2018, *239*, 46–51.
154. Ning, J.; Niu, Q.; Liu, Z.; Li, L. Aerobic oxidation of a covalent organic framework facilitating photocatalytic CO_2 reduction with water. *Green Chem.* 2025, *27*, 6804–6812.
155. Wei, Z. W.; Wang, H. J.; Zhang, C.; Xu, K.; Lu, X. L.; Lu, T. B. Reversed charge transfer and enhanced hydrogen spillover in platinum nanoclusters anchored on titanium oxide with rich oxygen vacancies boost hydrogen evolution reaction. *Angew. Chem.* 2021, *133*, 16758–16763.
156. Nematulloev, S.; Sagadevan, A.; Alamer, B.; Shkurenko, A.; Huang, R.; Yin, J.; Dong, C.; Yuan, P.; Yorov, K. E.; Karluk, A. A.; Mir, W. J. Atomically precise defective copper nanocluster catalysts for highly selective C–C cross-coupling reactions. *Angew. Chem. Int. Ed.* 2023, *62*, e202303572.
157. Liu, X.; Xu, J.; Zhang, T.; Zhang, J.; Xia, D.; Du, Y.; Jiang, Y.; Lin, K. Construction of Ag nanocluster-modified Ag_3PO_4 containing silver vacancies via in situ reduction for enhanced photocatalytic degradation of sulfamethoxazole. *J. Colloid Interface Sci.* 2023, *629*, 989–1002.
158. Hou, J.; Wang, K.; Zhang, X.; Wang, Y.; Su, H.; Yang, C.; Zhou, X.; Liu, W.; Hu, H.; Wang, J.; Li, C. Synergistic defect sites and CoO_x nanoclusters in polymeric carbon nitride for enhanced photocatalytic H_2O_2 production. *ACS Catal.* 2024, *14*, 10893–10903.
159. Yamazaki, Y.; Tomoyasu, Y.; Kawawaki, T.; Negishi, Y. Activation of photocatalytic CO_2 reduction by loading hydrophobic thiolate-protected Au_{25} nanocluster cocatalyst. *Nanoscale Adv.* 2025, *7*, 1518–1523.
160. Lu, R.; Yao, A.; Dai, Y.; Yin, H.; Li, C.; Du, Y.; Zhu, M. Atomically precise metal nanocluster sandwich heterojunction for robust and efficient photocatalytic CO_2 reduction to methanol. *Inorg. Chem. Front.* 2025.
161. 161. Wang, Q. F.; Jia, M. Q.; Yin, X. Y.; Zheng, S.; Yang, W. X.; Ma, C.; Ni, L. B.; Diao, G. W.; Zhang, L. N. Cobalt nanoparticles coupled with polyoxometalate nanoclusters to boost electrocatalytic conversion of nitrite to ammonia at low potentials. *Inorg. Chem. Front.* 2026.
162. Li, Z.; Li, J.; Wang, J.; Li, L.; Yuan, W.; Zhang, T.; Shen, J.; Ma, Y.; Fan, Z.; Liao, F.; Huang, H. Operando interfacial kinetic study of H_2O_2 photoproduction over carbon dots stabilized gold nanoclusters. *Appl. Catal. B: Environ. Energy* 2025, *361*, 124679.

163. Liu, K.; Wang, Z.; Xie, Y.; Wei, Y.; Liu, W.; Feng, T.; Liu, Y.; Zhu, H.; Yuan, X. Bioinspired pathway engineering in Au nanoclusters: Dopamine ligands as molecular switches for exclusive photocatalytic H_2O_2 generation. *Chin. Chem. Lett.* 2025, 111701.
164. Ke, J.; Jiang, L.; Sun, Q.; Wu, S.; Zheng, H.; Ye, J.; Zheng, H.; Zhong, Y.; Huang, D.; Wu, Y.; Wang, B. BPEI-stabilized photocatalytic Au/TiO_2 nanoclusters with enhanced antimicrobial activity for wound healing applications. *Int. J. Nanomedicine* 2025, 11197–11210.
165. Patra, A.; Shinde, K.; Mandal, S.; Kudlu, A.; Si, W. D.; Francis, M.; Das, A.; Sun, D.; Roy, S. Bulky (imino)phosphide- and mixed bis(dimethylsiloxane)/(imino)phosphide-supported redox-active Cu_5 and Cu_6 nanoclusters: Luminescence and photocatalytic studies. *Inorg. Chem.* 2025, *64*, 20666–20678.
166. Lin, Y.; Lai, X.; Huang, G.; Luo, J.; Chen, Q.; Huang, G.; Bi, J. Spatial confinement of Pd nanoclusters in pyrene-based covalent organic frameworks for boosting photocatalytic CO_2 reduction. *Chem.–Eur. J.* 2025, *31*, e202500766.
167. Cai, L.; Cai, Y. S.; Zhao, W.; Liang, J.; Chen, Q.; Xiao, F. X. Coupling transition metal chalcogenides with metal nanoclusters for steering photoredox catalysis. *Inorg. Chem.* 2025, in press.
168. Li, Y. B.; Xiao, F. X. Surmounting the instability of atomically precise metal nanoclusters toward boosted photoredox organic transformation. *Chem. Sci.* 2025, *16*, 2661–2672.
169. Zheng, B. X.; Yuan, J. N.; Su, P.; Yan, X.; Chen, Q.; Yuan, M.; Xiao, F. X. Alloy nanocluster artificial photosystems steering photoredox organic transformation. *J. Mater. Chem. A* 2025, *13*, 4908–4920.
170. Zhang, Y.; Liu, Y.; Bai, W.; Zhang, Z.; Zhang, J.; Li, D.; Feng, L. In situ self-growing CuO nanoclusters on titanium dioxide for high-efficient photocatalytic degradation of norfloxacin under visible light. *Inorg. Chem. Commun.* 2025, *178*, 114524.
171. Jin, H.; Zhu, M.; Nie, C.; Liu, J.; Hong, K.; Li, C.; Wang, Q. In situ interspersed geopolymer nanoclusters on nitrogen-defective g-C_3N_4 to promote the matching of adsorption and photocatalytic kinetics. *Surf. Interfaces* 2025, *60*, 106050.
172. Wang, Y.; Ben, J.; Guan, H.; Hu, X.; Ye, Y.; Hu, Y.; Zhou, P.; Wu, L. Rapid photocatalytic dechlorination of polychlorinated biphenyls by Cu nanocluster-modified $ZnIn_2S_4$. *Surf. Interfaces* 2025, 107430.
173. Cheng, Y.; Yu, T.; Zheng, C.; Lei, X.; Li, J.; Liu, X.; Guo, R. Bi nanoclusters construction and oxygen vacancy engineering for enhanced piezo-photocatalytic degradation performance of $BiVO_4$. *Chem. Eng. J.* 2025, 167714.
174. Si, F.; Wang, G.; Lv, M.; Bai, J.; Li, Y.; Hou, T.; Li, Y. Interfacial dual active centers bridged by oxygen vacancies promoting photocatalytic oxidation of methane. *Appl. Catal. B: Environ. Energy* 2025, *365*, 124934.
175. Si, F.; Bai, J.; Li, Y.; Lan, R.; Cheng, S.; Hou, T.; Li, Y. Regulating reactive oxygen species via orbital rehybridization between intermediate and active site for selective methane photooxidation to methanol. *Angew. Chem. Int. Ed.* 2025, *64*, e202505267.
176. Wu, P.; Chu, Y.; Wang, M.; Feng, N.; Xu, J.; Ma, D.; Ye, J.; Deng, F. Subnanometric MoO_x clusters limit overoxidation during photocatalytic CH_4 conversion to oxygenates over TiO_2. *Nat. Commun.* 2025, *16*, 4207.
177. Song, H.; Meng, X.; Wang, S.; Zhou, W.; Song, S.; Kako, T.; Ye, J. Selective photo-oxidation of methane to methanol with oxygen over dual-cocatalyst-modified titanium dioxide. *ACS Catal.* 2020, *10*, 14318–14326.
178. Ni, Z.; Liu, N.; Zhao, C.; Mi, L. Hexanuclear nickel-added silicotungstates as high-efficiency electrocatalysts for nitrate reduction to ammonia. Polyoxometalates 2024, 3, 9140044.
179. Xu, S.; Shi, W.; Huang, J.; Yao, S.; Wang, C.; Lu, T.; Zhang, Z. Single-cluster Functionalized TiO2 Nanotube Array for Boosting Water Oxidation and CO2 Photoreduction to CH3OH. Angew. Chem. Int. Ed. 2024, 63, e202406223.
180. Yin, H.; Zhang, Z.; Lu, T. Ordered Integration and Heterogenization of Catalysts and Photosensitizers in Metal-/Covalent-Organic Frameworks for Boosting CO2 Photoreduction. Acc. Chem. Res. 2023, 56, 2676.

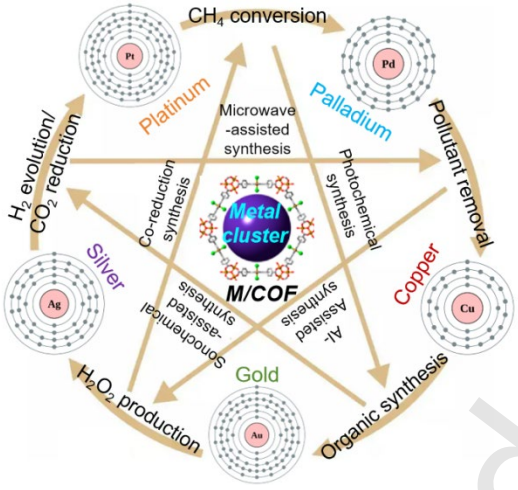

This review highlights emerging synthetic methodologies, modification strategies, and photocatalytic applications (CO_2 reduction, H_2 evolution, H_2O_2 production, organic synthesis, pollutant removal, and CH_4 conversion).